TALCOS SINTÉTICOS APLICADOS COMO CARGA EM NANOCOMPÓSITOS DE POLIURETANO

Guilherme Thomas Gerevini Dias

Pontifícia Universidade Católica do Rio Grande do Sul
Programa de Pós-Graduação em Engenharia e Tecnologia de Materiais

TALCOS SINTÉTICOS APLICADOS COMO CARGA EM NANOCOMPÓSITOS DE POLIURETANO

TALCS SYNTHÉTIQUES COMME CHARGES AVEC NANOCOMPOSITES DE POLYURÉTHANE

GUILHERME THOMAS GEREVINI DIAS
QUÍMICO INDUSTRIAL
MESTRE EM ENGENHARIA E TECNOLOGIA DE MATERIAIS

TESE PARA A OBTENÇÃO DO TÍTULO DE DOUTOR EM ENGENHARIA E TECNOLOGIA DE MATERIAIS

Porto Alegre

20 Março, 2019

Pontifícia Universidade Católica do Rio Grande do Sul
Programa de Pós-Graduação em Engenharia e Tecnologia de Materiais

TALCOS SINTÉTICOS APLICADOS COMO CARGA EM NANOCOMPÓSITOS DE POLIURETANO

TALCS SYNTHÉTIQUES COMME CHARGES AVEC NANOCOMPOSITES DE POLYURÉTHANE

GUILHERME THOMAS GEREVINI DIAS

QUÍMICO INDUSTRIAL

MESTRE EM ENGENHARIA E TECNOLOGIA DE MATERIAIS

ORIENTADOR: PROF(a). DR(a) SANDRA EINLOFT.

CO-ORIENTADOR: Prof(a). Dr(a) FRANÇOIS MARTIN.

Tese realizada no Programa de Pós-Graduação em Engenharia e Tecnologia de Materiais (PGETEMA) da Pontifícia Universidade Católica do Rio Grande do Sul, como parte dos requisitos para a obtenção do título de Mestre/Doutor em Engenharia e Tecnologia de Materiais.

Porto Alegre
Março, 2019

ATA Nº 87

Aos vinte dias do mês de março do ano de dois mil e dezenove, no Prédio 30, do Campus Universitário da Pontifícia Universidade Católica do Rio Grande do Sul, realizou-se a 87ª sessão de defesa de tese do Programa de Pós-Graduação em Engenharia e Tecnologia de Materiais. O candidato Guilherme Thomas Gerevini Dias apresentou a tese, "Talcos sintéticos aplicados como carga em nanocompósitos de poliuretano.", orientado pela Profa. Dra. Sandra Mara Oliveira Einloft e co-orientado pelo Prof. Dr. François Martin, para obtenção de grau de Doutor em Engenharia e Tecnologia de Materiais. A comissão esteve constituída pelos professores, Dra. Sandra Mara Oliveira Einloft, que a presidiu, Dr. Carlos Arthur Ferreira, PPGE3M, da UFRGS, Dra. Franciele Longaray Bernard, Escola de Ciências, da PUCRS e Dr. Felipe Dalla Vecchia, PGETEMA, da PUCRS. A comissão APROVOU o candidato neste requisito parcial e último para obtenção do grau de Doutor em Engenharia e Tecnologia de Materiais, desde que as correções sugeridas pela banca examinadora sejam efetuadas no prazo de sessenta dias. Nada mais havendo a constar, eu, Sandra Mara Oliveira Einloft, na qualidade de presidente da comissão examinadora, lavrei a presente ata que vai assinada por mim e pelos demais membros da Comissão de Avaliação.

Sandra Einloft

DRA. SANDRA MARA OLIVEIRA EINLOFT - ORIENTADORA

DR. FRANÇOIS MARTIN - CO-ORIENTADOR

BANCA EXAMINADORA

DR. CARLOS ARTHUR FERREIRA - PPGE3M - UFRGS

Franciele Longaray B.

DRA. FRANCIELE LONGARAY BERNARD - ESCOLA DE CIÊNCIAS - PUCRS

DR. FELIPE DALLA VECCHIA - PGETEMA - PUCRS

Sábio é aquele que conhece os limites da própria ignorância.
(Sócrates)

DEDICATÓRIA

Dedico este trabalho a meus pais, Marcolina Maria Gerevini Dias e Jorge Luiz Aguiar Dias, que sempre me apoiaram independente de minhas escolhas.

Á minha esposa, Liane Souto da Silva Dias por todo carinho, amor e suporte durante todo o desenvolvimento do trabalho.

E a todos que me ajudaram durante todo o caminho percorrido até o presente momento.

AGRADECIMENTOS

A todos que fizeram parte deste trabalho.

A professora Sandra Einloft pela orientação, colaboração e apoio durante a realização deste trabalho.

Ao professor François Martin pela orientação, colaboração e apoio durante o processo de desenvolvimento do trabalho.

Ao amigo Dr. Christophe Le Roux por toda ajuda e aprendizado durante todo o período em Toulouse.

A colega de Doutorado Manoela pela ajuda durante todos os trabalhos realizados.

A todos do Laboratório de Organometálicos e Resinas. Em especial ao Wesley, Leonardo, Rafael Duczinski, Franciele, Cristiane e todos os outros que conviveram juntos no LOR.

As professoras Jeane Dullius e Rosane Ligabue, por todo suporte desde os trabalhos de iniciação científica.

As secretarias da FAQUI e as do PGETEMA.

Ao pessoal do Almoxarifado (Beto, Luciane, Paulo, Marcus e Fernando) que sempre me ajudou dando as primeiras oportunidades de trabalho.

Ao vidreiro Nelson Goes, sempre ajudando e auxiliando com os equipamentos necessários para o desenvolvimento dos trabalhos.

A CAPES pela concessão da bolsa sem a qual nada poderia ter sido desenvolvido.

A FAQUI e PGETEMA pela estrutura.

SUMÁRIO

LISTA DE FIGURAS

LISTA DE SÍMBOLOS

AFM Microscopia de Força Atômica (do inglês, Atomic Force Microscopy)

BET Método Brunauer-Emmet-Teller

DMPA ácido dimetilpropiônico

DMTA Análise termo dinâmico mecânica (do inglês, Dinamic Mechanical Thermal Analysis)

DPU dispersão aquosa de poliuretano

DRX Difração de Raio-X

DSC Calorimetria Exploratória Diferencial (do inglês, Differential Scanning Calorimetry)

FTIR Infravermelho com Transformada de Fourier (do inglês, Fourier Transform Infrared Spectroscopy)

GPC Cromatografia de Permeação em Gel (do inglês, Gel Permeation Chromatography)

MEV Microscopia Eletrônica de Varredura

PA12 poliamida 12

PA6 poliamida

PP Poli(propileno)

PU Poliuretano

TEM Microscopia de Transmissão Eletrônica (do inglês, Transmission Eletronic Microscopy)

TGA Análise termogravimétrica (do inglês, Thermogravimetric Analysis)

μm micrometros

RESUMO

DIAS, Guilherme. **Talcos sintéticos aplicados como carga em nanocompósitos de poliuretano.** Porto Alegre. 2018. Tese. Programa de Pós-Graduação em Engenharia e Tecnologia de Materiais, PONTIFÍCIA UNIVERSIDADE CATÓLICA DO RIO GRANDE DO SUL.

Os poliuretanos abrangem diversos segmentos industriais. Suas propriedades podem ser adaptadas a sua aplicação apenas modificando seu processo de síntese e reagentes. A adição de talco natural e/ou sintético como carga na produção de nanocompósitos resulta na obtenção de materiais com propriedades térmicas e mecânicas superiores. Neste trabalho foram estudadas a interação e incorporação de talcos sintéticos com diferentes tratamentos hidrotérmicos em dispersões aquosas de poliuretano e poliuretanos base solvente. Foram obtidos nanocompósitos com talcos sintéticos por meio de mistura física e por meio da polimerização *in situ*. Os materiais obtidos foram caracterizados por DRX, TEM, BET, FTIR, DSC, TGA, GPC, DMA, AFM e MEV-FEG. Por meio de mistura física foram obtidos nanocompósitos de dispersão aquosa de poliuretano, utilizando três talcos sintéticos obtidos por meio de diferentes tratamentos hidrotérmicos. Nanocompósitos fluorescentes de poliuretano base solvente foram obtidos através mistura física, utilizando talcos sintético e talco natural funcionalizados com cloreto de berberina (agente fluorescente). Nanocompósitos ternários de poliuretano foram obtidos por meio da polimerização *in situ* com uma mistura de talcos sintéticos e uma argila comercial. Talco sintético em gel e em pó foi utilizado como catalisador e carga na obtenção de nanocompósitos de poliuretano base aquosa pela polimerização *in situ*. De um modo geral, foi possível observar que os talcos sintéticos foram bem dispersos dentro das matrizes de poliuretano. As propriedades térmicas e mecânicas tendem a aumentar com a introdução dos talcos sintéticos na matriz polimérica, em relação ao polímero puro. A utilização dos talcos sintéticos como carga, agente fluorescente e catalisador amplia a gama de aplicações deste material para produção de nanocompósitos com multifuncionalidades.

Palavras-Chaves: Poliuretano, talco sintético, nanocompósitos, propriedades mecânicas

ABSTRACT

DIAS, Guilherme. **Synthetic talcs applied as filler for polyurethane nanocomposites.** Porto Alegre. 2018. PhD Thesis. Graduation Program in Materials Engineering and Technology, PONTIFICAL CATHOLIC UNIVERSITY OF RIO GRANDE DO SUL.

Polyurethanes encompass several industrial segments. Its properties can be adapted to its application only by modifying its synthesis process and reagents. The addition of natural and/ or synthetic talc as a filler in the production of nanocomposites results in materials with superior thermal and mechanical properties. In this work the interaction and incorporation of synthetic talcs with different hydrothermal treatments in aqueous dispersions of polyurethane and solvent based polyurethanes were studied. Nanocomposites with synthetic talcs were obtained by physical mixing and by in situ polymerization. The obtained materials were characterized by DRX, TEM, BET, FTIR, DSC, TGA, GPC, DMA, AFM and MEV-FEG. By means of physical mixing, aqueous dispersion nanocomposites of polyurethane were obtained, using three synthetic talcs obtained by means of different hydrothermal treatments. Fluorescent nanocomposites of solvent-based polyurethane were obtained by physical mixing using synthetic talc and natural talc functionalized with berberine chloride (fluorescent agent). Polyurethane ternary nanocomposites were obtained by in situ polymerization with a mixture of synthetic talcs and a commercial clay. Synthetic gel and powder talc was used as catalyst and filler to obtain aqueous base polyurethane nanocomposites by in situ polymerization. In general, it was possible to observe that the synthetic talcs were well dispersed within the polyurethane matrices. The thermal and mechanical properties tend to increase with the introduction of the synthetic talcs into the polymer matrix, in relation to the neat polymer. The use of synthetic talcs as a filler, fluorescent agent and catalyst extends the range of applications of this material for the production of multifunctional nanocomposites.

Keywords: Polyurethane, synthetic talc, nanocomposites, mechanical properties.

RÉSUMÉ

DIAS, Guilherme. **Utilisation des talcs synthtétiques comme charges pour la préparation de nanocomposites à base de polyurethane.** Porto Alegre. 2018. Thése. Programme d'études supérieures en ingénierie des matériaux et technologie, UNIVERSITÉ PONTIFICALE CATÓLICA RIO GRANDE DO SUL.

Les polyuréthanes englobent plusieurs segments industriels et sont uttilisés dans les revêtements, les adhésifs, les mousses, les fibres, les thermoplastiques. Leurs propriétés ne peuvent être adaptées à leurs application qu'en modifiant leurs processus de synthèse et les réactifs utilisés. Dans ce contexte, les nanocomposites polymères se distinguent, car avec de petites quantités de charges, des changements dans les propriétés des polymères sont observés. L'ajout de talc naturel et / ou synthétique comme charge dans la production de nanocomposites permet d'obtenir des matériaux présentant des propriétés thermiques et mécaniques supérieures à ceux chargés avec d'autres charges.

Dans ce travail, été étudiée l'interaction et l'incorporation de trois poudres synthétiques de talc préparées par différents traitements hydrothermaux dans des dispersions aqueuses de polyuréthane. Les matériaux composites obtenus ont été caractérisés par DRX, TEM, BET, FTIR, DSC, TGA, GPC, DMTA, AFM et MEB-FEG. Ces nanocomposites issus des dispersions aqueuses de polyuréthane ont montré une bonne dispersion de la charge même en présence de grandes quantités de talc synthétique. Les propriétés mécaniques ont ainsi été améliorées. De plus, des nanocomposites de polyuréthane ont été obtenus par utilisation de talc naturel et de talcs synthétiques fonctionnalisés par du chlorure de berbiérine (agent fluorescent) par mélange physique. Ces nanocomposites de polyuréthane fluorescents ont montré une bonne dispersion de la charge au sein de la matrice polymère. Les nanocomposites produits avec les talcs synthétiques fluorescents, comparés au talc fluorescent naturel, indiquent une meilleure émission de fluorescence. L'utilisation de talcs synthétiques fluorescents a ainsi permis de fabriquer des matériaux aux propriétés thermiques et mécaniques améliorées.

Une autre étude réalisée avec des talcs synthétiques a présenté la synthèse de nanocomposites ternaires à l'aide de deux talcs synthétiques obtenus par différents procédés de traitement hydrothermal et une argile commerciale, en faisant

varier les proportions de talc synthétique/argile commerciale. Les résultats ont été comparés aux nanocomposites binaires. Les charges ont montré une bonne dispersion (exfoliation) et les propriétés mécaniques et thermiques sont meilleures que celle des nanocomposites binaires. Les deux charges influencent l'augmentation significative du module de Young par rapport au polymère pur.

Enfin, des talcs synthétiques ont été produits dans le but d'utiliser les talcs synthétiques non seulement comme charge mais aussi comme catalyseur pour la réaction de polymérisation. Le talc synthétique a été utilisé comme i) comme catalyseur lors de la réaction de polymérisation (dont l'activité catalytique sera comparée à un catalyseur commercial comme les sels d'étain tel que le DBTDL), et ii) comme agent de renforcement des nanocomposites formés. Les dispersions aqueuses ont été préparées en utilisant 0.5%, 1% et 3% en masse de talc synthétique en comparaison avec une dispersion aqueuse de polyuréthane pure. La structure des matériaux analysés par FTIR a montré qu'il est possible de synthétiser une dispersion aqueuse de polyuréthane en utilisant du talc synthétique comme catalyseur et qu'il existe des liaisons hydrogènes entre la matrice de polyuréthane et le talc synthétique qui apparait bien dispersé dans la matrice. Les propriétés thermiques et mécaniques des nanocomposites ont ainsi été améliorées avec l'ajout des talcs synthétiques. Les talcs synthétiques utilisés comme catalyseur / charge ont donné naissance à des nanocomposites dotés de propriétés thermiques et mécaniques supérieures, qui constituent un nouveau moyen d'utiliser les talcs synthétiques pour obtenir des matériaux multifonctionnels.

Mots clés: Polyuréthane, talc synthétique, nanocomposites, propriétés mécaniques

1. INTRODUÇÃO

Poliuretanos (PU) são amplamente utilizados na produção de revestimentos, adesivos, espumas, fibras, termoplásticos, etc. Suas propriedades podem ser ajustadas modificando seus componentes (segmento rígido e flexível) ou as condições de processamento (Jin, 2010). As propriedades dos diferentes tipos de poliuretano dependem das massas molares, das forças intermoleculares, da rigidez das cadeias e da cristalinidade. Devido às muitas variáveis envolvidas na produção destes polímeros, os poliuretanos são considerados polímeros multifuncionais. (Kaushik, 2011).

No entanto, os poliuretanos apresentam algumas desvantagens, tais como baixa estabilidade térmica e baixa propriedade de barreira. Para melhorar ainda mais suas propriedades, usualmente se adicionam partículas inorgânicas na estrutura do poliuretano. É relatado que o desempenho final do compósito está conectado a forma, tamanho e área superficial das cargas (Saha, 2013; Zhang, 2003). Quando as partículas são dispersas no polímero, as propriedades físicas do polímero são fortemente influenciadas por vários fatores, como a forma e tamanho das partículas da carga, o processo de fabricação, as interações carga-matriz, a quantidade de carga, área superficial e grau de dispersão (Bajsic, 2012).

O talco é um filossilicato mineral com uma estrutura em lamelas 2:1, que tem como célula unitária: $Mg_3(Si_4O_{10})$ - $(OH)_2$ (Dumas, 2013). A estrutura em lamelas é composta por uma folha octaédrica central contendo o metal (Mg, Ni, etc.) intercalada entre duas folhas de sílica tetraédricas. O talco é um mineral versátil, encontrado em uma ampla gama de processos industriais, é comumente empregado como carga em compósitos para reduzir seus custos de produção, melhorar suas propriedades físicas e fornecer novas funcionalidades. Também

aplicado em diferentes segmentos industriais (papéis, tintas, cerâmicas, cosméticos e polímeros). (Dumas, 2013; Zhao 2012; Song, 2003).

Porém, o talco natural apresenta algumas limitações. A estrutura do talco apresenta impurezas na forma de substituições catiônicas, diferentes elementos (Mg^{2+}, Fe^{2+}, Mn^{2+} e Ni^{2+}) podem aparecer na estrutura cristalina por meio de substituições isomórficas, fazendo com que o mineral apresente uma não homogeneidade na estrutura química, na fase cristalina e na distribuição de tamanho das partículas (Dumas, 2013). A síntese de nanopartículas de talco é uma metodologia refinada para se produzir materiais com características distintas, podendo-se controlar sua cristalinidade, composição, tamanho das partículas e das lamelas. Por exemplo, variando-se em alguns graus a temperatura da reação hidrotérmica, o tamanho médio das partículas pode variar em várias centenas de nanômetros (Yousfi, 2013).

Alguns trabalhos demonstraram que o uso de talco natural e/ou sintético como carga promoveu um aumento nas propriedades térmicas, mecânicas e de barreira do polímero utilizado como matriz (Yousfi, 2013, Yousfi, 2014; Bajsic, 2012; Wang, 2013; Castillo, 2013).

Pesquisas referentes à produção de nanocompósitos de poliuretanos (base aquosa ou base solvente) utilizando talcos sintéticos como carga demostraram que é possível desenvolver materiais multifuncionais com propriedades superiores (térmicas, mecânicas e magnéticas). (Dias, 2015; Dias, 2016; Dos Santos, 2015; Dos Santos, 2017; Prado 2015).

Neste trabalho foram desenvolvidos nanocompósitos de poliuretano base solvente e aquosa, produzidos por meio de misturas físicas entre os talcos sintéticos e as matrizes de PU. Diferentes tipos de talcos sintéticos foram utilizados como cargas. Talcos sintéticos com Mg na sua estrutura em forma de gel com diferentes tempos de síntese foram misturados com PUs base aquosa, foram avaliadas as propriedades térmicas, mecânicas e morfológicas dos nanocompósitos. Talcos sintéticos em pó com cloreto de berberina (agente fluorescente) em sua estrutura foram misturados com PUs base solvente, foram avaliadas as propriedades térmicas, mecânicas, morfológicas e fluorescentes dos nanocompósitos. Também

foram produzidos nanocompósitos de poliuretano base solvente feitos com uma mistura de cargas (argila comercial SPR; talcos sintéticos 7h e 24h) por meio de polimerização *in situ*. Por último, nanocompósitos de poliuretano base aquosa utilizando talcos sintético (300°C; 6h) em forma de gel e em forma de pó foram obtidos através da polimerização *in situ*, como mostra o fluxograma (Fig 1.1).

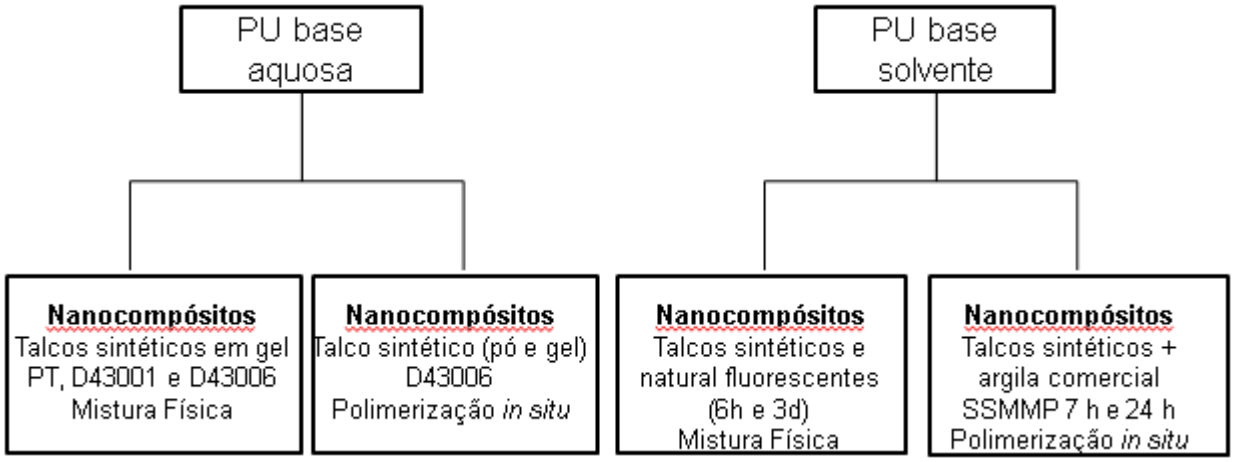

Figura 1.1. Fluxograma dos trabalhos desenvolvidos.

INTRODUCTION

Les polyuréthannes (PU) sont largement utilisés dans la production de revêtements, d'adhésifs, de mousses, de fibres, de thermoplastiques, etc... Leurs propriétés peuvent être ajustées en modifiant leurs composants (segment rigide et flexible) ou leurs conditions de traitement (Jin, 2010). Les propriétés des différents types de polyuréthane dépendent des masses molaires, des forces intermoléculaires, de la rigidité des chaînes et de la cristallinité. En raison des nombreuses variables impliquées dans la production de ces polymères, les polyuréthannes sont considérés comme des polymères multifonctionnels. (Kaushik, 2011).

Cependant, les polyuréthannes présentent certains inconvénients, tels qu'une faible stabilité thermique et une faible propriété de barrière. Pour améliorer encore leurs propriétés, des particules inorganiques sont généralement ajoutées au squelette des polyuréthanes. Il a été rapporté que la performance finale du composite est liée à la

forme, à la taille et à la surface des charges (Saha, 2013; Zhang, 2003). Lorsque les particules sont dispersées dans le polymère, les propriétés physiques du polymère sont fortement influencées par plusieurs facteurs, tels que la forme et la taille des particules de la charge, le processus de fabrication, les interactions charge-matrice, la quantité de charge, la surface et le degré de dispersion (Bajsic, 2012).

Le talc est un phyllosilicate minéral ayant une structure lamellaire 2:1, de formule structurale $Si_4Mg_3O_{10}(OH)_2$. La structure lamellaire est composée d'une couche octaédrique contenant le métal (Ni, etc...) sandwiché entre deux couches de tétraèdres de Si. Le talc est un minéral polyvalent, utilisé dans une large gamme de procédés industriels comme les papiers, les peintures, les céramiques, les cosmétiques et les polymères (Song, 2003 et Dumas 2013). Il est utilisé comme charge minérale pour réduire les coûts de production, améliorer les propriétés physiques et fournir de nouvelles fonctionnalités.

Cependant, le talc naturel présente certaines limites. En effet comme toute substance naturelle, il est extrait de carrières et l'existence d'une phase minéralogique unique est très exceptionnelle même pour les talcs les plus purs. Il est donc fréquemment associé avec d'autres phases minérales voisines et phyllosilicatées comme la chlorite dans des proportions définissant les classes commerciales, les plus pures en tant pouvant coûter 1000 euros la tonne, les moins pures avec 60% de chlorite 100 euros la tonne. Cette chlorite n'apporte aucun bénéfice pour les propriétés mais peut nuire si sa quantité est trop grande par rapport au talc dans certaines applications. Mais fréquemment les gisements de talc présente des associations avec d'autres minréaux comme les calcites et les dolomites (ce qui peut luire à la qualité du produit dans certaines applications) mais aussi avec d'autres minéraux qui eux sont interdits en application (pyrite, oxyde de fer) ou interdisant l'utilisation du talc (amiantes comme du chrysotile, ou de la trémolite). De plus, la structure du talc présente systématiquement des impuretés sous la forme de substitutions cationiques (Mg^{2+} substitué par Fe^{2+}, Mn^{2+}, Ni^{2+}, Co^{2+}, Fe^{3+}, Al^{3+}) et anioniques(OH^- par F^-), ce qui peut induire des variations cristallochimiques et modifier par exemple la distribution granulométrique (Dumas, 2013). La synthèse de nanoparticules de talc est une méthodologie raffinée permettant de produire des matériaux dotés de caractéristiques distinctes,

minéralogiquement purs et cristallochimiquement purs. Leur cristallinité, leur composition, leur taille et leurs formes peuvent être contrôlées. Par exemple, en modifiant de quelques degrés la température de la réaction hydrothermale, la taille moyenne des particules peut varier de plusieurs centaines de nanomètres (Yousfi, 2013, Dumas, 2013).

De récentes études ont montré que l'utilisation de talc naturel et / ou synthétique en tant que charge favorisait l'augmentation des propriétés thermiques, mécaniques et des effets barrières du polymère utilisé comme matrice (Bajsic, 2012, Castillo, 2013, Wang, 2013, Yousfi, 2013, Yousfi, 2014).

Les recherches sur la production de nanocomposites de polyuréthane (à base aqueuse ou à base de solvant) utilisant du talc synthétique comme charge ont montré qu'il est possible de développer des matériaux multifonctionnels dotés de propriétés supérieures à ceux utilisant des charges minérales commerciales (thermique, mécanique et magnétique) (Dias, 2015, Dos Santos, 2015, Prado 2015, Dos Santos, 2017).

Dans ce travail, des nanocomposites de polyuréthane (PU) aqueux et à base de solvant, produits par des mélanges physiques entre des talcs synthétiques et des matrices en PU, seront développés.

Différents types de talcs synthétiques ont été utilisés comme charges. 1) des poudres de talcs synthétiques avec du Mg dans la structure et des gels de talcs synthétiques de même composition obtenus avec différents temps de synthèse ont ainsi été mélangées avec des PU aqueux, les propriétés thermiques, mécaniques et morphologiques des nanocomposites ayant été ensuite évaluées ; 2) des poudres de talcs synthétiques avec du chlorure de berbiérine (agent fluorescent) dans leur structure ont été mélangées avec des PU à base de solvant, les propriétés thermiques, mécaniques, morphologiques et de fluorescence des nanocomposites ont été ensuite évaluées ; 3) des nanocomposites à base de solvant de polyuréthane constitués d'un mélange de charges (argile SPR commerciale, talcs synthétiques 7h et 24h) ont été frabriqués par polymérisation in situ ; 4) et enfin, des nanocomposites de polyuréthane à base aqueuse utilisant du talc synthétique (300 ° C, 6h) sous forme de gel et sous forme de poudre ont été obtenus par polymérisation in situ.

Le but de ces expériences sont de montrer l'intérêt de développer des charges nanométriques qui quand la dispersion dans la matrice est maitrisée permettent d'obtenir des matériaux composites avec des propriétés renforcées et permettant d'étendre les domaines d'application, MAIS aussi de créer de nouveaux métariaux multicomposites non présents sur les marchés, et qui peuvent conquérir des domaines d'applications nouveaux et dans lesquels ces matériaux ne sont pas présents actuellement. Le corollaire de ceci est d'aussi comprendre les effets des charges nanométriques sur les propriétés physiques et chimiques des polymères créés en comparaison des autres charges microniques utilisées, les charges nanométriques de type talc présentant des surfaces spécifiques supérieures à $300m^2/g$ et pouvant aller juqu'à $1000m^2/g$, engendrant un nombre de liaisons avec les polymères bien supérieur (la surface spécifique d'untalc commercial est de $10m^2/g$ maximum).

2. OBJETIVOS

Este trabalho tem como objetivo estudar nanocompósitos de PU utilizando talcos sintéticos produzidos em diferentes condições de tratamento hidrotérmico como carga.

2.1. Objetivos Específicos

- Obter os nanocompósitos PU/talcos sintéticos, variando a proporção de carga das misturas: talcos sintéticos em gel (PU base aquosa), talco sintético-berberina em pó (PU base solvente) e utilizando uma mistura de cargas (talcos sintéticos e argila comercial) ;

- Avaliar os nanocompósitos obtidos em relação ao polímero puro e a cargas comerciais através das propriedades térmicas, mecânicas, morfológicas e de fluorescência;

- Avaliar a interação entre a matriz de PU com os diferentes talcos sintéticos;

- Síntese de novos talcos sintéticos com diferentes funcionalidades

3. REVISÃO BIBLIOGRÁFICA

3.1. Poliuretanos

Poliuretanos (PUs) estão entre os materiais mais versáteis. Sua gama de aplicações varia desde espumas flexíveis em móveis estofados, espuma rígida para isolamento de paredes, telhados e eletrodomésticos, poliuretanos termoplásticos usados em dispositivos médicos, calçados, revestimentos, adesivos, selantes, etc. PUs são polímeros termoplásticos ou termofixos que podem ter suas propriedades mecânicas, térmicas e químicas adaptadas pela reação de vários polióis e poliisocianatos (Fig 3.1). Os PUs incluem aqueles polímeros que contêm um número significativo de grupos uretano (–NH–COO–), independentemente do que o resto da molécula possa ser (Zia, 2007).

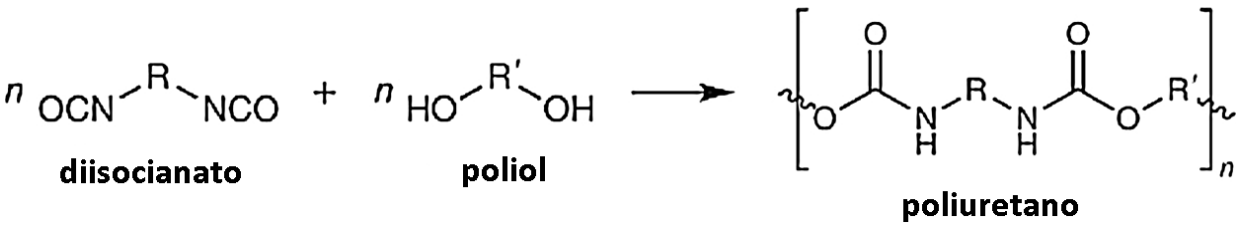

Figura 3.1. Reação de formação do poliuretano (adaptado de Czonka, 2018).

Estes materiais podem ter suas propriedades adaptadas modificando seus reagentes precursores ou seu processo de síntese. A ligação de uretano é formada pela reação de um grupo isocianato com o grupo hidroxila do poliol (Sattar, 2015). Os poliuretanos são copolímeros constituídos de segmentos flexíveis e rígidos alternados, o segmento rígido consiste em diisocianato e extensor de cadeia e o segmento flexível consiste de poliol. Os segmentos rígidos e flexíveis são termodinamicamente incompatíveis a baixas temperaturas, devido às ligações intermoleculares os dois segmentos constituem microdomínios (Fig 3.2). Geralmente, o PU pode ser adaptado de acordo com sua aplicação, escolhendo-se cuidadosamente os reagentes, sua proporção e o método de síntese. (Pohkarel, 2015). Em particular, os grupos uretano e/ou ureia dos segmentos rígidos formam fortes ligações por pontes de hidrogênio, resultando numa estrutura organizada desenvolvida pela separação dos microdomínios (Yamasaki, 2016).

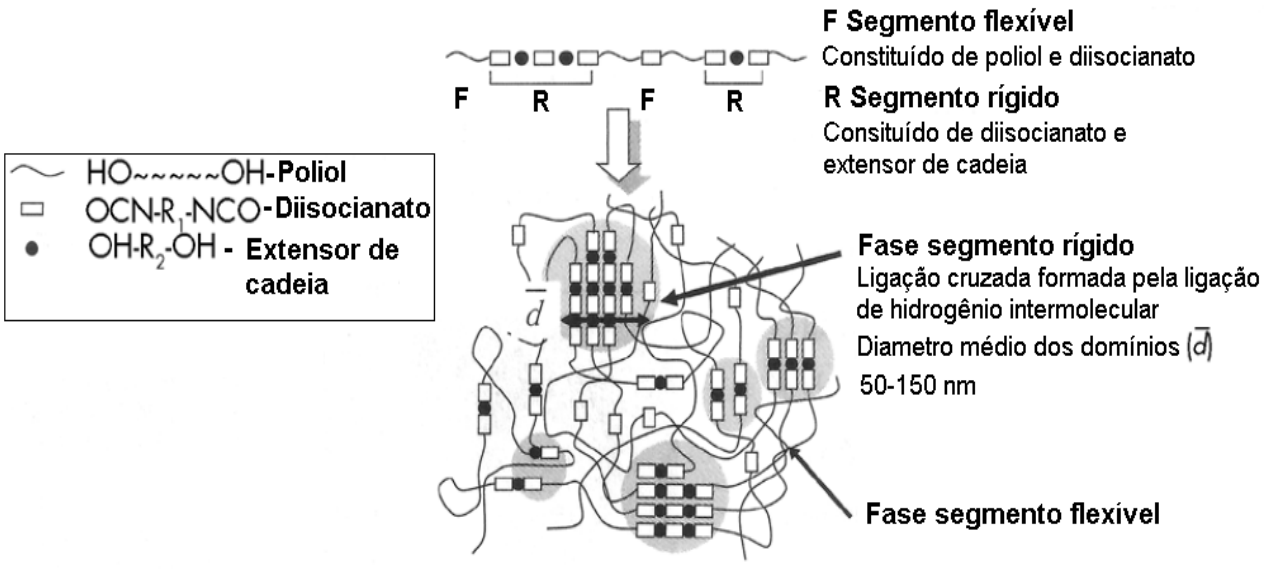

Figura 3.2. Estrutura das cadeias de um poliuretano (Adaptado de Yamasaki, 2016).

O desenvolvimento do PU teve início com o trabalho de Otto Bayer e seus colegas no começo da Segunda Guerra Mundial, quando o PU foi desenvolvido pela primeira vez como substituto da borracha. Bayer é conhecido como o “pai” da indústria de PUs por sua invenção do processo básico de poliadição de diisocianato. Durante a Segunda Guerra Mundial, os revestimentos PU foram usados para a impregnação de papel e a fabricação de roupas resistentes a gás mostarda, acabamentos de alto brilho para aeronaves e revestimentos resistentes a produtos químicos e corrosivos para proteger metal, madeira e alvenaria (Lee, 2006). Ao mesmo tempo, os primeiros adesivos metal-plástico de poliuretano foram desenvolvidos. As dispersões aquosas de poliuretano (DPU) também estavam sendo desenvolvidas, com o látex sendo divulgado em 1961 pela DuPont (Noreen, 2016).

A cadeia de valor agregado dos poliuretanos envolve três atores principais. Os primeiros são os químicos industriais que produzem as matérias-primas para a síntese de polímeros. Os segundos são os formuladores que produzem poliuretanos a partir de matérias-primas; e os últimos são os fabricantes, que incluem poliuretanos em seus produtos finais. Os atores econômicos estão envolvidos em um, dois ou nesses três setores. Em 2016, com uma produção global de 18 Mt, os PUs ocuparam o sexto lugar entre todos os polímeros, com base na produção anual mundial. A maior parte desta produção é realizada na Ásia, com cerca de 8 Mt, depois na Europa, com cerca de 4 Mt e, finalmente, nos Estados Unidos da América, com cerca de 3 Mt. O mercado global de poliuretano está avaliado em cerca de 53 bilhões de euros e as cinco primeiras empresas, BASF, Bayer, Dow, Huntsman e Yantai Wanhua, respondem por mais de 35% do mercado total (Fig 3.3) (Cornille,2017).

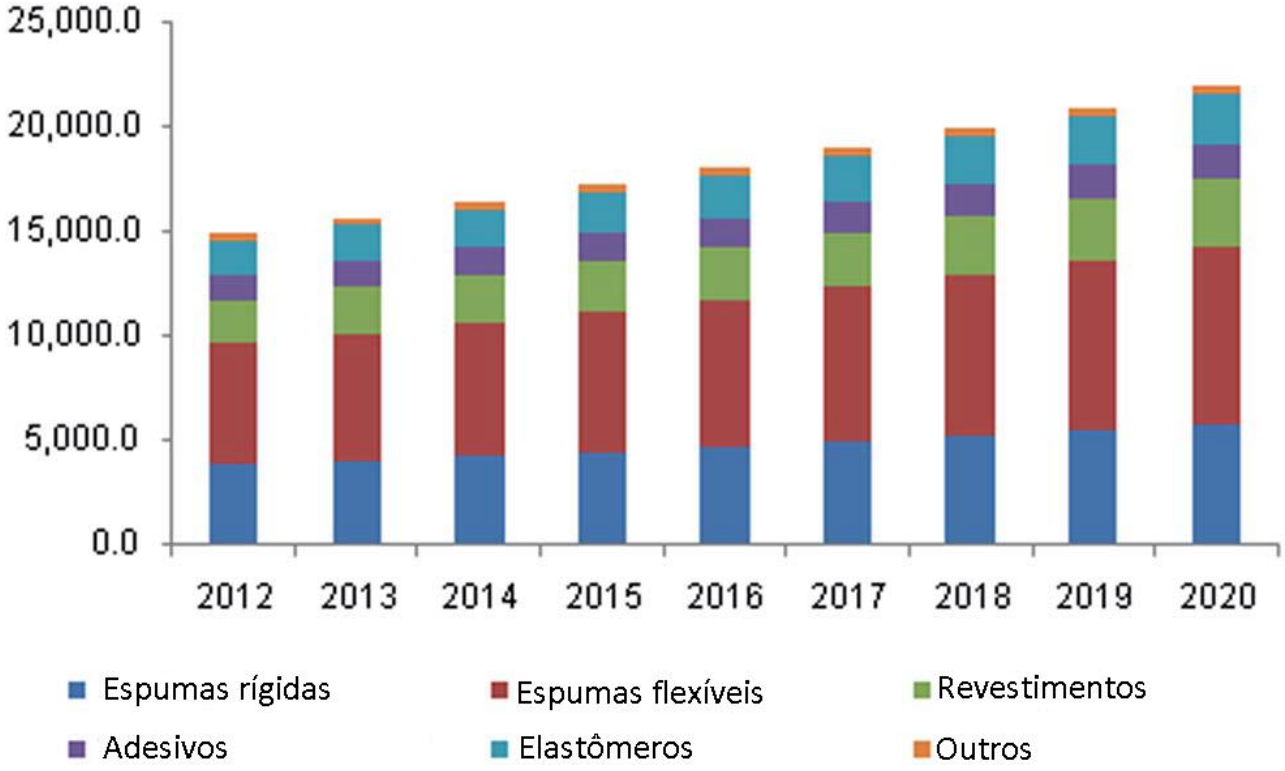

Figura 3.3. Produção mundial de PU (t) e uma estimativa de produção até 2020 (Adaptado de Akyndoyo, 2016).

3.1.1. Dispersões aquosas de poliuretano

Poliuretanos convencionais geralmente contêm uma quantidade significativa de solventes orgânicos e, às vezes, até monômeros de isocianato livres. Devido à limitação global às quantidades de compostos orgânicos voláteis liberados na atmosfera, dispersões aquosas de poliuretanos vêm sendo estudados devido à sua baixa concentração de compostos orgânicos voláteis. DPUs são poliuretanos dispersos em água, utilizados atualmente em diferentes aplicações industriais como: eletrônicos, adesivos, revestimentos, membranas e biológicas. Além disso, os DPUs possuem várias vantagens quando comparados aos PUs convencionais à base de solventes orgânicos, tais como baixa viscosidade em alto peso molecular, não toxicidade e não poluição (Cao,2009; Gao, 2011; Zhang, 2013; Heck, 2015).

É importante destacar que a viscosidade das DPUs independe da massa molar do polímero. Além disso, as DPUs podem ser preparadas com um alto teor de sólidos e com uma massa molar suficientemente alta capaz de formar filmes com excelente qualidade simplesmente por meio da evaporação da água. As DPUs são consideradas como um sistema coloidal de duas fases em que as partículas de poliuretano são dispersas em água (fase contínua) (Gurunathan, 2015). Inerentemente, os poliuretanos não se dispersam em água devido à presença de isocianatos hidrofóbicos (que também reagem com água), enquanto os DPUs conseguem se dispersar em meio aquoso devido à presença de grupos iônicos nas cadeias do poliuretano (Fig 3.4.) (Gurunathan, 2015; Noreen, 2016). O ácido dimetilpropiônico (DMPA) é comumente utilizado como emulsificante. O íon carboxílico do DMPA no polímero é hidrofílico e serve como um centro aniônico bem como emulsificante interno. Os grupos carboxílicos nas DPUs fornecem carga às superfícies das micelas de PU (partículas), causando repulsão entre as partículas de PU, resultando numa distribuição uniforme no tamanho das partículas de PU dentro da dispersão aquosa. Por conseguinte, a percentagem em peso de DMPA utilizada no pré-polímero não influencia apenas o tamanho das partículas e a estabilidade da dispersão, mas também na hidrofobicidade dos materiais. Por exemplo, o uso de uma maior quantidade de DMPA resulta em um menor tamanho médio de partícula e alta hidrofilicidade no filme, o que reduz a resistência à água do revestimento. Portanto, uma quantidade ideal de DMPA deve ser utilizada para se obter um material de alto desempenho (Chattopadhyay, 2007).

Vários processos foram desenvolvidos para a preparação de DPUs. Em todos estes processos, um polímero de peso molecular médio (o pré-polímero) é formado pela reação de dióis ou polióis adequados com um excesso de diisocianatos ou poliisocianatos na presença de um emulsificante interno. O emulsificante é diol com um grupo iônico (carboxilato, sulfonato ou um sal de amônio quaternário) ou um grupo não-iônico [poli (óxido de etileno)] é normalmente adicionado para permitir a dispersão do polímero em água (Chattopadhyay, 2007; Zhou, 2015).

O processo da acetona para preparação de uma DPU é o mais antigo e que permanece tecnicamente importante. Durante as últimas décadas, vários novos

processos foram desenvolvidos como: polimerização homogênea em solução (Wang, 2008), polimerização por miniemulsão (Zhang, 2012), polimerização radicalar por transferência de átomos (Zhou, 2015), etc. Uma característica comum a estes processos é, no entanto, que o primeiro passo é preparar os pré-polímeros de PU de peso molecular médio com grupos de NCO em excesso. A etapa que difere os processos é a extensão da cadeia (Kim, 1996).

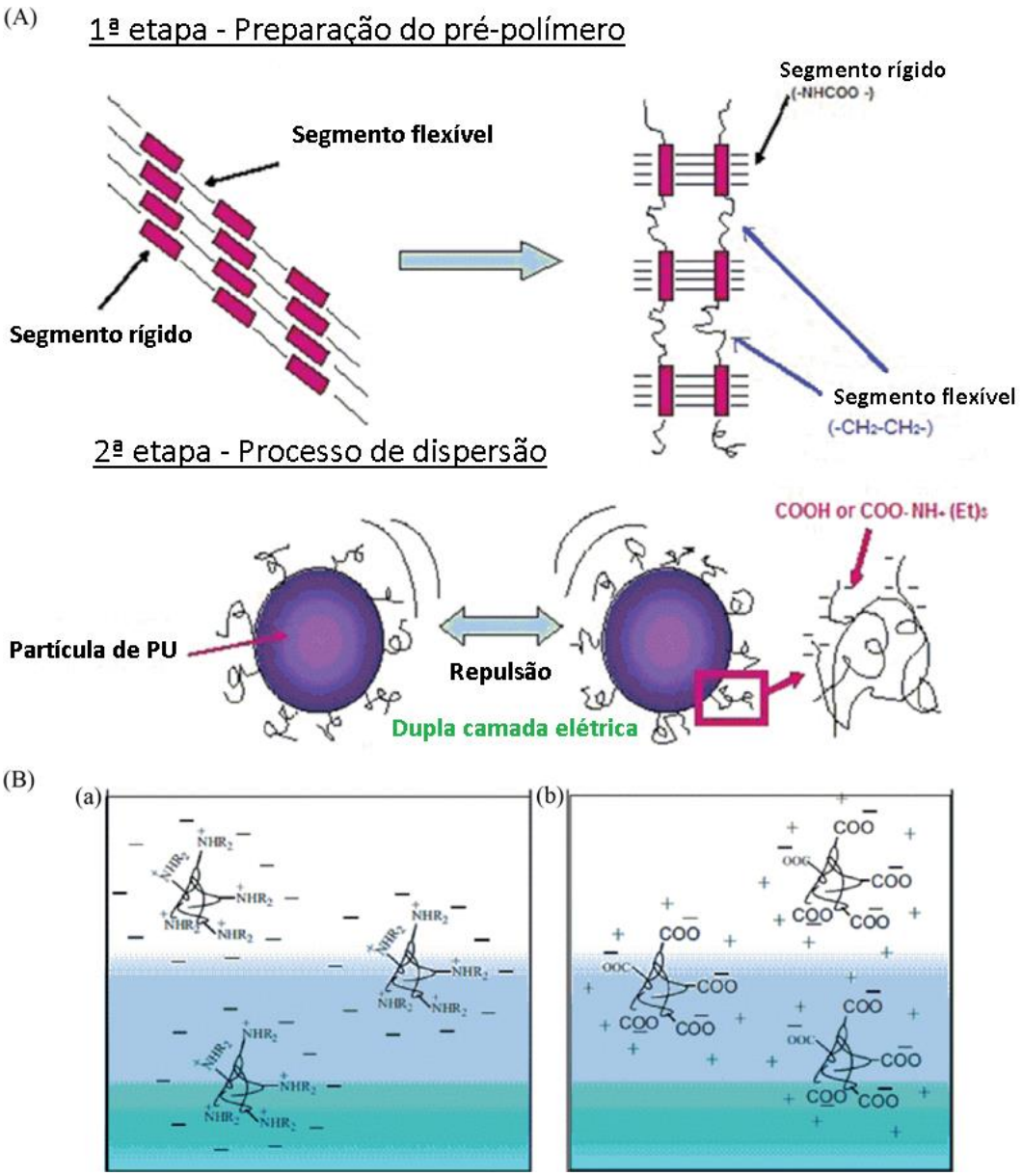

Figura 3.4. (A) Representação da dispersão do DPU; (B) Representação das micelas (a) catiônicas e (b) aniônicas dispersas em água. (Adaptado de Noreen, 2016).

3.1.1.1. Processo da acetona

No processo da acetona, um solvente (acetona) é adicionado ao pré-polímero, e a dispersão é formada pela adição de água a esta solução. A extensão é normalmente realizada pela adição de uma diamina à solução de pré-polímero ou após a dispersão em água. A acetona é então removida por evaporação (Barni, 2003).

Os pré-polímeros de PU com excesso de NCO tem sua cadeia estendida com uma diamina em meio solvente orgânico tal como acetona, metileticetona, ou tetrahidrofurano, seguido pela dispersão em água, e por último ocorre a remoção do solvente por destilação. Este processo bem estabelecido usa um solvente orgânico para controlar a viscosidade durante a etapa de extensão da cadeia. A acetona é especialmente adequada porque é inerte com as reações de formação de PU, miscível em água e tem um baixo ponto de ebulição. Além disso, reduz a alta reatividade de NCO-NH. As vantagens do processo de acetona incluem amplo escopo de variação na estrutura e emulsão, alta qualidade dos produtos e reprodutibilidade confiável. Estas vantagens são importantes porque a formação do polímero é realizada em uma solução homogênea. No entanto, PU obtido em processo de acetona é predominantemente linear e solúvel em acetona, uma vez que a extensão da cadeia é realizada em acetona. A destilação de grande quantidade de acetona torna o processo economicamente desfavorável. Este processo também apresenta um baixo rendimento devido às grandes quantidades de solvente usado (Kim,1996).

3.1.1.2. Processo do pré-polímero

No processo do pré-polímero, o pré-polímero modificado hidrofilicamente é disperso diretamente em água. Se a viscosidade da mistura for muito alta, uma pequena quantidade de solvente, tal como N-metilpirrolidona, pode ser adicionada antes da etapa de dispersão. A extensão da cadeia é realizada pela adição de diaminas à dispersão do pré-polímero aquoso (Barni, 2003).

O processo do pré-polímero evita o uso de grandes quantidades de solvente. Os pré-polímeros PU com excesso de grupos NCO modificados hidrofílicamente são dispersos em água para formar emulsão. A viscosidade do pré-polímero é importante e deve ser controlada durante o processo de dispersão. Portanto, este processo é adequado para um pré-polímero de baixa viscosidade. A extensão da cadeia é realizada pela adição de aminas (diaminas, poliaminas, etc.) à dispersão aquosa. A dispersão dever ser realizada em uma temperatura suficientemente baixa para que a reação entre NCO-água seja insignificante. Por esta razão, os diisocianatos cicloalifáticos são mais frequentemente utilizados devido à sua baixa reatividade com a água (Kim, 1996).

3.2. Nanocompósitos

Nanocompósitos poliméricos são uma nova classe de materiais compósitos derivados de nanopartículas com pelo menos uma dimensão na faixa dos nanômetros (até 100 nm). Estas nanopartículas são dispersas na matriz polimérica em uma quantidade de carga relativamente baixa (normalmente menor que 6% em massa) (Lei, 2006). Devido ao fato das nanopartículas (nanoargilas, nanofibras, nanotubos de carbono, etc.) serem muito pequenas e sua área superficial elevadas, mesmo com pequenas quantidades de carga algumas propriedades do polímero podem ser aprimoradas sem prejudicar as características físicas originais do material polimérico, o que pode ocorrer quando se utilizam cargas convencionais (Pavlidou, 2008; Maji, 2012). Em geral, as nanopartículas

podem melhorar significativamente a rigidez, a estabilidade térmica, as propriedades de barreira, a condutividade elétrica e a resistência ao fogo da matriz polimérica (Maji, 2012).

Os nanocompósitos orgânicos/inorgânicos são geralmente constituídos de polímeros orgânicos com partículas inorgânicas nanométricas (Nguyen, 2006). Eles combinam as vantagens do material inorgânico (por exemplo, rigidez, estabilidade térmica) e do polímero orgânico (por exemplo, flexibilidade, dutilidade e processabilidade) (Salahuddin, 2010). Além disso, os nanocompósitos também apresentam propriedades derivadas das nanocargas levando a obtenção de materiais com propriedades superiores. É importante destacar que devido as cargas estarem na escala dos nanômetros existe uma maior área interfacial entre polímero\carga, o que favorece a melhora nas propriedades, em relação ao polímero puro, mesmo utilizando-se uma pequena fração de carga (Zou, 2008).

Dependendo de quantas dimensões estão na escala nanométrica, pode-se classificar as nanopartículas: isodimensionais (quando as três dimensões são da ordem de nanômetros), nanotubos (quando duas dimensões estão na escala nanométrica) e, finalmente, cristais lamelares ou argilas (na forma de folhas onde a espessura varia de um até alguns nanômetros) (Pavlidou,2008).

Existem metodologias que podem favorecer a dispersão das nanopartículas nos nanocompósitos, como a polimerização *in situ*, mistura física por fusão, mistura física em solução, sonificação, intercalação por fusão, entre outras (Khudyakov, 2009). As metodologias mais empregadas para sintetizar nanocompósitos de silicatos lamelares são: por meio da inserção da carga na polimerização *in situ*, mistura física da carga com o polímero em meio solvente e mistura simples do polímero fundido com a carga (Song,2003). No método da polimerização *in situ* (Fig.3.5-III), o monômero é utilizado como um agente solubilizante do silicato lamelar facilitando a intercalação e\ou esfoliação. A polimerização ocorre após a mistura do silicato lamelar e do monômero, permitindo assim a formação de cadeias poliméricas entre as folhas do silicato lamelar intercaladas. Outro método é a mistura em solução onde ocorre a mistura da carga com o polímero em meio solvente (Fig.3.5-II). Este método requer um solvente adequado que pode tanto solubilizar o polímero como dilatar as lamelas do silicato.

Quando o silicato lamelar é disperso dentro da solução contendo o polímero, as cadeias poliméricas se intercalam entre as galerias do silicato lamelar. O nanocompósito polimérico é obtido após a remoção do solvente, seja por evaporação do solvente ou precipitação do polímero. As desvantagens destes dois métodos citados são os pré-requisitos de se ter solventes e reagentes adequados, o que eleva os custos associados com os solventes, a sua eliminação e o seu impacto no ambiente. E por último o método da mistura simples do polímero fundido com a carga (Fig.3.5-I), não requer o uso de um solvente compatível ou monômero adequado. Neste método, um polímero e uma mistura de silicato lamelar são aquecidos (exemplo, extrusão) acima do ponto de fusão do polímero. Durante o processo de aquecimento, as cadeias poliméricas se difundem do polímero fundido para as galerias do silicato lamelar, formando estruturas intercaladas e\ou esfoliadas, dependendo do grau de dispersão. Este método se destaca devido a simplicidade, baixo custo e pequeno impacto ambiental (Nguyen, 2006).

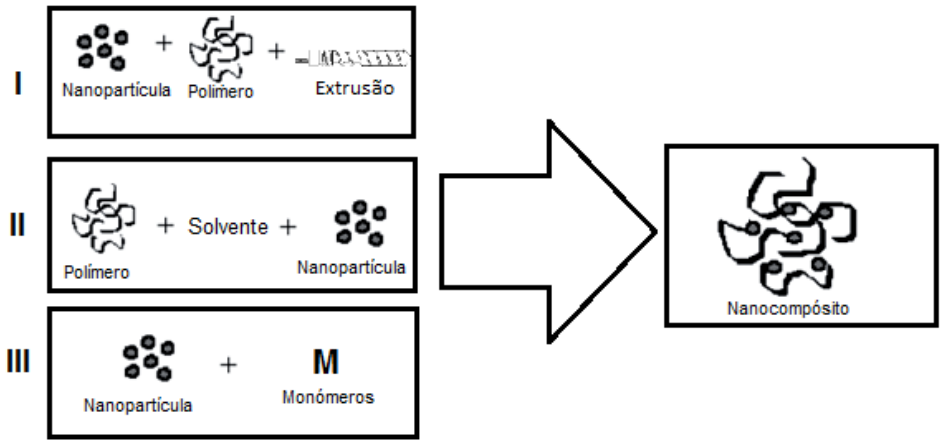

Figura 3.5. Métodos de preparação dos nanocompósitos: I) mistura simples dos componentes (extrusão), II) preparação de nanopartículas por mistura física (em solvente) e III) Polimerização da matriz *in situ*. (Moreira Dos Santos,2013).

Nanocompósitos de polímero/silicato lamelar são sistemas de duas fases, que consistem em uma matriz polimérica e nanopartículas dispersas na matriz. As cargas inorgânicas mais utilizadas em nanocompósitos poliméricos pertencem à família dos filossilicatos 2:1, que possuem uma estrutura de silicato lamelar. Existem três tipos de morfologias para nanocompósitos com base no grau de dispersão do

silicato lamelar: agregada, intercalada e esfoliada (Fig.3.6). Na estrutura agregada, as folhas de silicato lamelar estão bem distribuídas na matriz polimérica, mas as camadas individuais de silicato lamelar não estão esfoliadas. Na estrutura intercalada, as folhas de silicato lamelar estão esfoliadas em alguma extensão: assim cadeias poliméricas podem se difundir nas galerias entre elas. Na estrutura esfoliada, as folhas de silicato lamelar estão completamente separadas em folhas de uma única camada, que estão homogeneamente dispersas na matriz polimérica. A estrutura esfoliada é a estrutura ideal quando se trabalha com nanocompósitos, pois pode fornecer excelentes propriedades térmicas e mecânicas quando se utiliza quantidades muito baixas de silicatos lamelares. No entanto, a maioria dos nanocompósitos poliméricos apresenta uma estrutura intercalada e esfoliada (Tan,2016).

O mecanismo para se obter melhorias significativas nas propriedades dos nanocompósitos é dispersar ou esfoliar as partículas (lamelas) individuais do silicato lamelar mineral dentro da matriz polimérica aproveitando sua alta área superficial específica. A afinidade do polímero à superfície do silicato lamelar mineral e/ou aos surfactantes intercalados no mesmo é essencial para promover interações favoráveis entre carga/polímero e, assim, obter altos níveis de esfoliação (Salahuddin, 2010).

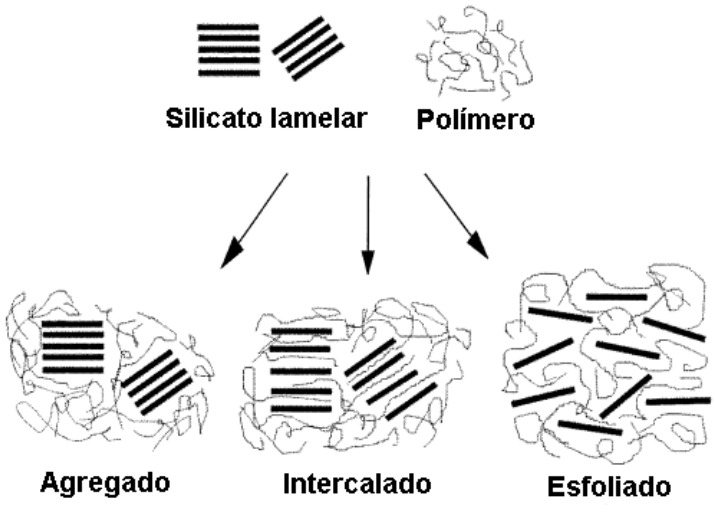

Figura 3.6. Morfologias possíveis em nanocompósitos de silicatos lamelares (Adaptado de Alexandre e Dubois, 2000).

3.3. Silicatos Lamelares

Silicatos lamelares são minerais naturais e\ou sintéticos muito utilizados para sintetizar nanocompósitos, consistindo basicamente de folhas com espessura muito finas que geralmente são ligadas a contra-íons. Sua estrutura cristalina básica consiste de folhas tetraédricas, nas quais o silício é circundado por quatro átomos de oxigênio, e folhas octaédricas, nas quais um metal, como o alumínio, é circundado por oito átomos de oxigênio. Portanto, em estruturas de camadas 1:1 (por exemplo, a caulinita), uma folha tetraédrica é ligada a uma folha octaédrica, onde os átomos de oxigênio são compartilhados (Pavlidou,2008).

Os filossilicatos com estrutura em lamelas 2:1 (Fig 3.7), são constituídos de uma rede cristalina em camadas bidimensionais onde uma folha octaédrica central com um metal (Al, Mg, etc.) é ligada a dois tetraedros de sílica, de modo que os íons de oxigênio são compartilhados pelas folhas octaédricas e tetraédricas. A espessura das lamelas é de cerca de 1 nm e as dimensões laterais dessas camadas podem variar de 300 Å a vários micrometros, dependendo do silicato lamelar em particular. Essas lamelas se organizam formando folhas empilhadas com um intervalo regular entre elas, chamado de espaço interlamelar ou galeria. A substituição isomórfica dentro das lamelas (por exemplo, Al_3 substituído por Mg_2, ou Mg_2 substituído por Li) gera cargas negativas que são contrabalanceadas por cátions alcalinos ou alcalino-terrosos situados no espaço interlamelar ou galeria. Como as forças que atuam mantendo as folhas empilhadas (forças de van der Walls) são relativamente fracas, a intercalação de moléculas pequenas entre lamelas é fácil (Alexandre e Dubois, 2000).

Cargas derivadas de silicatos lamelares apresentam um grande potencial para aumentar as propriedades de matrizes poliméricas. Devido a sua alta área superficial, nanocompósitos poliméricos de silicatos lamelares apresentam propriedades superiores quando comparadas as do polímero puro (Song,2003; Yu,2012).

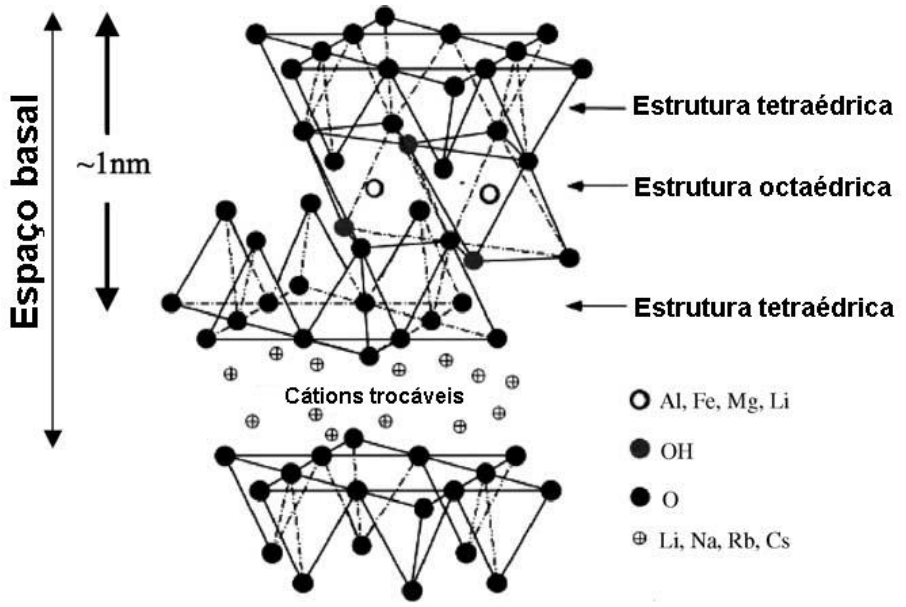

Figura 3.7. Estrutura 2:1 de silicatos lamelares (filossilicatos) (Adaptado de Ray e Okamoto,2003).

3.4. Talco

O talco é um silicato lamelar mineral de magnésio tendo como fórmula ideal $Mg_3Si_4O_{10}(OH)_2$ (Fig.3.8), sendo normalmente utilizado como carga em compósitos causando uma redução nos custos de manufatura dos mesmos, melhoria em suas propriedades físicas e químicas e fornecendo novas funcionalidades. Sua gama de aplicações abrange diferentes áreas da indústria como: papéis, tintas, cerâmicas, cosméticos e polímeros (Dumas, 2013). Sua estrutura elementar é formada por uma folha octaédrica de hidróxido de magnésio ($Mg_{12}O_{12}H_4$) ensanduichada entre duas folhas tetraédricas de sílica (SiO_2), o talco é constituído de uma superposição indefinida de lamelas. O tamanho de uma folha individual de talco (alguns milhares de lamelas) pode variar de, aproximadamente, 1 até 100 µm, dependendo das condições de formação do mineral. O espaço ou lacuna de van der Waals (espaço

interlamelar ou galeria) entre as lamelas é formado devido ao empilhamento, o que pode ser uma vantagem para se obter materiais onde o talco esteja completamente esfoliado dentro da matriz polimérica. A carga das lamelas é zero ou muito baixa, não havendo íons livres entre as lamelas (Castillo,2013).

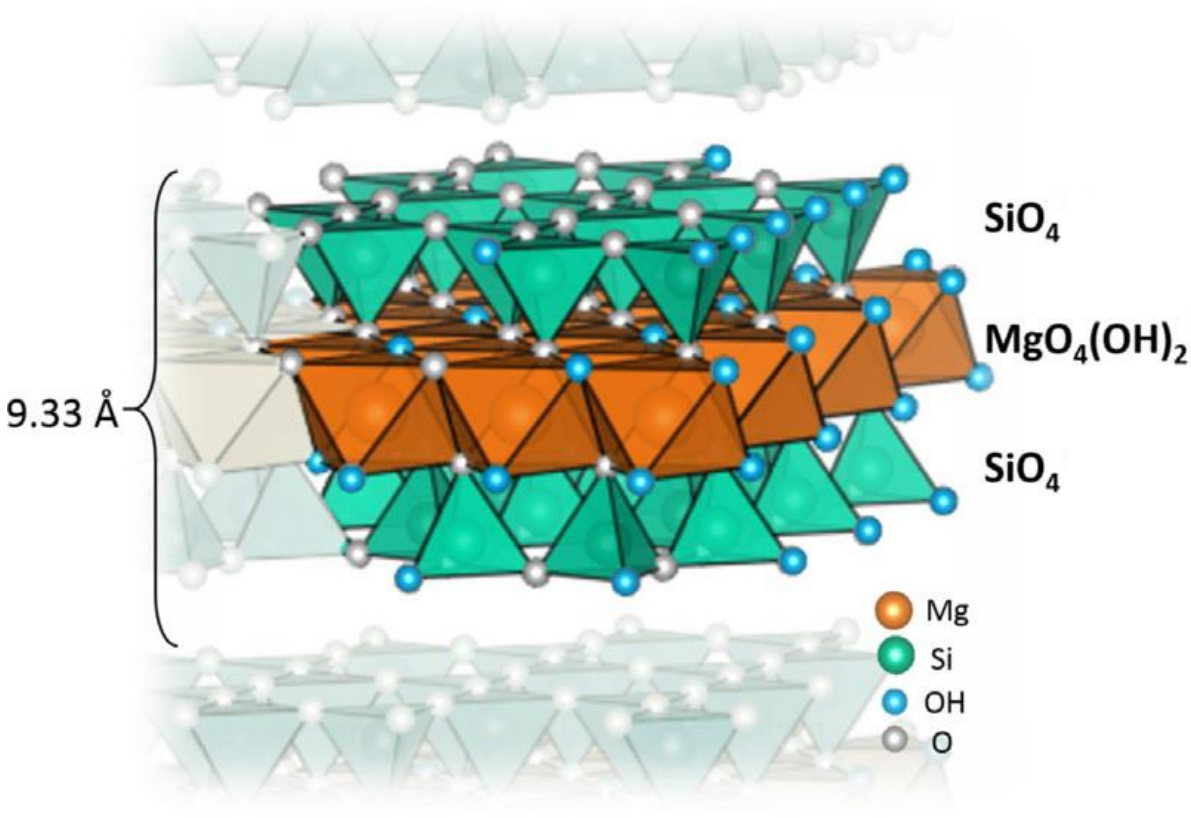

Figura 3.8. Estrutura tridimensional do talco (Adaptado de Claverie, 2018).

O talco se destaca como carga devido a sua estrutura ser no formato de folhas, facilitando seu processamento junto a matriz polimérica. Os silicatos lamelares (filossilicatos) tem uma área superficial elevada, o que facilita a interação carga-matriz polimérica. As superfícies basais das folhas representam 90% da superfície total e não contêm grupos hidroxila ou íons ativos contrários às faces laterais que contêm poucos grupos -SiOH e -MgOH. A superfície lateral, que é mais reativa, apresenta acidez de Brønsted, enquanto a superfície basal do talco, formada por ligações Si-O-Si siloxano, apresenta baixo nível de basicidade de Lewis. Devido à geometria lamelar, a predominância de superfícies basais

hidrofóbicas explica a difícil dispersão do talco natural em meio aquoso (Claverie, 2018). Como carga, o talco é usualmente aplicado em materiais compósitos para por exemplo, aumentar as propriedades mecânicas de diferentes tipos de materiais na indústria de plásticos (Zhao,2012).

O talco por ter uma alta área superficial (diâmetro da partícula / espessura ≈ 20:1) é considerado uma boa carga para matrizes poliméricas. Isso ocorre devido sua estrutura ser em forma de folhas, com dimensões de comprimento e largura na escala micrométrica, com uma espessura na escala manométrica (Castillo, 2013). Porém o talco natural apresenta algumas desvantagens. Especificamente, o talco natural consiste de uma mistura de minerais, sua estrutura apresenta algumas substituições catiônicas e, consequentemente, sua estrutura química, fase cristalina e distribuição do tamanho das partículas não são homogêneas (Yousfi,2013).

Dentro deste contexto, os talcos sintéticos com uma estrutura bem definida e um alto grau de pureza surgem como uma nova plataforma para a produção de materiais com diferentes funcionalidades voltados a diferentes aplicações. Nas últimas décadas, os processos de síntese dos talcos sintéticos vêm sendo estudados, atualizados e aprimorados como bem descrito por Claverie et. al. (2018).

As principais vantagens do talco sintético frente ao mineral de talco natural é sua homogeneidade, sua estrutura química bem definida e a possibilidade do controle de tamanho das partículas e da espessura das lamelas. A variação de alguns graus Celsius na temperatura da reação hidrotérmica faz com que o tamanho médio das partículas varie em algumas centenas de nanômetros (Yousfi, 2013). Tipicamente, as propriedades físicas resultantes de nanocompósitos poliméricos contendo partículas de talco sintético de tamanho nanométrico são superiores às que contêm partículas de talco de tamanho micrométrico (Chabrol, 2010; Fiorentino, 2015). Portanto, um talco sintetizado com uma composição bem definida, tamanhos de partículas regulares é de grande interesse científico e prático, tendo em vista sua aplicação como carga em nanocompósitos poliméricos. Além disso, uma vantagem dos talcos sintéticos é a possibilidade de se obtê-lo em forma de uma suspensão aquosa (em gel) diretamente do reator de síntese. Por conseguinte, as partículas contidas no gel são mais estáveis (Yousfi, 2013).

3.5. Nanocompósitos poliméricos x talcos sintéticos.

Nos últimos anos, muitos artigos vêm sendo publicados a respeito de nanocompósitos poliméricos utilizando talcos sintéticos como carga.

Fiorentino et al. (2015) investigaram a influência do nanotalco sintético como agente nucleante e seu grau de dispersão em uma matriz de polipropileno (PP). O nanotalco sintético também foi funcionalizado com organosilanos buscando uma melhor interação entre a carga e a matriz. Além disso, um compatibilizante foi utilizado para melhorar a incorporação de nanotalco sintético. Em ambos os casos observou-se um aumento da estabilidade térmica, destacando-se uma melhor dispersão das amostras funcionalizadas com organosilanos.

O uso de nanotalcos sintéticos também foi estudado por Yousfi et al. (2013) em uma matriz não polar de PP e em uma matriz de poliamida polar (PA6) para avaliar sua contribuição nas propriedades mecânicas e térmicas do compósito. A estabilidade térmica dos sistemas PP preenchidos com nanotalco sintético foi aprimorada e uma melhor dutilidade foi observada. Nos materiais de PA6, foi possível observar uma boa dispersão do nanotalco sintético e um aumento significativo no módulo de Young. Os autores atribuíram esses fenômenos à alta afinidade entre o talco sintético hidrofílico e a matriz PA6 polar.

Além disso, novos nanotalcos sintéticos e um talco natural comercial foram escolhidos para estabelecer um estudo comparativo em termos de suas contribuições na melhoria da morfologia, bem como nas propriedades finais das blendas de PP/PA6 preparadas pelo processo de mistura física por fusão (extrusão). Em ambos os casos, a adição de cargas de talco induziu uma diminuição significativa do tamanho dos domínios de PA6, mas a compatibilização foi melhorada na presença dos nanotalcos sintéticos. Neste trabalho, destacou-se que

os nanotalcos sintéticos favoreceram melhorias na cinética de cristalização e na morfologia final. Também foi relatada uma melhor dispersão quando se utilizou os nanotalcos sintéticos em comparação ao talco natural. Esta melhor dispersão levou a obtenção de melhores propriedades térmicas e mecânicas (+ 40% no modulo de Young) das blendas PP/PA6 (Yousfi, 2014).

Os autores também utilizaram líquidos iônicos à temperatura ambiente como compatibilizadores de blendas PP/PA6/talcos sintéticos. O nanotalco foi funcionalizado com dois tipos de líquidos iônicos baseados em cátions de fosfônio. Eles observaram um aumento tanto das propriedades térmicas do PP/PA6/talco sintético (+ 80 °C) quanto das propriedades mecânicas. Eles demonstraram uma boa interação entre os líquidos iônicos e os talcos sintéticos (Yousfi, 2015).

Em seu estudo, Beuguel et al. (2015) inseriu talco sintético em matrizes PA6 e PA12, analisando as propriedades reológicas e estruturais dos nanocompósitos. Os resultados mostram que o talco sintético foi melhor disperso na matriz PA6 do que na matriz PA12 (devido à polaridade da matriz). Outro estudo, no entanto, comparou o talco sintético com a argila montmorilonita quando disperso na matriz PA12, mostrando que os talcos sintéticos são uma alternativa as argilas comerciais uma vez que os talcos sintéticos apresentam uma estrutura principalmente nanométrica (Beuguel, 2017).

Prado et al. (Prado, 2015) focaram no uso de talco sintético de Níquel (Ni) como carga na preparação de nanocompósitos de PU por meio da polimerização *in situ*. Os nanocompósitos de PU apresentaram uma coloração verde homogênea, o que corrobora com uma boa dispersão das partículas de Ni-talco sintético. Esta dispersão significativa pode ser explicada pelas interações dos grupos OH do Ni-talco sintético com o grupo uretano da matriz polimérica. Os nanocompósitos de PU/Ni-talco sintético também apresentaram um aumento na estabilidade térmica e na temperatura de cristalização em comparação aos compósitos PU/talco natural e com o PU puro.

L.M dos Santos et al. (L.M dos Santos, 2015) utilizaram um novo nanotalco-Fe_3O_4 como carga para a produção de nanocompósitos poliméricos magnéticos. Os

nanocompósitos apresentaram uma boa dispersão do nanotalco-Fe_3O_4 dentro da matriz de PU, mesmo com alto teor de carga de 10%. Foi demonstrado que é possível obter nanocompósitos magnéticos, levando a produção materiais com propriedades superiores com uma maior temperatura de cristalização e estabilidade térmica.

Também foi relatado por L.M dos Santos et.al. (L.M dos Santos, 2017) a síntese de nanocompósitos com dispersões aquosas de poliuretano utilizando nanotalco-Fe_3O_4 em gel. Esta carga apresenta numerosos grupos (Si-O e Mg-O) e grupos OH que formam facilmente ligações de hidrogênio e apresentam uma interação polar com água pelo seu caráter hidrofílico, consequentemente, melhorando sua dispersão dentro de uma matriz polimérica à base de água. O nanotalco-Fe_3O_4 pode ser disperso mesmo quando usadas grandes quantidades de carga. O uso de talco sintético Fe_3O_4 para obtenção de nanocompósitos magnéticos resultou em materiais com propriedades mecânicas superiores.

Dias et.al. (Dias, 2015) sintetizaram e caracterizaram nanocompósitos de poliuretano utilizando dois talcos sintéticos distintos produzidos com condições hidrotérmicas de processamento diferentes (talco 7h/315 °C e talco 24h/205°C) por meio da polimerização *in situ*. Ambas cargas foram bem dispersas/esfoliadas na matriz polimérica. A alta área superficial dos talcos sintéticos favoreceu no aumento das temperaturas de cristalização e nas estabilidades térmicas. O talco sintético (talco 7h/315 °C) com menor tamanho de partícula mostrou um maior aumento das propriedades mecânicas quando comparado ao outro talco sintético e ao PU puro. Os resultados demonstraram ser possível obter nanocompósitos PU/talco sintético com propriedades desejadas.

Dias et. al. (Dias, 2016) também publicou um estudo comparando a síntese de nanocompósitos de PU, pela técnica de polimerização *in situ*, utilizando diferentes talcos sintéticos como carga inorgânica. As cargas foram sintetizadas a partir de dois tratamentos hidrotérmicos e com composições diferentes (talco-Mg e talco-Ni). Quando o talco-Ni foi utilizado como carga, o nanocompósito resultante apresentou uma morfologia intercalada, enquanto o talco-Mg apresentou uma morfologia esfoliada dentro da matriz de poliuretano. Ambas as cargas aumentaram

as propriedades térmicas do polímero e as temperaturas de cristalização, mas o nanocompósito esfoliado proporcionou maior estabilidade térmica.

4. MATERIAIS, MÉTODOS E RESULTADOS

Neste capítulo serão apresentados os materiais, métodos e resultados já publicados em revistas internacionais e que irão compor essa seção da tese.

Primeiramente, serão apresentados os resultados referentes a produção de nanocompósitos de dispersões aquosas de poliuretano (DPU) utilizando talcos sintéticos com diferentes condições de tratamento hidrotérmico em forma de gel.

A segunda parte é composta pelos resultados referentes a obtenção de nanocompósitos de poliuretano base solvente usando talcos sintéticos fluorescentes com diferentes tratamentos hidrotérmicos comparados frente a um talco natural fluorescente.

A terceira parte mostra resultados obtidos quando se utilizou uma mistura de cargas (talco + argila) para obtenção de nanocompósitos de poliuretano híbridos.

A quarta parte mostra a síntese e caracterização dos talcos sintéticos realizadas durante o período de doutorado sanduíche no laboratório GET em Toulouse, França. Os nanocompósitos serão produzidos através da polimerização *in situ*, utilizando os talcos sintéticos como catalisador e como reforço da matriz polimérica.

4.1. Análise da influência de três talcos sintéticos diferentes na obtenção de nanocompósitos de dispersões aquosas de poliuretano

No artigo intitulado "*Analyzing the influence of different synthetic talcs in waterborne polyurethane nanocomposites obtainment*", publicado na revista "Journal of Applied Polymer Science" é apresentada a mistura física de três talcos sintéticos na forma de gel obtidos em três condições de tratamento hidrotérmico para obtenção de nanocompósitos de dispersões aquosas de poliuretano a fim de melhorar suas propriedades mecânicas, térmicas e morfológicas entre si e frente ao polímero puro. Os nanocompósitos foram caracterizados por BET, FTIR, DRX, TEM, AFM, DMTA, TGA e MEV-FEG. Os talcos sintéticos apresentaram uma boa dispersão na matriz polimérica, mesmo o processo sendo por mistura física. As propriedades mecânicas dos nanocompósitos tiveram um aumento com a adição dos talcos sintéticos na forma de gel. A alta área superficial das cargas pode ter influenciado na boa interação observada entre carga-polímero, corroborando com os resultados dos módulos de armazenamento e perda e de infravermelho. Foi demonstrado que a utilização de talcos sintéticos em forma de gel surge como uma forma de se obter nanocompósitos de dispersões aquosas de poliuretano com propriedades mecânicas superiores via mistura física.

JOURNAL OF Applied Polymer SCIENCE

Analyzing the influence of different synthetic talcs in waterborne polyurethane nanocomposites obtainment

Guilherme Dias,[1] Manoela Prado,[1] Christophe Le Roux,[2] Mathilde Poirier,[2] Pierre Micoud,[2] Rosane Ligabue,[1,3] François Martin,[2] Sandra Einloft [1,3]

[1]Programa de Pós-Graduação em Engenharia e Tecnologia de Materiais (PGETEMA), Pontifícia Universidade Católica do Rio Grande do Sul (PUCRS), Porto Alegre, Brazil

[2]ERT 1074 géomatériaux, GET UMR 5563 CNRS, Université de Toulouse, Toulouse, France

[3]Faculdade de Química (FAQUI), Pontifícia Universidade Católica do Rio Grande do Sul (PUCRS), Porto Alegre, Brazil

Correspondence to: S. Einloft (E-mail: einloft@pucrs.br)

ABSTRACT: Waterborne polyurethane (WPU) nanocomposites were produced utilizing synthetic talc in gel form in order to improve its physical–chemical properties. Synthetic talc manufactured in nano-gel form are interesting because their interaction with water occurs through hydrogen bonding favoring fillers dispersion within the WPU matrix. WPUs are environmental friendly materials because no organic solvents are used in its production. The nanocomposites obtained with the three synthetic talc nano-gel fillers presented a good dispersion even when higher amounts of fillers were added, as seen by X-ray diffraction, transmission electron microscopy, field emission scanning electron microscopy, and atomic force microscopy analyses. The addition of synthetic talcs improved WPU nanocomposites mechanical properties. Storage and loss modulus results proved fillers incorporation into the WPU matrix corroborating with Fourier transform infrared spectroscopy results. Results demonstrated that synthetic talcs in nano-gel form are interesting to obtain WPU nanocomposites with superior mechanical properties. © 2017 Wiley Periodicals, Inc. J. Appl. Polym. Sci. **2018**, *135*, 46107.

KEYWORDS: mechanical properties; nanoparticles; nanowires; nanocrystals; polyurethane

Received 14 August 2017; accepted 23 November 2017

DOI: 10.1002/app.46107

INTRODUCTION

Waterborne polyurethanes (WPU) are known for their wide range of applications such as flexible films, coatings, and medical applications.[1,2] When compared to traditional solvent-based polyurethanes, WPU are environmental friendly materials. The use of water as solvent attend to environmental requirements limiting the quantity of volatile organic components released to the environment.[2,3] Nevertheless, WPU have some disadvantages as low thermal–mechanical properties, low adhesion, low drying rate, and so on.[2,4,5] The incorporation of inorganic particles in the WPU matrix is a solution to improve its physical–chemical properties.[5,6] Organic–inorganic nanocomposites have been widely discussed,[7] improvements promoted by nanofillers are frequently associated to their concentration, shape, size, degree of aggregation, surface area, degree of dispersion, and the interaction between nanofiller/polymer.[8] Dispersed nanofillers improve physical/chemical properties of nanocomposites such as mechanical strength, conductivity, thermal stability, and optical properties.[9] Literature describes that different fillers have been introduced into WPU such as silver nanoparticles,[1,17] halloysite nanotubes,[2] metallic oxides,[4,9,10,13] graphene,[5] silica,[6,15] nanoclays,[7,8,11,12,18,19] nano-Fe_3O_4,[14] and cellulose nanocrystals.[16] Talc is also a good alternative due to its low cost and availability. Natural talc presents some disadvantages namely mineralogical and crystallochemical impurities, hydrophobicity, and the impossibility of being ground to nano-sizes.[20–22] Synthetic talc can be produced in a form of a hydrophilic nano-gel suspension since it presents numerous edges (Si—O and Mg—O) and OH groups forming hydrogen bonds and polar interaction with water.[23] The filler in a gel form improves its dispersion within WPU matrix.[23] The usage of synthetic talc as nanofillers has been reported to obtain new materials such as solvent-borne polyurethanes,[22,24–26] polypropylene (PP), and polyamide 6 (PA6) nanocomposites,[21] PP/PA6 blends,[27] and also WPU.[28] The main objective of this work is to obtain and characterize new WPU/synthetic talcs nanocomposites produced by physical mixture. Three synthetic nano-gel talcs were used as fillers aiming to compare the talc syntheses conditions effects with the WPU matrix properties.

Additional Supporting Information may be found in the online version of this article.

EXPERIMENTAL

Synthetic Talc Syntheses

Synthetic talcs were prepared as described in literature.[20,29] D43001 10,4% dry extract (synthetic talc heated at 300 °C for 1 h), D43006 8.7% dry extract (synthetic talc heated at 300 °C for 6 h) and Prototalc (PT) (Mg100, 25 °C for 30 min) 16.4% dry extract, all samples were used in gel form without any functionalization.

Materials

To synthesize WPU, isophorone diisocyanate (IPDI, for synthesis, Bayer, Germany), polyester diol ($M_n = 1000$ g/mol) and 2,2-bis(hydromethyl) propionic acid (DMPA, 99%, Perstorp, Sweden) were used. Dibutyl tin dilaurate [DBTDL Miracema-Nuodex Ind., Brazil (0.1% w/w)] was used as catalyst. The NCO/OH molar ratio of 1.7 was utilized. DMPA carboxylic acid was neutralized with trimethylamine (J.T Baker, Center Valley, Pennsylvania, USA). The free NCO content was measured by titration with *n*-dibutylamine (Bayer, Leverkusen, Germany) and hydrazine (Merck, Kenilworth, New Jersey, USA) was used as chain extender.

WPU Nanocomposites Syntheses

The WPU syntheses were performed in a glass reactor utilizing the following reagents: IPDI, a polyester diol ($M_n = 1000$ g/mol) and DMPA (NCO/OH molar ratio of 1.7:5% w/w of DMPA in relation to the prepolymer solids content). The NCO terminated prepolymer reaction was carried out under constant mechanical stirring and inert atmosphere (N_2) at 80 °C for 1 h. To quantify the residual free isocyanate content, titrations were performed with *n*-dibutylamine based on the ASTM 2572 standard technique. Then, to neutralize the acid groups from DMPA, molar equivalent of trimethylamine was added to the reactor and stirred for 30 min at 50 °C. Lastly, a mixture of the previously neutralized prepolymer and hydrazine (chain extender in amount equivalent to the residual free NCO content) was poured in water and kept under mild agitation (200 rpm) at room temperature for 30 min. After that, synthetic talc filler were mixed with pristine WPU under mild agitation for 30 min, regarding the total mass of non-volatile, to form the WPU/nanocomposites. Filler contents were of 1, 3, 5, and 10% w/w. The average solids content for the WPU and WPU nanocomposites was 33% w/w.

Characterization Methods

WPU nanocomposites and neat WPU characterizations were performed using dried films, samples of these films were analyzed by: nitrogen adsorption–desorption isotherms determined at 77 K, using a volumetric method, with a Quantachrome Autosorb-1 apparatus (GET laboratory, University of Toulouse). The isotherms were recorded in the 0.05–0.3 relative pressure range and high purity nitrogen was used. Samples were outgassed for 15 h at 120 °C under vacuum before analysis. Surface areas were calculated using a Brunauer–Emmett–Teller (BET) method[30]; Fourier transform infrared spectroscopy (FTIR, PerkinElmer, spectrometer model Spectrum100) from film samples in transmission mode in the range 4000–650 cm^{-1}, was used to ascertain the structural properties of the fillers and nanocomposites; X-ray diffraction (Shimadzu XRD-7000) patterns were recorded with CuKα Bragg–Brentano geometry θ–θ radiations, between 5 and 80° with a step size of 0.02°, current of 40 kV and voltage of 30 mA; transmission electron microscopy (TEM, Tecnai G2 T20 FEI) was used to determine morphology and the degree of dispersion of nanocomposites. The samples were cryomicrotomed and analyzed at 200 KV; differential scanning calorimetry (DSC equipment, Q20 model, TA Instruments) was used to determine the glass transition temperature (T_g) from −90 to 200 °C, with a heating rate of 10 °C/min under an inert atmosphere of nitrogen, from the heat second cycle; Thermogravimetric analysis (SDT equipment, Q600 model, TA Instruments) was carried out with a heating rate of 20 °C/min, from an ambient temperature to 800 °C under nitrogen atmosphere; mechanical tests were performed in triplicate according to ASTM D822 standard technique (DMTA equipment, Q800 model, TA Instruments) for determination of Young's modulus and stress × strain tests. The field emission scanning electron microscopy (FESEM, FEI Inspect F50) analyses were performed in secondary electrons (SE) mode and used for assessment of fillers distribution in the polymer matrix. Atomic force microscopy (AFM) was used to collect roughness data of the WPU and its nanocomposites. The analyses were performed in tapping mode to construct phase/height contrast images at different locations on the top surface of the samples using a Bruker Dimension Icon PT equipped with a TAP150A probe (Bruker, resonance frequency of 150 kHz and 5 N/m^{-1} spring constant). The equipment was calibrated prior to samples measurements. The scanned area of images was 5 × 5 μm^2 with a resolution of 512 frames per area.

RESULTS AND DISCUSSION

BET Analysis

BET tests were performed aiming to compare the influence of different hydrothermal treatments in surface area of synthesized nano-gel talcs. Literature described that specific surface area decreases as synthesis time increased, consequently decreasing the hydroxyl group number on layers edges.[20] D43006 (300 °C; 6 h) and D43001 (300 °C; 1 h) presented specific surface area of 130 and 222 $m^2 g^{-1}$, respectively. Yet, the prototalc (25 °C; 30 min) presented a specific surface area of 214 $m^2 g^{-1}$. This results evidenced that the specific surface area values for synthetic talcs are much higher than for natural talc (20 $m^2 g^{-1}$).[21,29] The possibility of obtaining synthetic fillers with distinct specific surface area offers a platform of possibilities to promote desired changes in physical–chemical properties of WPU nanocomposites adapting it for different applications in coatings or films industry.

FTIR Analysis

Figure 1(A–C) shows the results of FTIR analyses for synthetic nano-gel talcs, WPU nanocomposites with 10% w/w of synthetic talcs and neat WPU. In synthetic talc spectra, the band around 700–600 cm^{-1} is related to the free OH of the talc structure[22,31] and the characteristic band around 1000–900 cm^{-1} is attributed to Si—O and Si—O—Si bond[28,31,32] as can be seen in Figure 1(A.c), (B.c), and (C.c). For neat WPU and nanocomposites [Figure (1A.a–c, B.a–c, and C.a–c)] the bands in regions of 3500–3400 cm^{-1} are attributed to urethane linkage N—H. This spectrum region is affected by polymer/filler interaction [Figure 1(D.a–c, E.a–c, and F.a–c)]. The bonded NH

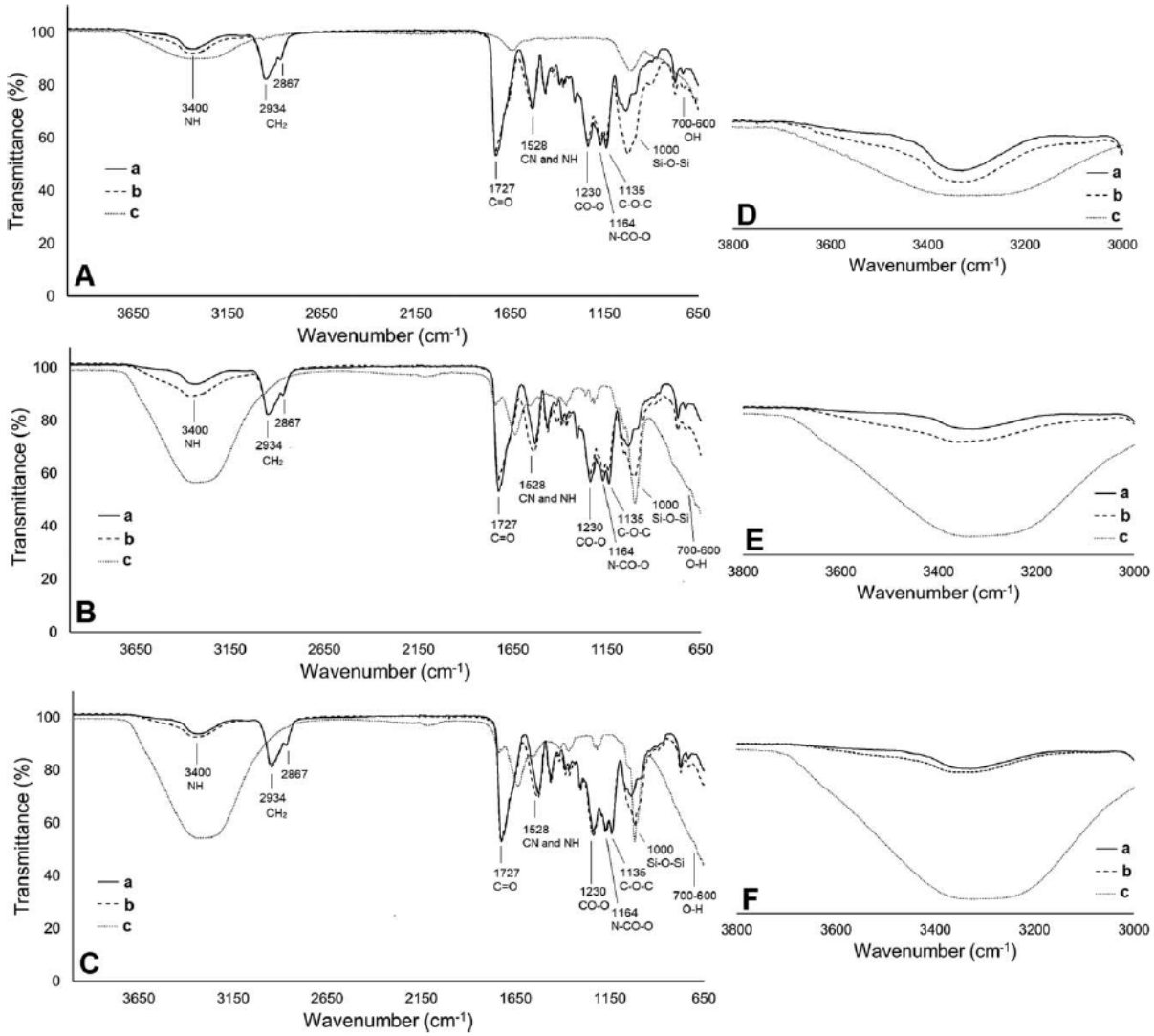

Figure 1. FTIR overlays (A) (a) WPU, (b) WPU/PT 10%, (c) Prototalc (PT). (B) (a) WPU, (b) WPU/D43001 10%, (c) D43001. (C) (a) WPU, (b) WPU/D43006 10%, (c) D43006 and FTIR overlays around 3400 cm^{-1}. (D) (a) WPU, (b) WPU/PT 10%, (c) Prototalc (PT). (E) (a) WPU, (b) WPU/D43001 10%, (c) D43001. (F) (a) WPU, (b) WPU/D43006 10%, (c) D43006.

stretching vibration exhibited a strong absorption peak at ~3400 cm^{-1} due to hydrogen bonding while the free N—H stretching vibration appears at ~3500 cm^{-1}.[33] One can observe from Figure 1(D.a–c, E.a–c, and F.a–c) that with the increasing of synthetic talc concentration the N—H bands shifted to the free N—H region indicating hydrogen bonding between WPU/fillers.[34] The bands in 2934 and 2867 cm^{-1} are associated to different vibrational modes of CH_2 group of polymeric chain. The band in 1727 cm^{-1} is characteristic of C=O of urethane bond. The region in 1528 cm^{-1} is related to CN and NH of the urethane bonds. The CO—O group appears in the region of 1230 cm^{-1}. In 1164 and 1135 cm^{-1} appears the bands associated to N—CO—O and C—O—C groups.[22,24–26,28] It can be highlighted that with the increasing of fillers amount into the matrix the characteristic band around 1000 cm^{-1} attributed to Si—O—Si bonds becomes more prominent, proving fillers incorporation into WPU matrix. Previous works demonstrated similar results.[22,24–26,28]

TEM–XRD Structure Analysis

TEM analyses evidenced the nanoscale dispersion of fillers for WPU nanocomposites as presented in Figure 2. The dark entities that appears in the brighter background of the matrix represent synthetic talc layers; some individual layers appears even at higher fillers content evidencing that some synthetic talc layers are "exfoliated" and some points of agglomeration are presented.[19] Cross-section TEM micrographs (Figure 2) of the WPU nanocomposites demonstrates that talc layers were parallel to the surface of the films and well dispersed in WPU matrix.[35] The different processes used to manufacture the synthetic nanogel talcs modified its structures and influenced fillers distribution into the WPU matrix.

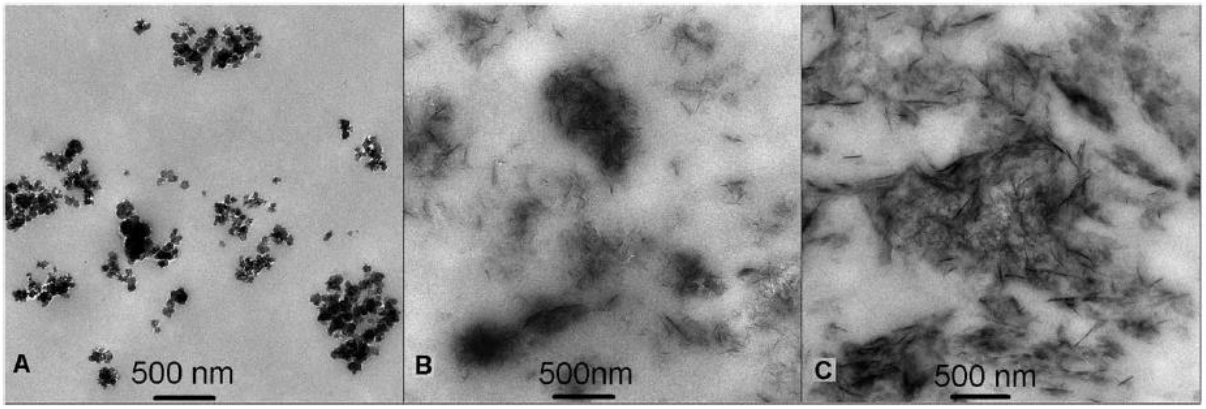

Figure 2. TEM micrographs, magnification of 13,500× (a) WPU/PT 10%, (b) WPU/D43001 10%, and (c) WPU/D43006 10%.

Figure 3 presents crystalline structures of fillers, pristine WPU and its nanocomposites. Fillers characteristic XRD diffraction peaks associated with natural talc are observed, but for synthetic talcs these diffraction peaks are broader and less intense. This behavior indicates that synthetic talc layers are smaller than for natural talc.[20,21] The augmentation in the diffraction peak at $2\theta \cong 9°$ is noticed as the quantity of filler content increases indicating fillers intercalation between WPU chains.[36,37] For neat WPU, a broad diffraction halo related with WPU amorphous phase is seen close $2\theta = 20°$.[38] All the nanocomposites presented the same amorphous nature of neat WPU, but it can be noticed that as synthetic talc content increases, the intensities of diffraction peaks increased as well, indicating that synthetic talc in nanocomposites tended to self-aggregate with an increase in fillers content.[39,40]

Mechanical Properties

Table I presents stress/strain properties of neat WPU and WPU nanocomposites. With a higher content of synthetic talc, Young Modulus, stress, and strain values increased. The nanocomposites do not break at the tests conditions. Hydrogen bonding interaction among fillers/WPU matrix, as evidenced in FTIR section, can be responsible for this behavior.[41] Unlike the others samples the WPU nanocomposite with 3% w/w of synthetic talc D43001 as filler achieved higher values of Young Modulus and stress/strain when compared to 5 and 10% w/w (Figure S1). This improvement in mechanical properties in lower filler concentration can be somehow associated to a good filler dispersion due to filler–polymer interaction alternatively to filler–filler interaction with the increase in fillers content.[22,24] Furthermore, layered silicates as synthetic talcs can improve the elongation at break of the nanomaterials, as reported for WPU/clay nanocomposites by Kuan *et al.*,[35] corroborating with strain results for WPU nanocomposites obtained with synthetic talcs D43001 and D43006. These results corroborate with TEM results and reinforce the fact that dispersion affects nanocomposites mechanical properties.[24]

The storage modulus, loss modulus and tan δ of the WPU nanocomposites films with different synthetic talcs and neat WPU as a function of temperature are shown in Figure 4. The

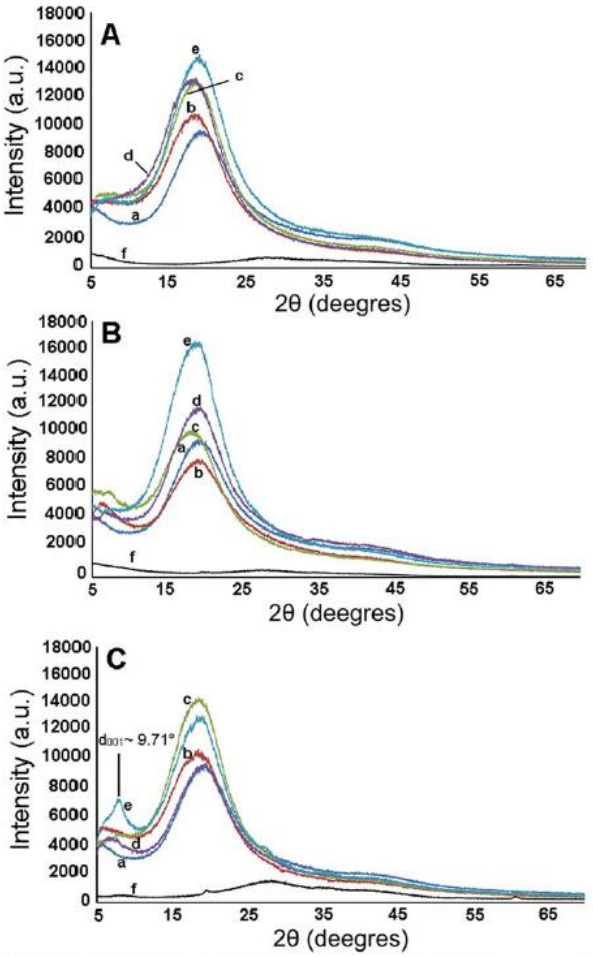

Figure 3. XRD diffractograms. (A) (a) WPU, (b) WPU/PT 1%, (c) WPU/PT 3%, (d) WPU/PT 5%, (e) WPU/PT 10%, and (f) Prototalc (PT). (B) (a) WPU, (b) WPU/D43001 1%, (c) WPU/D43001 3%, (d) WPU/D43001 5%, (e) WPU/D43001 10%, and (f) D43001. (C) (a) WPU, (b) WPU/D43006 1%, (c) WPU/D43006 3%, (d) WPU/D43006 5%, (e) WPU/D43006 10%, and (f) D43006. [Color figure can be viewed at wileyonlinelibrary.com]

Table I. Mechanical Properties of the Nanocomposites and Neat WPU

Sample	Young modulus (MPa)	Stress (MPa)	Strain (%)
WPU	58 ± 0.9	10 ± 0.6	137 ± 12.6
WPU/PT 1%	44 ± 0.5	7 ± 0.2	126 ± 4.8
WPU/PT 3%	57 ± 1.5	9.5 ± 0.1	128 ± 3.8
WPU/PT 5%	58 ± 0.9	10 ± 0.6	137 ± 12.6
WPU/PT 10%	126 ± 12.1	13 ± 2.5	128 ± 18.9
WPU/D43001 1%	91 ± 7	11 ± 0.6	144 ± 6.4
WPU/D43001 3%	138 ± 9.6	16 ± 1.6	146 ± 3.3
WPU/D43001 5%	93 ± 6.5	12 ± 0.2	150 ± 0.5
WPU/D43001 10%	73 ± 1.1	10 ± 0.2	134 ± 8
WPU/D43006 1%	89 ± 3.8	10 ± 0.8	139 ± 17.9
WPU/D43006 3%	89 ± 1.7	10 ± 0.2	138 ± 18.7
WPU/D43006 5%	105 ± 16.7	11 ± 0.8	142 ± 14.3
WPU/D43006 10%	109 ± 11.9	9 ± 1.1	154 ± 10.6

Table II. TGA and DSC Analyses Results for Pristine WPU and its Nanocomposites

Samples	T_{onset} (°C)	$T_{peakmax}$ (°C)	$T_{g\text{-}DSC}$ (°C)
WPU	325	348	−33.0
WPU/PT 1%	332	350	−33.7
WPU/PT 3%	325	347	−34.6
WPU/PT 5%	325	344	−33.5
WPU/PT 10%	323	339	−34.1
WPU/D43001 1%	324	344	−32.9
WPU/D43001 3%	318	340	−33.2
WPU/D43001 5%	309	338	−33.0
WPU/D4300110%	305	329	−33.7
WPU/D43006 1%	328	352	−32.1
WPU/D43006 3%	314	337	−33.9
WPU/D43006 5%	311	340	−32.8
WPU/D4300610%	307	330	−34.0

value of the storage modulus [Figure 4 (A,D,G)] of the nanocomposites films increased significantly upon filler addition as compared to the neat WPU proving fillers incorporation into the WPU matrix and a strong interaction between filler/polymer,[42] comparing neat WPU (1020 MPa), WPU/PT 10% (2892 MPa), WPU/D43001 10% (4560 MPa), and WPU/D43006 10% (3930 MPa). The nanocomposites capability to maintain higher modulus values even at temperatures above T_g is an advantage, dos Santos *et al.*[28] noticed the same behavior for WPU/Fe_3O_4-synthetic talc composites. T_g was provided by the tan δ maximum values.[43] Tan δ curves [Figure 4(C,F,I)] intensity tended to decrease with D43001 and D43006 fillers addition, probably because synthetic talcs fillers restricted the mobility of the WPU chains.[44] From the loss modulus curves [Figure 4-(B,E,H)], a transition peak can be noticed and the temperature at the peak is assigned as the T_g of the soft segments of WPU matrix.[45] The

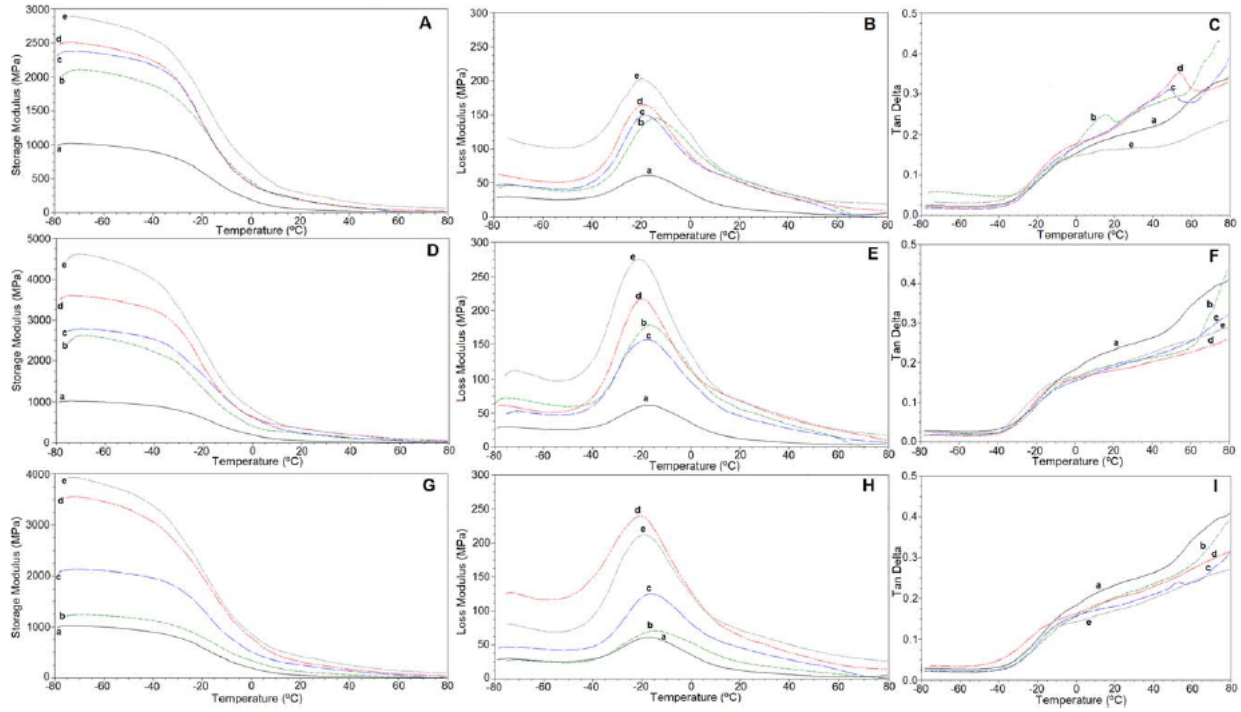

Figure 4. Storage modulus, loss modulus, and tan delta of the nanocomposites and neat WPU films. (A–C) (a) WPU, (b) WPU/PT 1%, (c) WPU/PT 3%, (d) WPU/PT 5%, and (e) WPU/PT 10%. (D–F) (a) WPU, (b) WPU/D43001 1%, (c) WPU/D43001 3%, (d) WPU/D43001 5%, and (e) WPU/D43001 10%. (G–I) (a) WPU, (b) WPU/D43006 1%, (c) WPU/D43006 3%, (d) WPU/D43006 5%, and (e) WPU/D43006 10%. [Color figure can be viewed at wileyonlinelibrary.com]

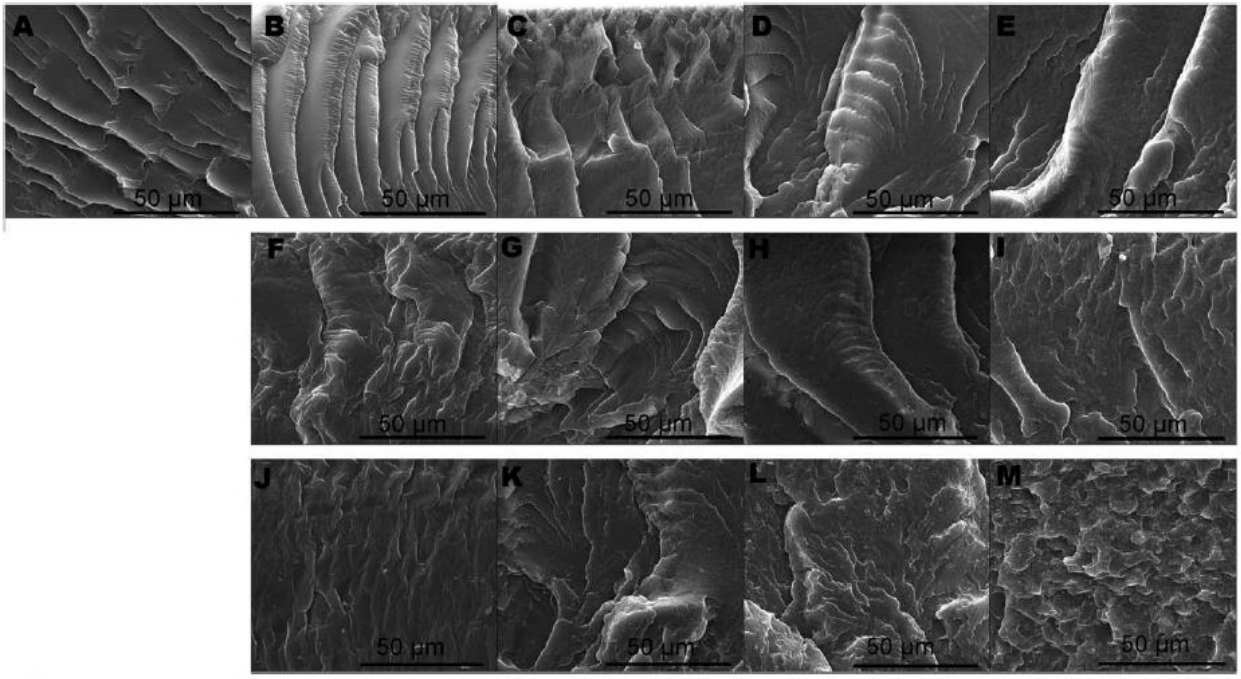

Figure 5. Micrographs from cryogenically fractures of the materials at magnification of 3000×, mode SE, (a) WPU, (b) WPU/PT 1%, (c) WPU/PT 3%, (d) WPU/PT 5%, (e) WPU/PT 10%, (f) WPU/D43001 1%, (g) WPU/D43001 3%, (h) WPU/D43001 5%, (i) WPU/D43001 10%, (j) WPU/D43006 1%, (k) WPU/D43006 3%, (l) WPU/D43006 5%, and (m) WPU/D43006 10%.

loss modulus and T_g augmentation (neat WPU: 61.2 MPa at −17.3 °C; WPU/PT10%: 203.3 MPa at −20.2 °C; WPU/D43001 10%: 275.1 MPa at −20.8 °C; and WPU/D43006 10%: 211.5 MPa at −19.9 °C) are related with the incorporation of the fillers into the polymeric matrix which is attributed to the confinement of the intercalated polymer chains into the fillers layers, which corroborates with XRD and TEM results. Moreover, the enlargement in the T_g peak can be related to the

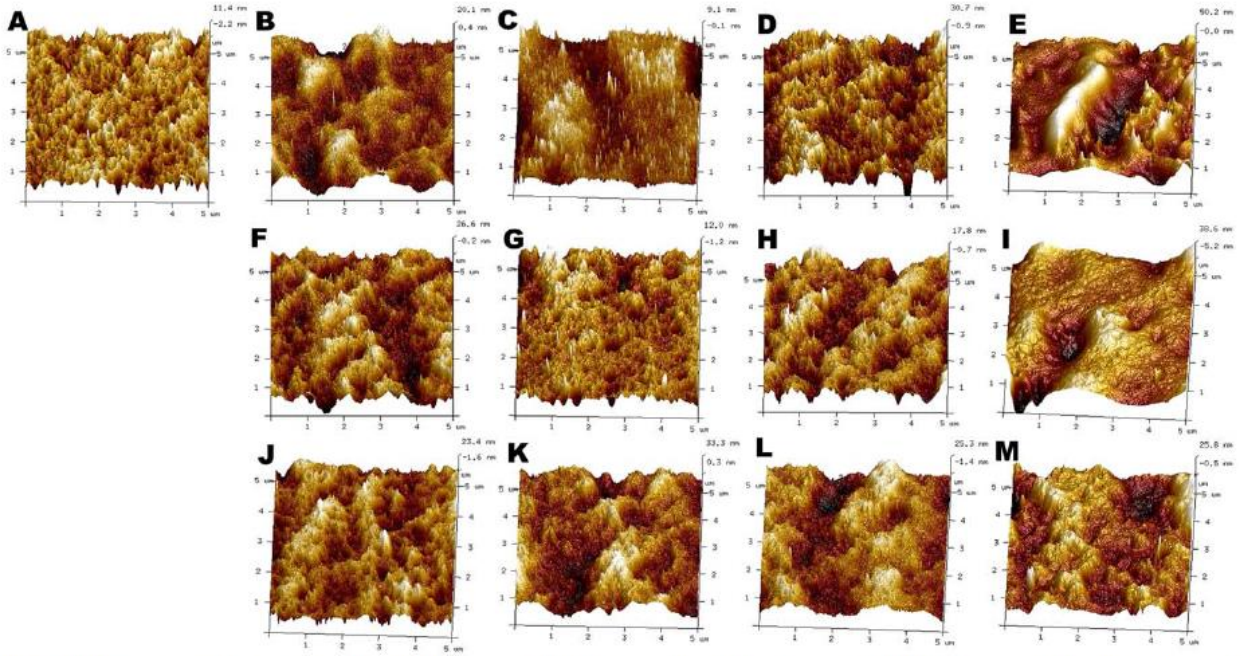

Figure 6. AFM images (height). (a) WPU, (b) WPU/PT 1%, (c) WPU/PT 3%, (d) WPU/PT 5%, (e) WPU/PT 10%, (f) WPU/D43001 1%, (g) WPU/D43001 3%, (h) WPU/D43001 5%, (i) WPU/D43001 10%, (j) WPU/D43006 1%, (k) WPU/D43006 3%, (l) WPU/D43006 5%, and (m) WPU/D43006 10%. [Color figure can be viewed at wileyonlinelibrary.com]

Table III. AFM Results: Average Roughness (R_a), Root Mean Square Roughness (R_q), and Maximum Height Roughness (R_{max}) of Neat WPU and its Nanocomposites

Sample	R_a (nm)	R_q (nm)	R_{max} (nm)
WPU	2.3	3.2	38.3
WPU/PT 1%	4.3	5.4	42.4
WPU/PT 3%	5.6	7.0	57.1
WPU/PT 5%	7.5	9.4	94.6
WPU/PT 10%	11.9	16.0	98.3
WPU/D43001 1%	6.5	8.1	53.9
WPU/D43001 3%	6.2	7.8	70.5
WPU/D43001 5%	6.4	8.6	195.0
WPU/D43001 10%	8.0	11.8	176.0
WPU/D43006 1%	5.5	6.9	54.7
WPU/D43006 3%	7.5	9.5	75.1
WPU/D43006 5%	6.2	7.8	51.4
WPU/D43006 10%	5.9	7.5	71.9

motion of the polymer chains at the polymer-filler matrix interface.

Thermal Properties (TGA–DSC)

Table II and Figure S2 presents thermogravimetric analysis values and DSC analyses results for neat WPU and nanocomposites films. It can be highlighted that the first stage of initial weight loss is related to the removal of residual water (Figure S2).[46] Two-step weight loss was observed for all samples, thermal decomposition temperature range in first step was between 305 and 325 °C and thermal decomposition temperature range in second step was between 390 and 420 °C, associated to the earlier decomposition of the hard segment and the later decomposition of the soft segment, respectively.[7,14] It could be observed that initial degradation temperature of the nanocomposites decreased with the addition of synthetic talcs, this result indicates that nanocomposites decompose at lower temperatures than neat WPU matrix; same results were described for WPU/ZnO composites.[47] The available hydroxyl groups located at fillers layers edges interaction with the WPU hard segments can result in a deleterious effect on the nanocomposites thermal stability, breaking urethane and urea bonds of the hard segments as described for WPU/halloysite nanotubes nanocomposites.[2] DSC analyses showed no significant changes on the glass transition temperature (T_g) with values varying from −33 to −34 °C for the neat WPU and the nanocomposites.

FESEM

Figure 5 shows the FESEM micrographs of the neat WPU and WPU nanocomposites having 1, 3, 5, and 10% w/w of synthetic talc fillers. All samples showed deeper and longer cracks because of brittle fractures in the liquid nitrogen but, compared with neat WPU [Figure 5(a)], WPU nanocomposites [Figure 5(b–m)] samples presented rougher fractured surfaces.[2] A homogeneous distribution of the fillers into the polymeric matrix was observed without agglomeration points in all nanocomposites, implying that the miscibility between the synthetic talcs and the polymer matrix is good. Uniform distribution of the fillers in the WPU matrix played an important role in improving the mechanical performance of the resulting nanocomposite films as discussed.[7,14]

AFM

Figure 6 shows the three-dimensional height AFM topographic images and Table III shows the average roughness (R_a), root mean square roughness (R_q), and maximum height roughness (R_{max}) for neat WPU and its nanocomposites measured by AFM in tapping mode. In WPU matrix, dark regions are associated with amorphous domains (soft segments) and bright regions are associated with crystalline domains (hard segments).[16] The results of R_a, R_q, and R_{max} demonstrates that with fillers addition the surface roughness of the nanocomposites increased, indicating the fillers influence on the surface morphology of the systems. As seen in Figure 6, with the addition of fillers on the nanocomposites the rugged domains come more prominent evidencing the interactions between filler/polymer probably by hydrogen bonding among fillers and hard segments of the WPU.[6,11] This interactions corroborates the mechanical properties improvements in nanocomposites once compared to pristine WPU.

CONCLUSIONS

WPU nanocomposites were prepared by physical mixture in order to obtain new environmental friendly materials with superior mechanical properties. Synthetic talcs specific surface area influenced the final WPU nanocomposites properties. XRD, TEM, FESEM, and AFM analyses indicated that synthetic talc fillers are well dispersed into the polymer matrix. Storage modulus and loss modulus improvement proved the good fillers incorporation into the WPU matrix. The compatibility of synthetic talcs in nano-gel form with WPU is related to the interaction with water occurring through hydrogen bonding. This interactions favor fillers dispersion within the WPU matrix. Yet, the distinct fillers synthesis conditions resulting in different specific surface areas provides an interesting platform to obtain WPU nanocomposites with a range of possible mechanical and thermal properties. These newly developed synthetic talc-WPU system can found potential application niches in coatings and flexible films industry.

ACKNOWLEDGMENTS

The authors would like to thank CAPES and CNPq for doctorate, post-doc, and research scholarship.

REFERENCES

1. El-Sayed, A. A.; Salama, M.; Salem, T.; Rehan, M. *Indian J. Sci. Technol.* **2016**, *9*. DOI: 10.17485/ijst/2016/v9i17/87216.
2. Wu, Y.; Du, Z.; Wang, H.; Cheng, X. *J. Appl. Polym. Sci.* **2016**, *133*, DOI: 10.1002/app.43949.
3. Wang, H.; Zhou, Y.; He, M.; Dai, Z. *Colloid Polym. Sci.* **2015**, *293*, 875.
4. Gao, X.; Zhu, Y.; Zhou, S.; Gao, W.; Wang, Z.; Zhou, B. *Colloids Surf. A Physicochem. Eng. Asp.* **2011**, *377*, 312.
5. Kim, Y. J.; Kim, B. K. *Colloid Polym. Sci.* **2014**, *292*, 51.

6. Han, Y.; Chen, Z.; Dong, W.; Xin, Z. *High Perform. Polym.* **2015**, *27*, 824.
7. Peng, L.; Zhou, L.; Li, Y.; Pan, F.; Zhang, S. *Compos. Sci. Technol.* **2011**, *71*, 1280.
8. Romo-Uribe, A.; Santiago-Santiago, K.; Zavala-Padilla, G.; Reyes-Mayer, A.; Calixto-Rodriguez, M.; Arcos-Casarrubias, J. A.; Baghdachi, J. *Prog. Org. Coat.* **2016**, *101*, 59.
9. Christopher, G.; Kulandainathan, M. A.; Harichandran, G. *J. Coat. Technol. Res.* **2015**, *12*, 657.
10. Soares, R. R.; Carone, C.; Einloft, S.; Ligabue, R.; Monteiro, W. F. *Polym. Bull.* **2014**, *71*, 829.
11. Kuan, H. C.; Chuang, W. P.; Ma, C. C. M.; Chiang, C. L.; Wu, H. L. *J. Mater. Sci.* **2005**, *40*, 179.
12. Ayres, E.; Oréfice, R. L. *Polím.: Ciên. Tecnol.* **2007**, *17*, 339.
13. Wu, D. M.; Qiu, F. X.; Xu, H. P.; Yang, D. Y. *Plast. Rubber Compos.* **2011**, *40*, 449.
14. Zhang, S.; Li, Y.; Peng, L.; Li, Q.; Chen, S.; Hou, K. *Compos. Part A Appl. Sci. Manuf.* **2013**, *55*, 94.
15. Heck, C. A.; dos Santos, J. H. Z.; Wolf, C. R. *Int. J. Adhes. Adhes.* **2015**, *58*, 13.
16. Santamaria-Echart, A.; Ugarte, L.; García-Astrain, C.; Arbelaiz, A.; Corcuera, M. A.; Eceiza, A. *Carbohydr. Polym.* **2016**, *151*, 1203.
17. Hsu, S. H.; Tseng, H. J.; Lin, Y. C. *Biomaterials* **2010**, *31*, 6796.
18. Barboza, E. M.; Delpech, M. C.; Garcia, M. E. F.; Pimenta, F. D. *Polymer* **2014**, *24*, 94.
19. Stratigaki, M.; Choudalakis, G.; Gotsis, A. D. *J. Coat. Technol. Res.* **2014**, *11*, 899.
20. Dumas, A.; Martin, F.; Le Roux, C.; Micoud, P.; Petit, S.; Ferrage, E.; Brendlé, J.; Grauby, O.; Greenhill-Hooper, M. *Phys. Chem. Miner.* **2013**, *40*, 361.
21. Yousfi, M.; Livi, S.; Dumas, A.; Le Roux, C.; Crépin-Leblond, J.; Greenhill-Hooper, M.; Duchet-Rumeau, J. *J. Colloid Inter. Sci.* **2013**, *403*, 29.
22. dos Santos, L. M.; Ligabue, R.; Dumas, A.; Le Roux, C.; Micoud, P.; Meunier, J. F.; Martin, F.; Einloft, S. *Eur. Polym. J.* **2015**, *69*, 38.
23. Dumas, A.; Claverie, M.; Slostowski, C.; Aubert, G.; Careme, C.; Le Roux, C.; Micoud, P.; Martin, F.; Aymonier, C. *Angew. Chem.* **2016**, *128*, 10022.
24. Prado, M. A.; Dias, G.; Carone, C.; Ligabue, R.; Dumas, A.; Le Roux, C.; Micoud, P.; Martin, F.; Einloft, S. *J. Appl. Polym. Sci.* **2015**, *132*, DOI: 10.1002/app.41854.
25. Dias, G.; Prado, M. A.; Carone, C.; Ligabue, R.; Dumas, A.; Martin, F. L.; Roux, C.; Micoud, P.; Einloft, S. *Polym. Bull.* **2015**, *72*, 2991.
26. Dias, G.; Prado, M.; Carone, C.; Ligabue, R.; Dumas, A. L.; Roux, C.; Micoud, P.; Martin, F.; Einloft, S. *Macromol. Symp.* **2016**, *367*, 136.
27. Yousfi, M.; Livi, S.; Dumas, A.; Crépin-Leblond, J.; Greenhill-Hooper, M.; Duchet-Rumeau, J. *J. Appl. Polym. Sci.* **2014**, *131*, DOI: 10.1002/app.40453.
28. dos Santos, L. M.; Ligabue, R.; Dumas, A. L.; Roux, C.; Micoud, P.; Meunier, J. F.; Martin, F.; Corvo, M.; Almeida, P.; Einloft, S. *Polym. Bull.* **2017**, 1.
29. Dumas, A.; Martin, F.; Ferrage, E.; Micoud, P.; Le Roux, C.; Petit, S. *Appl. Clay Sci.* **2013**, *85*, 8.
30. Brunauer, S.; Emmett, P. H.; Teller, E. *J. Am. Chem. Soc.* **1938**, *60*, 309.
31. Martin, F.; Micoud, P.; Delmotte, L.; Marichal, C. L.; Dred, R. D.; Parseval, P.; Mari, A.; Fortuné, J. P.; Salvi, S.; Béziat, D.; Grauby, O.; Ferret, J. *Can. Miner.* **1999**, *37*, 997.
32. Zhang, M.; Hui, Q.; Lou, X. J.; Redfern, S. A. T.; Salje, E. K. H.; Tarantino, S. C. *Am. Miner.* **2006**, *91*, 816.
33. Peruzzo, P. J.; Anbinder, P. S.; Pardini, F. M.; Pardini, O. R.; Plivelic, T. S.; Amalvy, J. I. *Mater. Today Commun.* **2016**, *6*, 81.
34. Jena, K. K.; Sahoo, S.; Narayan, R.; Tejraj, M.; Aminabhavic, T. M.; Rajua, K. V. S. N. *Polym. Int.* **2011**, *60*, 1504.
35. Kuan, H. C.; Ma, C. C. M.; Chuang, W. P.; Su, H. Y. *J. Polym. Sci. Part B Polym. Phys.* **2005**, *43*, 1.
36. Paul, D. R.; Robeson, L. M. *Polymer* **2008**, *49*, 3187.
37. Ray, S. S.; Okamoto, M. *Prog. Polym. Sci.* **2003**, *28*, 1539.
38. Zhang, S.; Jiang, J.; Yang, C.; Chen, M.; Liu, X. *Prog. Org. Coat.* **2011**, *70*, 1.
39. Chen, G.; Wei, M.; Chen, J.; Huang, J.; Dufresne, A.; Chang, P. R. *Polymer* **2008**, *49*, 1860.
40. Chang, P. R.; Ai, F.; Chen, Y.; Dufresne, A.; Huang, J. *J. Appl. Polym. Sci.* **2009**, *111*, 619.
41. Han, W. *Polym. Compos.* **2013**, *34*, 156.
42. Rahman, M. M.; Kim, H. D.; Lee, W. K. *J. Appl. Polym. Sci.* **2008**, *110*, 3697.
43. Lorandi, N. P.; Cioffi, M. O. H.; Ornaghi, H. Jr. *Sci. Cum. Ind.* **2016**, *4*, 48.
44. Fu, H.; Yan, C.; Zhou, W.; Huang, H. *Comp. Sci. Technol.* **2013**, *85*, 65.
45. Cao, X.; Habibi, Y.; Lucia, L. A. *J. Mater. Chem.* **2009**, *19*, 7137.
46. García-Pacios, V.; Costa, V.; Colera, M.; Martín-Martínez, J. M. *Prog. Org. Coat.* **2011**, *71*, 136.
47. Ma, X. Y.; Zhang, W. D. *Polym. Degrad. Stab.* **2009**, *94*, 1103.

4.2. Talco sintético como uma nova plataforma na produção de nanocompósitos fluorescentes

No artigo intitulado “*Synthetic talc as a new platform for producing fluorescente clay nanocomposites*“, publicado na revista “Applied Clay Science” um talco natural e dois talcos sintéticos foram funcionalizados com cloreto de berberina (agente fluorescente) e depois utilizados como carga na produção de nancompósitos de poliuretano através de misturas físicas. Os materiais foram caracterizados por BET, FTIR, DRX, TEM, AFM, DMTA, TGA, MEV-FEG, GPC e emissão de fluorescência, afim de comparar as propriedades mecânicas, térmicas, morfológicas e de fluorescência dos materiais entre si e também frente ao polímero puro. Todos os talcos foram bem dispersos na matriz de poliuretano mesmo quando se misturou uma quantidade maior (5% em massa), como mostraram as análises de TEM e SEM. Alterações morfológicas foram confirmadas por AFM. As propriedades fluorescentes dos talcos fluorescentes, do polímero misturado somente com berberina e dos nanocompósitos foram comparados. Enquanto a mistura da berberina pura com o poliuretano apresentou menor fluorescência devido a aglomeração, a emissão dos nanocompósitos aumentou com o aumento da quantia de talco sintético. A melhor eficiência de emissão foi observada para o nanocompósito com o talco sintético fluorescente com menor tamanho de partículas. A utilização de talcos sintéticos fluorescentes resultou em materiais com propriedades térmicas e mecânicas superiores em relação ao polímero puro, e pode ser considerado como um novo método para produzir nanocompósitos fluorescentes multifuncionais.

Applied Clay Science 158 (2018) 37–45

Contents lists available at ScienceDirect

Applied Clay Science

journal homepage: www.elsevier.com/locate/clay

Research paper

Synthetic talc as a new platform for producing fluorescent clay polyurethane nanocomposites

Guilherme Dias[a], Manoela Prado[a], Rosane Ligabue[a,b], Mathilde Poirier[c], Christophe Le Roux[c], François Martin[c], Suzanne Fery-Forgues[d,*], Sandra Einloft[a,b,**]

[a] Programa de Pós-Graduação em Engenharia e Tecnologia de Materiais (PGETEMA), Pontifícia Universidade Católica do Rio Grande do Sul (PUCRS), Porto Alegre, Brazil
[b] Faculdade de Química (FAQUI), Pontifícia Universidade Católica do Rio Grande do Sul (PUCRS), Porto Alegre, Brazil
[c] ERT 1074 Géomatériaux, GET UMR 5563 CNRS, Université de Toulouse, Toulouse, France
[d] SPCMIB, CNRS UMR5068, Université Toulouse III Paul Sabatier, 118 route de Narbonne, 31062 Toulouse cedex 9, France

ARTICLE INFO

Keywords:
Clay polymer nanocomposite (CPN)
Synthetic talc
Fluorescence properties
Mechanical properties

ABSTRACT

As a non-swelling clay, talc generally interacts very weakly with organic molecules. However, two new nanometric synthetic talcs that incorporate berberine chloride were successfully used as fluorescent fillers in clay polyurethane nanocomposites obtained by the blending method. A micrometric natural talc filler was also used for comparison. The clay polymer nanocomposites (CPN) were characterized by FTIR, molar mass analysis and XRD. All talc fillers were well dispersed into the polyurethane matrix even at high filler content of 5 wt%, as supported by TEM and SEM analyses. Morphological changes were confirmed by AFM. The optical properties of the fluorescent talcs, dye-doped polymer and CPN were compared. While the dye-doped polymer suffered from conventional fluorescence quenching due to dye aggregation, the emission quantum yield of the CPN was increased with increasing the filler content. The best emission efficiency was observed for the CPN that contains the smallest talc-berberine hybrid particles. The use of fluorescent synthetic talc resulted in materials with good thermal and mechanical properties, and can be considered as a new method to produce fluorescent CPN in view of multiple applications.

1. Introduction

Over the past fifteen years, the development of inorganic-filler polymer nanocomposites has stimulated extensive research in both industry and academia (Hussain et al., 2006; Paul and Robeson, 2008). The nature of nanofillers, their immobilization and the structuration of the polymer matrix around them lead to strong changes in the physical and chemical properties, and govern all possible applications. In this context, clay polymer nanocomposites (CPN) are of special practical and commercial significance, since their strength, fire retardation and chemical stability are markedly enhanced with respect to conventional polymers and polymer composites (Da Silva et al., 2013; Galimberti et al., 2013; Gürses, 2015; Shunmugasamy et al., 2015; Taheri and Sadeghi, 2015). They may also display additional specific properties, in particular fluorescence, after introduction of appropriate organic compounds (Aloisi et al., 2010; Esposito et al., 2010; Diaz et al., 2013; Hao et al., 2014; Zhong et al., 2017). A smart way to ensure good dispersion of the photoactive agent into the CPN is to modify the clay filler by organic molecules before introduction into the polymer. To do so, two strategies can be considered. The most popular one requires synthesis efforts. It consists of covalently labeling the nanoclay with various dye molecules, as reported for montmorillonite linked to fluorescein, rhodamine and anthracene derivatives (Aloisi et al., 2010; Esposito et al., 2010; Diaz et al., 2013). Although it would be easier to implement, the non-covalent approach has seldom been used. For instance, the characteristic property of swelling clays, i.e. the replacement of interlayer inorganic cations by cationic organic molecules (Suzuki et al., 2011; Bujdák et al., 2011; Felbeck et al., 2013; Ley et al., 2015), has only recently been exploited to obtain a fluorescent CPN (Zhong et al., 2017). Besides, the non-covalent approach has not been extended to non-swelling clays, which do not contain inorganic charge-exchange cations, probably because they are known to interact very weakly with organic compounds.

The aim of the present work was to introduce fluorescence into CPN

* Corresponding author.
** Corresponding author at: Programa de Pós-Graduação em Engenharia e Tecnologia de Materiais (PGETEMA), Pontifícia Universidade Católica do Rio Grande do Sul (PUCRS), Porto Alegre, Brazil.
E-mail address: Einloft@pucrs.br (S. Einloft).

https://doi.org/10.1016/j.clay.2018.03.012
Received 23 November 2017; Received in revised form 5 March 2018; Accepted 6 March 2018

by using a non-swelling clay modified by a very simple and effective process. The clay is expected to confer both mechanical and spectroscopic properties to the polymer. Talc polyurethane nanocomposites were considered as the continuation of other works performed on this type of materials (Dias et al., 2015; Dos Santos et al., 2015; Prado et al., 2015). Polyurethanes (PU) are formed by hard and soft segment blocks that can be tailored by varying their chemical composition to enable a wide variety of applications such as coatings, foams, elastomers and biomaterials (Li et al., 2012; Amela-Cortes et al., 2015). The addition of talc particles decreases gas permeability, and improves corrosion resistance (Kantheti et al., 2015). However, in this system, the use of natural talc (NTlc) presents some disadvantages because talc particles cannot be ground homogenously below one micron without losing their structure and becoming amorphous (Dumas et al., 2013, 2015; Yousfi et al., 2013; Dos Santos et al., 2015). In contrast, synthetic talc (STlc), like the one developed in the team, has well-defined chemical composition, high purity, crystallinity, particle size and layer thickness control. Among numerous applications that have recently been reviewed (Claverie et al., 2018), STlc has been used successfully as nanofiller in CPN, in particular for the reinforcement of PU. The good compatibility of organic and inorganic phases has been attributed to hydrogen bonding interactions between the OH groups of the filler and the PU chain (Dumas et al., 2013, 2015; Dias et al., 2015; Dos Santos et al., 2015; Prado et al., 2015). Moreover, studies have shown that STlc has a remarkable capacity to adsorb colored and fluorescent organic molecules (Aymonier et al., 2017a,b). Berberine chloride (Fig. 1) was chosen as the fluorescent dye to be incorporated into the talc particles. This compound is emissive in organic phases (Díaz et al., 2009; Zhang et al., 2014), constrained media (Megyesi and Biczók, 2006; Gade and Sharma, 2014) and in the solid state (Soulié et al., 2016). Its fluorescence properties are closely dependent on the micro-environment and provide useful information in this regard. The incorporation into polymers has scarcely been investigated (Gade and Sharma, 2014). Besides, berberine is a natural alkaloid of wide therapeutic interest, and it can be used to mimic the behavior of drugs in systems designed for biomedical applications (Soulié et al., 2015; Duval and Duplais, 2017). Synthetic talc fillers were therefore synthesized, loaded with berberine, and introduced into PU matrices. A comparison was made with NTlc. Here, it is of significance to note that, for the sake of simplicity, all clay polymer composites have been called “nanocomposites” and abbreviated CPN, even if the inorganic filler is of micrometric size. At each stage, the compounds were characterized by various analytical methods. Special attention was brought to homogeneity because the simple dispersion of inorganic particles in a polymer matrix often leads to phase segregation, which is an obstacle in the preparation of CPN (Amela-Cortes et al., 2015). Present studies showed that modified STlc fillers can be used as original platforms to produce fluorescent CPN. This simple concept allows potential applications to be envisioned in various fields: materials for optics, light-emitting devices, and controlled released of drug molecules.

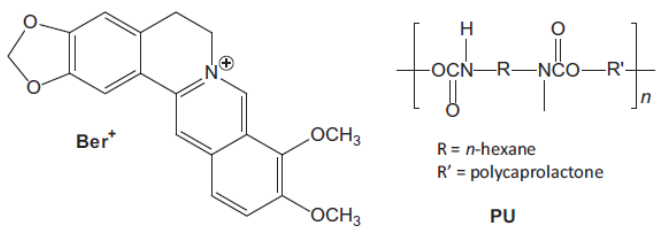

Fig. 1. Chemical formula of berberine chloride and the polyurethane used in this work.

2. Materials and methods

2.1. Preparation

The PU synthesis was performed by reacting poly(caprolactone) diol (PCL, MM = 2000 g/mol, Sigma–Aldrich) and 1,6-hexamethylene diisocyanate (HDI, Merck) in a molar ratio of NCO/OH of 1:1. Dibutyl tin dilaurate (DBTDL, Miracema-Nuodex Ind.) was used as catalyst (0.1% w/w) and methyl ethyl ketone (MEK, P.A., Merck) as solvent (about 50 mL). Commercial natural talc was obtained from IMERYS (Talc de Luzenac). STlc was prepared as described elsewhere (Le Roux et al., 2013). Fluorescent talcs were prepared by mixing an aqueous solution of berberine (9,10-dimethoxy-2,3-methylenedioxy-5,6-dihydrodibenzo [*a,g*] quinolizinium) chloride hydrate (Sigma Aldrich, 1 mg/mL) with dry STlc or NTlc in a ratio of 0.6 mg berberine/1 g of talc. A volume of 100 mL of water was added. The dispersions were then sonicated and placed in an oven at 100 °C for 12 h.

To prepare dye-doped PU, berberine chloride (1.2×10^{-4} g, 3.6×10^{-4} g and 6.0×10^{-4} g) dissolved in 100 mL of MEK was mixed with 20 g of PU. To prepare the CPN, 20 g of PU were solubilized in 100 mL of MEK, and then various talc filler contents were added (1 wt %, 3 wt% and 5 wt% in relation to pure PU). All dispersions were stirred for 30 min. After solvent evaporation at room temperature, the films were prepared using a hydraulic press (1 Pa; 50 °C), resulting in a thickness of approximately 0.10 mm.

2.2. Characterizations

Fourier transform infrared (FTIR) spectroscopy was performed with a Perkin Elmer FTIR spectrometer model Spectrum100. The nitrogen adsorption–desorption isotherms were measured at 77 K using a volumetric method, with a Quantachrome Autosorb-1 apparatus. They were recorded in the 0.05–0.30 relative pressure range, and high purity N_2 was used. Samples were outgassed for 15 h at 120 °C under vacuum before analysis. Specific surface areas were calculated using the Brunauer–Emmett–Teller (BET) method (Brunauer et al., 1938). The XRD patterns were recorded on a Shimadzu XRD-7000 diffractometer using CuKα Bragg-Brentano geometry θ-θ radiations, operating between 5 and 80° with a step size of 0.02°, at 40 kV and 30 mA. For transmission electron microscopy (TEM), the samples were cryomicrotomed and analyzed in a Tecnai G2 T20 FEI apparatus operating at 200 kV. Size exclusion chromatography (SEC) was performed using a liquid chromatograph equipped with an isocratic pump 1515 (eluent: tetrahydrofuran (THF), flow: 1 mL/min) and a refractive index detector 2414 from Waters Instruments with styragel column set at 45 °C. Differential scanning calorimetry (DSC) was carried out using a TA Instruments model Q20 equipment. Analyses were performed in two heating cycles, under N_2 in a temperature range from −90 °C to 200 °C with a heating/cooling rate of 10 °C min^{-1}. Thermogravimetric analysis (TGA) was made using a DSC-TGA coupled (SDT) equipment (TA Instruments Model Q600). Tests were carried out in a temperature range from 25 °C to 800 °C with a heating rate of 20 °C min^{-1} under constant N_2 flow. The analyzed samples weighted between 15 and 20 mg. Tensile tests (stress/strain) were performed using a dynamic mechanical thermal analysis in the static mode (DMTA) equipment (TA Instruments Model Q800). Tests were carried out at 25 °C with rectangular shape films (thickness ~ 0.15 mm, length 12 mm, width ~7.0 mm) with a force-ramp rate of 1 N min^{-1}. The Young's moduli of the materials were determined according to the standard test methods ASTM D638. The field emission scanning electron microscopy (FESEM) analyses were performed using a FEI Inspect F50 equipment in secondary electron (SE) mode. The samples in the form of 200 µm thick films were placed into a stub and covered with a thin gold layer. Atomic force microscopy (AFM) was performed in tapping mode using a Bruker Dimension Icon PT equipped with a TAP150A probe (Bruker, resonance frequency of 150 kHz and 5 N m^{-1} spring constant). The equipment was calibrated

prior to sample measurements. The scanned area of the images was $5 \times 5\,\mu m^2$ with a resolution of 512 frames per area. Corrected photoluminescence spectra of all solid samples were obtained using a SAFAS Xenius spectrofluorometer equipped with a $BaSO_4$ integrating sphere. The absolute photoluminescence quantum yield values (Φ_{PL}) were determined as described elsewhere (Soulié et al., 2016).

3. Results and discussion

3.1. Preparation of talc-berberine hybrids and CPN

Fluorescent STlc fillers were prepared via hydrothermal synthesis according to a procedure patented by Le Roux et al. (2013). In a first step, the talc precursor was formed by reacting sodium metasilicate pentahydrate with magnesium acetate tetrahydrate in proportion that fits the ratio Si/Mg = 4/3, in the presence of a catalyst. The second step turned the amorphous prototalc into well-crystallized nano-sized talc gel by subjecting it to thermal treatment under high pressure for a specified period of time. Two samples of STlc of formula $Si_4Mg_3O_{10}(OH)_2$ were therefore obtained and fully characterized by usual methods (Dumas et al., 2013). In sample STlc1, manufactured in only 6 h, the particle size was between 100 and 300 nm, and the specific surface area was $250\,m^2\,g^{-1}$. In sample STlc2, obtained via a 3-day process, the particle size was between 100 and 2300 nm, and the specific surface area was $130\,m^2\,g^{-1}$. A commercially available natural talc (NTlc) was used for comparison purposes. This high aspect ratio (length/thickness ratio) sample presents a particle size larger than 50 µm and a specific surface area of $10\,m^2\,g^{-1}$. Crystallinity was as its best for NTlc and comparatively weaker for STlc, for which it was increased with the duration of the hydrothermal process (Dumas et al., 2013).

The three talc samples were then placed in contact with an aqueous solution of berberine chloride. The total amount of berberine in modified talc was 0.6 mg (1.5×10^{-6} mol) for 1 g talc. After evaporation of water, the talc-berberine hybrids (STlc1-Ber, STlc2-Ber and NTlc-Ber) were powders. Their morphological characteristics were unchanged compared to the respective starting materials.

Clay polymer nanocomposites STlc1-Ber PU, STlc2-Ber PU and NTlc -Ber PU were finally prepared by incorporating various amounts of talc-berberine hybrids into PU dissolved in an organic solvent. After drying and pressing, the resulting samples were films of homogeneous thickness (0.10 mm). The hybrid concentration in the polymer ranged from 1 to 5 wt%.

3.2. Fourier transform infrared (FTIR) spectroscopy

Due to the small amount of organic compound in the mineral matrix, the characteristic peaks of berberine chloride (Fig. S1, Supplementary materials) were not visible in the FTIR spectra of the talc-berberine hybrids (Fig. 2). However, the FTIR spectra reflect the nature of talc. The band around $3672\,cm^{-1}$ arises from the Mg_3OH vibrations of STlc (Martin et al., 1999; Dos Santos et al., 2015; Dumas et al., 2015). Its intensity increases in the order STlc1-Ber < STlc2-Ber < NTlc-Ber because it is related to crystallinity (Dumas et al., 2013). The bands around 3400 and $1550\,cm^{-1}$ are related to the Mg—OH vibrations (Zhang et al., 2006), while that around 1000–900 cm^{-1} is characteristic of Si—O and Si—O—Si bonds (Martin et al., 1999; Zhang et al., 2006; Dos Santos et al., 2015; Prado et al., 2015). Fig. 2 also allows the comparison between PU and the CPN. In the PU spectrum, the bands around 3385, 1724, and $1526\,cm^{-1}$ correspond respectively to the NH, C=O and CN groups of urethane bonds (Dos Santos et al., 2015). The bands at 2940, 2866, and $732\,cm^{-1}$ are assigned to different vibrational modes of CH_2 group (Da Silva et al., 2013; Dias et al., 2015; Prado et al., 2015). The CO—O bond can be identified by bands at 1238 and $1162\,cm^{-1}$. The clay polymer composite spectra are characterized by bands around $1000\,cm^{-1}$ related to the Si—O bonds. The fingerprint of each talc filler therefore appeared in the FTIR spectra and this confirms incorporation.

3.3. Molar mass analysis

SEC was performed to obtain the number average and weight average molar mass (Mn and Mw, respectively). The Mn values for PU and CPN varied in the range of 190,000 Da to 219,000 Da, while the Mw were in the range of 344,000 Da to 379,000 Da. These very small variations showed that the incorporation of fillers into the polymer did not affect the molecular structure of the PU chains.

3.4. X-ray diffraction (XRD) analysis and transmission electron microscopy (TEM)

The crystalline structures were evaluated by XRD analysis (Fig. 3). The fillers presented the most characteristic reflections associated to natural talc (Yousfi et al., 2013; Dumas et al., 2015). However, the reflections of STlc1-Ber were broader and less intense than those of STlc2-Ber, which are themselves badly defined with respect to NTlc-Ber. This indicates that the number of talc layers and the size of the crystals were increased in the order STlc1-Ber < STlc2-Ber < NTlc-Ber, as it is the case for the precursors without organic dye (Dumas et al., 2013; Yousfi et al., 2013). The reflections of the hybrids were clearly found in the CPN patterns, showing that the crystallinity of each filler has been retained after incorporation into PU. Moreover, the appearance of new reflections in the XRD patterns of CPN evidenced that the STlc layers are intercalated between the polymer chains as is assumed to be the case when the CPN are not exfoliated (Ray and Okamoto, 2003; Paul and Robeson, 2008). From TEM images (Fig. 3, insets), it can be seen that the talc particles form elongated micro-domains, whose good dispersion was achieved for all samples, even at high concentration of filler. Similar morphological structures have been observed for CPN made of PU (Dias et al., 2015; Dos Santos et al., 2015), polypropylene (PP) and polyamide-6 (PA6) blends (Yousfi et al., 2014; Hemlata and Maiti, 2015) filled with STlc. Exfoliated silicate layers were also observed here in the TEM images for CPN obtained with STlc, even at 5 wt% filler. This observation is in line with the broadness of the XRD peak, which suggests a diversity of co-existing structures and possibly the influence of a local disorder within the crystallites (Morgan and Gilman, 2003). All these results highlight the good compatibility of the fillers with the polymer matrix and this is particularly significant because the CPN have been obtained by physical mixture.

3.5. Field emission scanning electron microscopy (FESEM)

The FESEM images displayed in Fig. 4 allow the surface of pristine PU and CPN to be visualized. Heterogeneities can be observed for all STlc2-Ber PU samples and for STlc1-Ber PU at 5 wt% filler. In contrast, NTlc-Ber PU had a very plain surface, comparable to that of pristine PU. In any case, the talc fillers seem to be well dispersed in the PU matrix and this suggests good interactions between these two components. These interactions should affect the molecular mobility and consequently the thermal and mechanical properties of the PU matrix (Zhou et al., 2005; Pavličević et al., 2013). The uniform dispersion of the filler should also prevent the formation of defects in the materials.

3.6. Atomic force microscopy (AFM)

AFM allows a more detailed analysis of the surface. The high values of the roughness parameters (Table S1) obtained for CPN with respect to PU confirm the presence of the fillers at the sample surface (Maji and Bhowmick, 2012). No obvious differences were found between CPN containing STlc and NTlc. Fig. 5 displays the 3D height images of pure PU and CPN. Hard segments are represented by the brightest regions

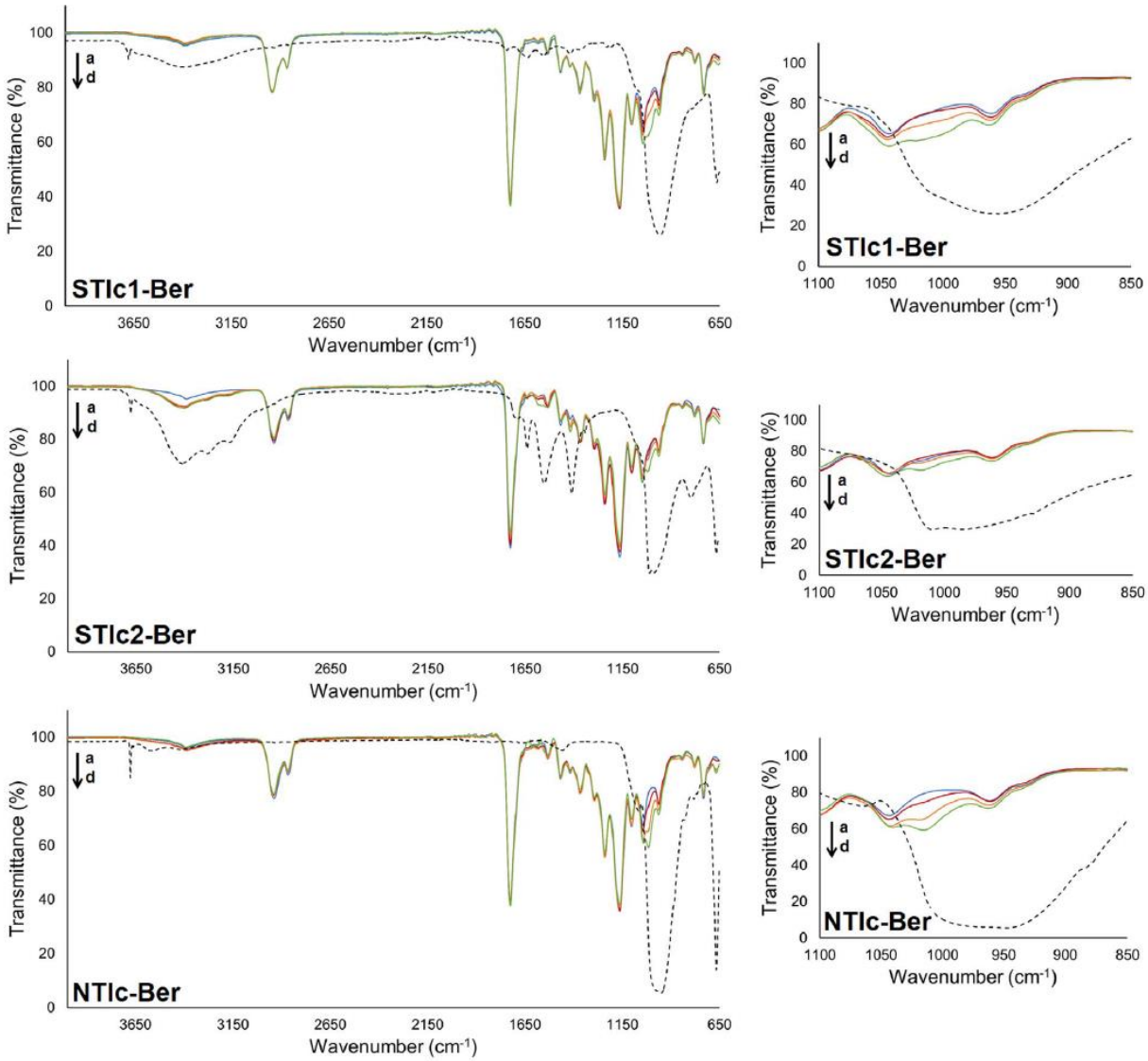

Fig. 2. I: Left: FTIR spectra of the three types of talc-berberine hybrids (i.e. STlc1-Ber, STlc2-Ber and NTlc -Ber, black dotted lines) and polyurethane (color solid lines) containing 0 wt% (a), 1 wt% (b), 3 wt% (c) and 5 wt% (d) of the corresponding hybrid. Right: expansion of the 1000–900 cm^{-1} region.

and soft segments appear dark, according to the resistance that they present to penetration by the AFM probe tip (Anandhan and Lee, 2014). It can be seen that the fillers are well distributed both in soft and hard domains of the PU matrix. Again, this good dispersion can be attributed to the hydroxyl groups of the fillers that significantly leverage the interactions with polymer (Verma et al., 2013).

It is noteworthy that the hard segments of PU and CPN with low content of fillers (1 wt%) (Fig. 5 A, B, E and H) show some connectivity, the bright regions being associated to one another. This behavior could be explained by some hydrogen bonding between hard/hard segments. In the presence of large filler contents, the polymer/filler and filler/filler interactions become more important than interactions between hard/hard and hard/soft segments (Fig. 5 D, G and J). In this case, the hard and soft segments reorganize, and their miscibility is increased due to the formation of new hydrogen bonds between the fillers and polymeric chains (Dos Santos et al., 2015).

3.7. Spectroscopic properties

3.7.1. Talc-berberine hybrids

During the preparation of the hybrids, the instant interaction between talc and berberine was visualized by a drastic change in the shape and intensity of the absorption spectrum, and the appearance of a strong fluorescence signal at 538 nm, while the berberine cation alone is virtually not emissive in water (Díaz et al., 2009) (Fig. 6). Since no cation-exchange interaction can take place in talc, this interaction is assumed to be adsorption at the talc surface, as will be thoroughly described in a forthcoming article.

After drying, the hybrids NTlc-Ber and STlc2-Ber were pale yellow powders, while STlc1-Ber was bright yellow. All of them were emissive in the yellow-green when illuminated by a hand-held UV lamp, and the emission intensity was particularly intense for STlc1-Ber (Fig. 7). The emission spectra showed a strong unresolved band at around 547 nm (Fig. S2). The photoluminescence quantum yield Φ_{PL} of modified NTlc was 0.02, comparable to that of the dye in the solid state (Soulié et al., 2016) and in solution in organic solvents (Díaz et al., 2009). Most interestingly, this value was markedly increased with passing from NTlc-Ber to STlc2-Ber (Φ_{PL} = 0.10) and then to STlc1-Ber (Φ_{PL} = 0.23), and to our knowledge, this high fluorescence efficiency is unprecedented for berberine (Table S2). The berberine molecules are probably well dispersed at the surface of the talc particles in STlc1-Ber, while some aggregation may occur in STlc2-Ber and even more in NTlc-Ber.

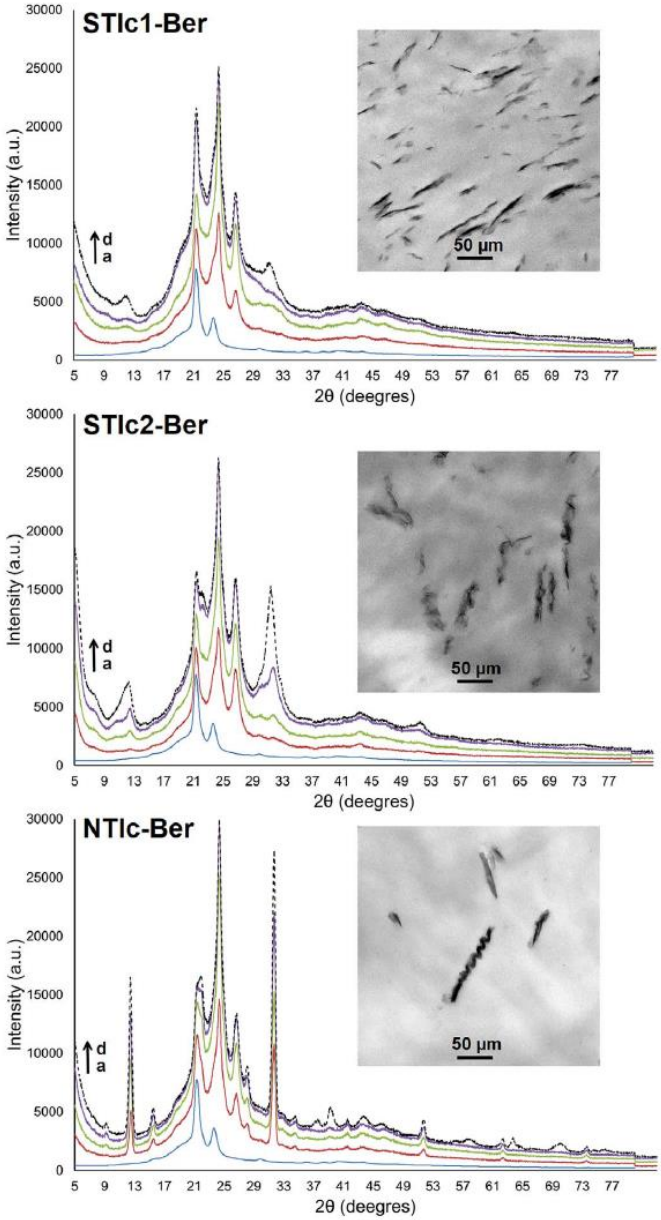

Fig. 3. XRD patterns of the three types of talc-berberine hybrids (i.e. STlc1-Ber, STlc2-Ber and NTlc-Ber, black dotted lines) and polyurethane (color solid lines) containing 0 wt% (a), 1 wt% (b), 3 wt% (c) and 5 wt% (d) of the corresponding hybrid. Insets: TEM micrographs of the CPN containing 5 wt% hybrid.

3.7.2. Direct incorporation of berberine into PU

Before going any further, it is instructive to study the behavior of berberine-doped PU (Ber PU samples). The polymer used in this work is hydrophobic and very weakly polar (Fig. 1). It emits weakly in the blue with a maximum around 504 nm, probably due to traces of aromatic compounds. Solid samples of PU incorporating berberine chloride at three different concentrations (6×10^{-4}, 1.8×10^{-3} and 3×10^{-3} wt %) were prepared. They were pale yellow and emitted yellow-green fluorescence with a maximum at 547 nm (Fig. S3). This observation suggests that the dye molecules interact with heteroatoms of PU because they emit at shorter wavelengths when dissolved in weakly polar media (Díaz et al., 2009). The Φ_{PL} value was between 0.03 and 0.04, similar to organic solutions, indicating that the medium rigidity has induced no fluorescence enhancement (Table S3). The fluorescence intensity was increased with passing from the least concentrated sample to the intermediate one, and then it was decreased again for the most

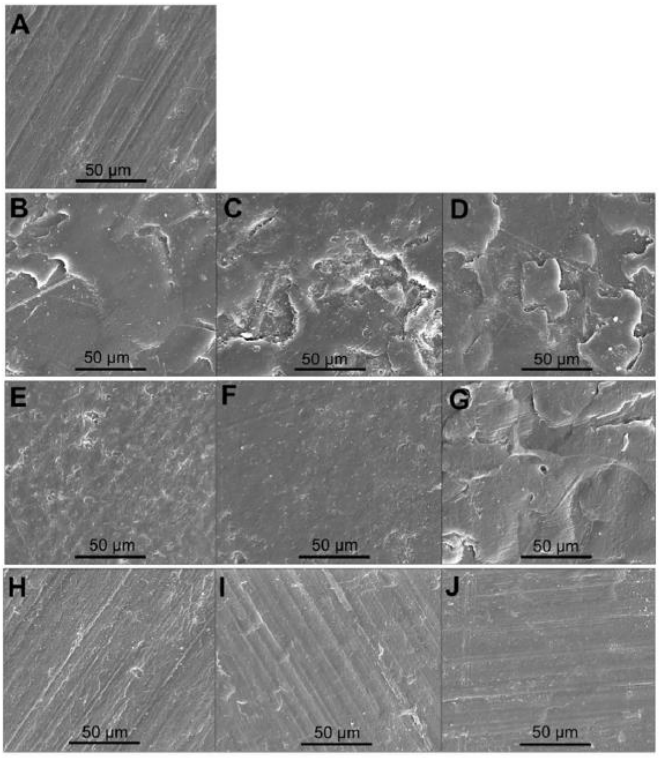

Fig. 4. FESEM Micrographs, mode SE, of the materials at magnification of 2000× (A) PU, (B) STlc1-Ber PU 1 wt%, (C) STlc1-Ber PU 3 wt%, (D) STlc1-Ber PU 5 wt%, (E) STlc2-Ber PU 1 wt%, (F) STlc2-Ber PU 3 wt%, (G) STlc2-Ber PU 5 wt%, (H) NTlc-Ber PU 1 wt%, (I) NTlc-Ber PU 3 wt% and (J) NTlc-Ber PU 5 wt%.

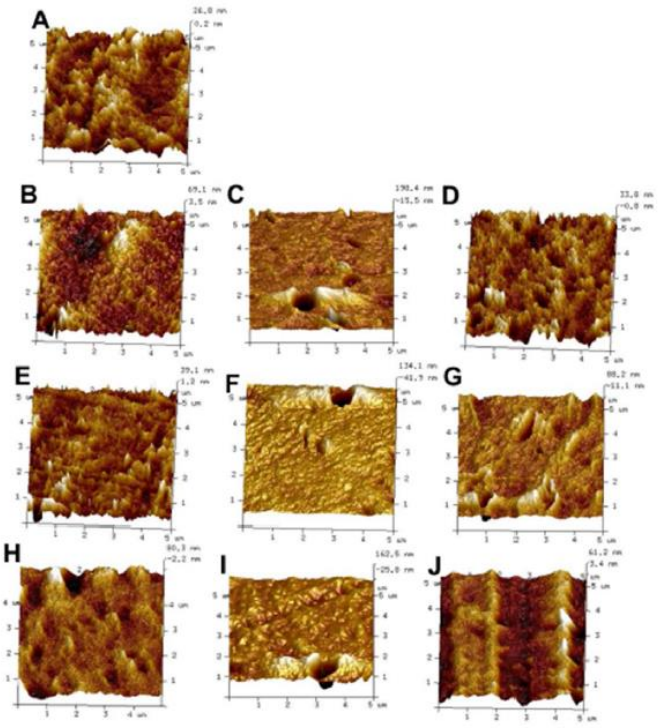

Fig. 5. AFM images (height) (A) PU, (B) STlc1-Ber PU 1 wt%, (C) STlc1-Ber PU 3 wt% (D) STlc1-Ber PU 5 wt%, (E) STlc2-Ber PU 1 wt%, (F) STlc2-Ber PU 3 wt%, (G) STlc2-Ber PU 5 wt%, (H) NTlc-Ber PU 1 wt%, (I) NTlc-Ber PU 3 wt% and (J) NTlc-Ber PU 5 wt%.

concentrated sample, probably due to dye stacking and formation of aggregates. It is noteworthy that other samples heavily loaded with 1 to 5 wt% berberine had a pronounced yellow color, their fluorescence

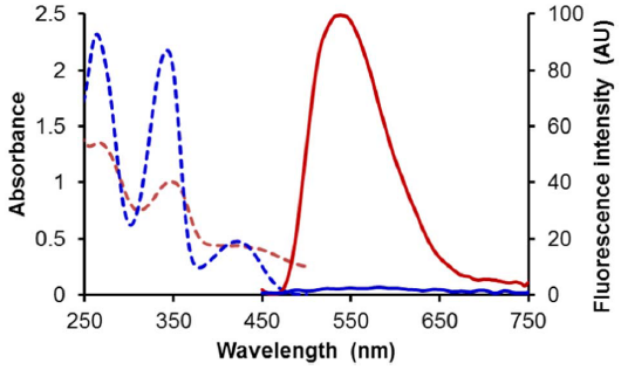

Fig. 6. Absorption (dotted lines) and fluorescence emission spectra (solid lines) of berberine chloride dissolved in water in the absence (blue lines) and in the presence (red lines) of synthetic talc STlc1. Dye concentration: 8.7×10^{-5} M for absorption and 8.7×10^{-6} M for emission. λ_{ex} = 420 nm. (For interpretation of the references to color in this figure legend, the reader is referred to the web version of this article.)

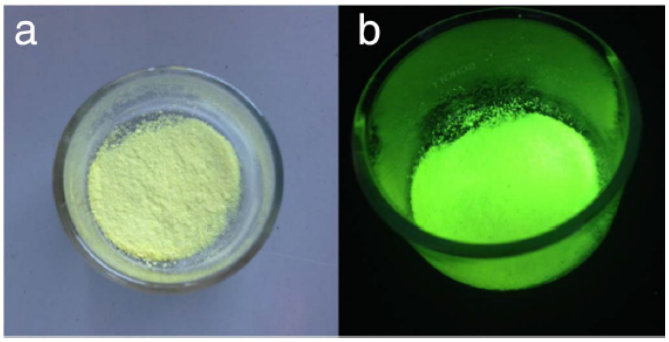

Fig. 7. Powder of STlc1-Ber hybrid observed (a) in natural light and (b) under illumination by a hand-held UV lamp (λ_{ex} = 365 nm).

spectra were red-shifted by about 10 nm and they were comparatively much less emissive than the weakly concentrated samples (Fig. S3 and Table S3), all this supporting the hypothesis of dye aggregation in the polymer.

3.7.3. Spectroscopic properties of the CPN

The talc-berberine hybrids were very stable and almost no leaching occurred in organic solvents like ethyl acetate. It may thus be assumed that the dye molecules remain at the surface of the talc particles after incorporation into PU. The resulting CPN were pale yellow films. When illuminated by UV light, all of them were luminescent to the naked eye. Due to the weak blue fluorescence of PU, the emitted color was varied from blue-green for the CPN samples that contain a weak amount of talc-berberine hybrid, to yellow-green for the most concentrated ones (Fig. 8). In CPN incorporating 1, 3, and 5 wt% talc-berberine hybrid, the dye concentration was 6×10^{-4}, 1.8×10^{-3} and 3.0×10^{-3} wt%, respectively, identical to the berberine-doped PU (Ber PU) samples studied above. Since all samples were studied in the same experimental conditions, they can be easily compared. The first observation is that no CPN emits more efficiently than the best Ber PU sample and the corresponding talc-berberine hybrids (Table S4). In particular, the excellent fluorescence properties of the STlc hybrids were not retained after incorporation into PU. This shows that the adsorption of the dye molecules on the talc particles does not prevent fluorescence quenching from PU. A second striking feature is that CPN incorporating STlc, and especially STlc1-Ber PU, emitted more strongly than the one incorporating NTlc. Therefore, the talc morphological characteristics and crystallinity influence the fluorescence emission intensity of the CPN.

Finally, it is noteworthy that fluorescence intensity was increased with increasing the filler content. A similar observation has been reported for pyrene-anchored ZnO PU nanocomposites (Kantheti et al., 2015). Most remarkably, the Φ_{PL} value was also increased with the filler content. This behavior is the exact opposite of the self-quenching effect that has been observed for the Ber PU samples. It was hoped that adsorption on the talc surface would prevent aggregation of the dye molecules, and the best case scenario was therefore that Φ_{PL} remains steady with increasing the filler concentration. But, the observed augmentation of fluorescence efficiency was much beyond what could have been expected. For example, the Φ_{PL} value passed from 0.006 to 0.04 when the filler concentration was increased from 1 to 5 wt% in STlc1-Ber PU. This phenomenon could be attributed to an increase of effective excitation energy due to internal scattering or reflection of the light beam within the CPN films (Lee et al., 2001). Most likely, a cooperative effect is taking place here. The TEM pictures have shown the formation of micro-domains resulting from the incorporation of the hybrids into PU. In these agglomerates, the dye molecules may be protected from the detrimental quenching effect of PU, and even more so as the hybrid concentration is high, and this could explain the spectacular fluorescence revival.

3.8. Thermal properties

The thermal properties of the CPN compared to pristine PU are presented in Table S5. The thermogravimetric analysis (TGA) showed a significant increase in the onset temperatures for the STlc1-Ber PU and NTlc-Ber PU samples. For example, this value passed from 321 °C for PU to 343 °C for STlc1-Ber PU 5 wt%, and 342 °C for NTlc-Ber PU 5 wt%, evidencing that the thermal resistance has been increased with addition of the fillers. This behavior can be related to the filler dispersion in the PU matrix and to the formation of a network structure between the fillers and the polymeric chains (Balamurugan and Maiti, 2010). Indeed, it was shown in previous works that the thermal stability of CPN is improved by the use of synthetic talc, because the large amount of hydroxyl groups present at the filler layer edges favors interactions with PU (Dumas et al., 2013, 2015; Dias et al., 2015; Prado et al., 2015). Curiously, a different behavior was noticed for all STlc2-Ber PU samples, the onset temperatures of which was lower than for pristine PU. The huge particle size distribution (100–2300 nm) of these CPN is probably detrimental to thermal stability.

The crystallization temperatures (Tc) of the CPN ranged between −1.2 and −1.9 °C. They were quite close to pristine PU (−1.4 °C) (Table S5), indicating that the synthetic talc fillers do not promote the crystallization of PU and do not act as nucleating agents. Fiorentino et al. (2015) have reported similar results for CPN made of PP and STlc. The melting temperature values of the CPN ranged between 37.0 °C and 37.7 °C, very similar to PU (37.3 °C).

3.9. Mechanical testing (DMTA)

The static mechanical properties were investigated by DMTA (Table 1 and Fig. S4). The stress at break did not present a significant change for the CPN when compared to pristine PU, probably due to the good dispersion and intercalation of the fillers in the polymeric chains. In contrast, the stiffness of the CPN, quantified by Young's modulus, was enhanced with respect to pure PU and depended markedly on the talc-berberine hybrid concentration. This effect may be due to filler–polymer interactions that are increased with the filler content, including the crosslinks formed between the fillers and the polymer matrix through hydrogen bonding (Da Silva et al., 2013; Dias et al., 2015; Dos Santos et al., 2015; Prado et al., 2015). Interestingly, the three samples investigated showed almost the same increase of Young's modulus. Similar observations have been reported as regards incorporation of NTlc, STlc and chemically modified STlc in PP, PA6 and PU (Castillo et al., 2013; Yousfi et al., 2013; Dias et al., 2015; Prado et al., 2015). The increase of Young's modulus has been associated with the orientation of talc particles, the good dispersion of the fillers (Saha et al., 2013), and the particle morphology (Castillo et al., 2013). In general, talcs with

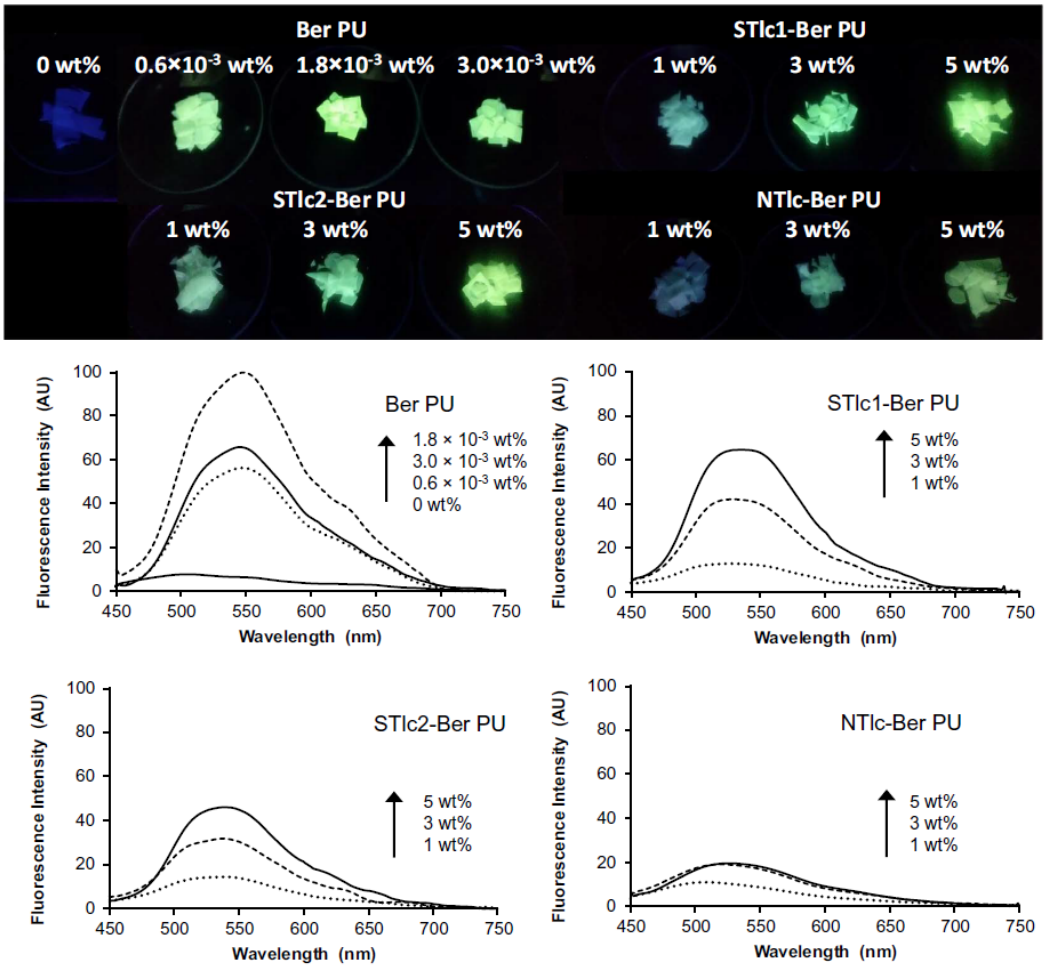

Fig. 8. Images of PU alone, PU loaded with three concentrations of berberine (Ber PU), and CPN STlc1-Ber PU, STlc2-Ber PU and NTlc-Ber PU loaded with 1, 3 and 5 wt% talc-berberine hybrid, under illumination by 365-nm UV light. Corresponding fluorescence spectra with λ_{ex} = 420 nm. All spectra were recorded in the same experimental conditions and their height is proportional to the fluorescence intensity.

high aspect ratio show a better stiffening effect than those with high particle symmetry, such as macroscopic talcs (Castillo et al., 2013). Here, the present results indicate that the close behavior of the three samples is in line with their high aspect ratio and the fact that they all form well-distributed micro-domains.

Finally, it might have been expected that filler-polymer interactions restrict the movement of the polymer chains, resulting in a reduction in the elastic behavior of the CPN when compared to pure polymer (Lapcik et al., 2008; Zhang et al., 2011; Castillo et al., 2013). The creep-recovery tests showed that this was actually not the case, meaning that the recovery properties of the CPN are maintained even with high contents of fillers.

4. Conclusions

New fluorescent CPN, which incorporate natural and synthetic talcs as fillers, have been obtained and characterized by various methods. It was proposed that the Mg-OH groups situated on the edges of the talc layers interact with the PU chains. Thanks to these interactions, the talc particles were well dispersed into the PU matrix even at high filler content, without addition of coupling agents or compatibilizers. The onset temperatures were increased in the presence of STlc1 and NTlc fillers with respect to pure PU, and the stiffness was increased for all the CPN, whatever the nature of the talc filler.

In contrast, the talc characteristics played an important role on

Table 1
Mechanical properties of PU and CPN.

Samples	Young's modulus (MPa)	Strain at break (%)	Stress at break (MPa)	Creep recovery (%)
PU	81 ± 5	90 ± 9	6 ± 0.4	90 ± 1
STlc1-Ber PU 1 wt%	81 ± 15	88 ± 16	5 ± 0.5	87 ± 1
STlc1-Ber PU 3 wt%	94 ± 11	125 ± 30	7 ± 0.3	85 ± 1
STlc1-Ber PU 5 wt%	96 ± 13	98 ± 31	6 ± 0.6	84 ± 3
STlc2-Ber PU 1 wr%	77 ± 6	92 ± 29	6 ± 0.5	87 ± 1
STlc2-Ber PU 3 wt%	86 ± 13	101 ± 33	6 ± 1.5	85 ± 7
STlc2-Ber PU 5 wt%	95 ± 10	104 ± 28	6 ± 0.4	87 ± 1
NTlc-Ber PU 1 wt%	81 ± 18	102 ± 21	6 ± 0.8	89 ± 2
NTlc-Ber PU 3 wt%	88 ± 9	99 ± 7	6 ± 0.3	89 ± 3
NTlc-Ber PU 5 wt%	97 ± 6	89 ± 32	6 ± 0.6	87 ± 3

the luminescence properties of the CPN. The STlc1 hybrid, where the talc particles are the smallest, brought strongest fluorescence. The originality of our CPN is that the fluorescent agent is molecularly dispersed at the surface of the talc filler, and so the ubiquitous aggregation-caused quenching effect was circumvented, contrary to what is observed in the dye-doped polymer. Berberine is not the best fluorescent probe, but the results obtained suggest that the concept can be easily applied to other fluorescent or electroluminescent dyes, thus opening new routes towards highly emissive materials also endowed with good thermal and mechanical properties. It must be emphasized that silicates polymer-layered nanocomposites are promising in the field of light-emitting devices (Lee et al., 2001), but are still in their infancy, and the incorporation of dye-loaded talc filler could be a distinct advantage. Finally, the strong adsorption of berberine on the talc filler suggests that many biologically-active molecules that are badly soluble in water should behave similarly. This method could be of great value for the controlled released of these molecules and would deserve further investigations.

Acknowledgements

GD and MP thanks CAPES for their PhD scholarship. SE acknowledges CNPq for DT grant (number 303467/2015-0).

Appendix A. Supplementary data

Supplementary data to this article can be found online at https://doi.org/10.1016/j.clay.2018.03.012.

References

Aloisi, G.G., Elisei, F., Nocchetti, M., Camino, G., Frache, A., Costantino, U., Latterini, L., 2010. Clay based polymeric composites: preparation and quality characterization. Mater. Chem. Phys. 123, 372–377.

Amela-Cortes, M., Paofai, S., Cordier, S., Folliot, H., Molard, Y., 2015. Tuned red NIR phosphorescence of polyurethane hybrid composites embedding metallic nanoclusters for oxygen sensing. Chem. Commun. 51, 8177–8180.

Anandhan, S., Lee, H.S., 2014. Influence of organically modified clay mineral on domain structure and properties of segmented thermoplastic polyurethane elastomer. J. Elastom. Plast. 46, 217–232.

Aymonier, C., Fery-Forgues, S., Le Roux, C., Martin, F., Micoud, P., Poirier, M., 2017a. Matériaux hybrides organique/inorganique photoluminescents et procédé pour leur préparation. (Fr. Pat. FR 1750612).

Aymonier, C., Fery-Forgues, S., Le Roux, C., Martin, F., Micoud, P., Poirier, M., 2017b. Matériaux hybrides organique/inorganique colorés et procédé pour leur préparation. (Fr. Pat. FR 1750613).

Balamurugan, G.P., Maiti, S.N., 2010. Effects of nanotalc inclusion on mechanical, microstructural, melt shear rheological, and crystallization behavior of polyamide 6-based binary and ternary nanocomposites. Polym. Eng. Sci. 50, 1978–1993.

Brunauer, S., Emmett, P.H., Teller, E., 1938. Surface area measurements of activated carbons, silica gel and other adsorbents. J. Am. Chem. Soc. 60, 309–319.

Bujdák, J., Czímerová, A., López Arbeloa, F., 2011. Two-step resonance energy transfer between dyes in layered silicate films. J. Colloid Interface Sci. 364, 497–504.

Castillo, L.A., Barbosa, S.E., Capiati, N.J., 2013. Influence of talc morphology on the mechanical properties of talc filled polypropylene. J. Polym. Res. 20, 152–161.

Claverie, M., Dumas, A., Carême, C., Poirier, M., Le Roux, C., Micoud, P., Martin, F., Aymonier, C., 2018. Synthetic talc and talc-like structures: preparation, features and applications. Chem. Eur. J. 24, 519–542.

Da Silva, V.D., Dos Santos, L.M., Subda, S.M., Ligabue, R., Seferin, M., Carone, C.L., Einloft, S., 2013. Synthesis and characterization of polyurethane/titanium dioxide nanocomposites obtained by in situ polymerization. Polym. Bull. 70, 1819–1833.

Dias, G., Prado, M.A., Carone, C., Ligabue, R., Dumas, A., Martin, F., Le Roux, C., Micoud, P., Einloft, S., 2015. Synthetic silico-metallic mineral particles (SSMMP) as nanofillers: comparing the effect of different hydrothermal treatments on the PU/SSMMP nanocomposites properties. Polym. Bull. 72, 2991–3006.

Díaz, M.S., Freile, M.L., Gutiérrez, M.I., 2009. Solvent effect on the UV/Vis absorption and fluorescence spectroscopic properties of berberine. Photochem. Photobiol. Sci. 8, 970–974.

Diaz, C.A., Xia, Y., Rubino, M., Auras, R., Jayaraman, K., Hotchkiss, J., 2013. Fluorescent labeling and tracking of nanoclay. Nanoscale 5, 164–168.

Dos Santos, L.M., Ligabue, R., Dumas, A., Le Roux, C., Micoud, P., Meunier, J.F., Einloft, S., 2015. New magnetic nanocomposites: polyurethane/Fe_3O_4-synthetic talc. Eur. Polym. J. 69, 38–49.

Dumas, A., Martin, F., Le Roux, C., Micoud, P., Petit, S., Ferrage, E., Greenhill-Hooper, M., 2013. Phyllosilicates synthesis: a way of accessing edges contributions in NMR and FTIR spectroscopies. Example of synthetic talc. Phys. Chem. Miner. 40, 361–373.

Dumas, A., Martin, F., Ferrage, E., Micoud, P., Le Roux, C., Petit, S., 2015. Synthetic talc advances: coming closer to nature, added value, and industrial requirements. App. Clay Sci. 85, 8–18.

Duval, R., Duplais, C., 2017. Fluorescent natural products as probes and tracers in biology. Nat. Prod. Rep. 34, 161–193.

Esposito, A., Raccurt, O., Charmeau, J.-Y., Duchet-Rumeau, J., 2010. Functionalization of Cloisite 30B with fluorescent dyes. Appl. Clay Sci. 50, 525–532.

Felbeck, T., Behnke, T., Hoffmann, K., Grabolle, M., Lezhnina, M.M., Kynast, U.H., Resch-Genger, U., 2013. Nile-red – nanoclay hybrids: red emissive optical probes for use in aqueous dispersion. Langmuir 29, 11489–11497.

Fiorentino, B., Fulchiron, R., Bounor-Legaré, V., Majesté, J.C., Leblond, J.C., Duchet-Rumeau, J., 2015. Chemical modification routes of synthetic talc: influence on its nucleating power and on its dispersion state. Appl. Clay Sci. 109–110, 107–118.

Gade, C.R., Sharma, N.K., 2014. Synthesis and spectroscopic studies of berberine immobilized modified cellulose material. RSC Adv. 4, 39337–39342.

Galimberti, M., Cipolletti, V.R., Coombs, M., 2013. Applications of clay-polymer nanocomposites (CPN). In: Bergaya, F., Lagaly, G. (Eds.), Handbook of Clay Science. Elsevier, Amsterdam, pp. 539–586 Chapter 4.4, Vol. 5 B.

Gürses, A., 2015. Introduction to Polymer-clay Nanocomposites. CRC Press, Boca Raton Florida, USA.

Hao, W., Ding, S., Zhang, L., Liu, W., Yang, W., 2014. Nacrelike nanocomposite films from fluorescent hyperbranched poly(amido amine)s and clay nanosheets. Chem. Plus Chem. 79, 211–216.

Hemlata, J., Maiti, S.N., 2015. Mechanical, morphological, and thermal properties of nanotalc reinforced PA6/SEBS-g-MA composites. J. Appl. Polym. Sci. 132, 41381.

Hussain, F., Hojjati, M., Okamoto, M., Gorga, R.E., 2006. Polymer-matrix nanocomposites, processing, manufacturing, and application: an overview. J. Compos. Mater. 40, 1511–1575.

Kantheti, S., Narayan, R., Raju, K.V., 2015. Pyrene-anchored ZnO nanoparticles through click reaction for the development of antimicrobial and fluorescent polyurethane nanocomposite. Polym. Int. 64, 267–274.

Lapcik, L., Jindrova, P., Lapcikova, B., Tamblyn, R., Greenwood, R., Rowson, N., 2008. Effect of the talc filler content on the mechanical properties of polypropylene composites. J. Appl. Polym. Sci. 110, 2742–2747.

Le Roux, C., Martin, F., Micoud, P., Dumas, A., 2013. Process for Preparing a Composition Comprising Synthetic Mineral Particles and Composition. (Int. Pat. WO 2013/004979 A1).

Lee, T.W., Park, O.O., Yoon, J., Kim, J.J., 2001. Polymer-layered silicate nanocomposite light-emitting devices. Adv. Mater. 13, 211–213.

Ley, C., Brendlé, J., Walter, A., Jacques, P., Ibrahim, A., Allonas, X., 2015. On the interaction of triarylmethane dye crystal violet with LAPONITEs clay: using mineral nanoparticles to control the dye photophysics. Phys. Chem. Chem. Phys. 17, 16677–16681.

Li, X., Ni, X., Liang, Z., Shen, Z., 2012. Synthesis of imidazolium-functionalized ionic polyurethane and formation of CdTe quantum dot–polyurethane nanocomposites. J. Polym. Sci. Part A. 50, 509–516.

Maji, P.K., Bhowmick, A.K., 2012. Efficacy of clay content and microstructure of curing agents on the structure–property relationship of new-generation polyurethane nanocomposites. Polym. Adv. Technol. 23, 1311–1320.

Martin, F., Micoud, P., Delmotte, L., Marichal, C., Le Dred, R., De Parseval, P., Mari, A., Fortuné, J.P., Salvi, S., Béziat, D., Grauby, O., Ferret, J., 1999. The structural formula of talc from the trimouns deposit, Pyrenees, France. Can. Mineral. 37, 997–1006.

Megyesi, M., Biczók, L., 2006. Considerable fluorescence enhancement upon supramolecular complex formation between berberine and *p*-sulfonated calixarenes. Chem. Phys. Lett. 424, 71–76.

Morgan, A.B., Gilman, J.W., 2003. Characterization of polymer-layered silicate (clay) nanocomposites by transmission electron microscopy and X-ray diffraction: a comparative study. J. Appl. Polym. Sci. 87, 1329–1388.

Paul, D.R., Robeson, L.M., 2008. Polymer nanotechnology: nanocomposites. Polymer 49, 3187–3204.

Pavličević, J., Špírková, M., Sinadinović-Fišer, S., Budinski-Simendić, J., Govedaric, O., Janković, M., 2013. The influence of organoclays on the morphology, phase separation and thermal properties of polycarbonate-based polyurethane hybrid materials, Macedon. J. Chem. Eng. 32, 151–161.

Prado, M.A., Dias, G., Carone, C., Ligabue, R., Dumas, A., Roux, C., Micoud, P., Martin, F., Einloft, S., 2015. Synthetic Ni-talc as filler for producing polyurethane nanocomposites. J. Appl. Polym. Sci. 132, 41854.

Ray, S.S., Okamoto, M., 2003. Polymer/layered silicate nanocomposites: a review from preparation to processing. Prog. Polym. Sci. 28, 1539–1641.

Saha, C., Chaki, T.K., Singha, N.K., 2013. Synthesis and characterization of elastomeric polyurethane and PU/clay nanocomposites based on an aliphatic diisocyanate. J. Appl. Polym. Sci. 130, 3328–3334.

Shunmugasamy, V.C., Xiang, C., Gupta, N., 2015. Clay/polymer nanocomposites: Processing, properties, and applications. In: Hybrid and Hierarchical Composite Materials. Springler International Publishing, pp. 161–200.

Soulié, M., Frongia, C., Lobjois, V., Fery-Forgues, S., 2015. Fluorescent organic ion pairs based on berberine: counter-ion effect on the formation of particles and on the uptake by colon cancer cells. RSC Adv. 5, 1181–1190.

Soulié, M., Carayon, C., Saffon, N., Blanc, S., Fery-Forgues, S., 2016. A comparative study of nine berberine salts in the solid state: optimization of the photoluminescence and self-association properties through the choice of the anion. Phys. Chem. Chem. Phys. 18, 29999–30008.

Suzuki, Y., Tenma, Y., Nishioka, Y., Kamada, K., Ohta, K., Kawamata, J., 2011. Efficient two-photon absorption materials consisting of cationic dyes and clay minerals. J. Phys. Chem. C 115, 20653–20661.

Taheri, S., Sadeghi, G.M.M., 2015. Microstructure–property relationships of organo-

montmorillonite/polyurethane nanocomposites: influence of hard segment content. Appl. Clay Sci. 114, 430–439.
Verma, G., Kaushik, A., Ghosh, A.K., 2013. Comparative assessment of nano-morphology and properties of spray coated clear polyurethane coatings reinforced with different organoclays. Prog. Org. Coat. 76, 1046–1056.
Yousfi, M., Livi, S., Dumas, A., Le Roux, C., Crépin-Leblond, J., Greenhill-Hooper, M., Duchet-Rumeau, J., 2013. Use of new synthetic talc as reinforcing nanofillers for polypropylene and polyamide 6 systems: thermal and mechanical properties. J. Colloid Interface Sci. 403, 29–42.
Yousfi, M., Livi, S., Dumas, A., Crépin-Leblond, J., Greenhill-Hooper, M., Duchet-Rumeau, J., 2014. Compatibilization of polypropylene/polyamide 6 blends using new synthetic nanosized talc fillers: morphology, thermal, and mechanical properties. J. Appl. Polym. Sci. 131, 46197.
Zhang, M., Hui, Q., Lou, X.J., Redfern, S.A., Salje, E.K., Tarantino, S.C., 2006. Dehydroxylation, proton migration, and structural changes in heated talc: an infrared spectroscopic study. Amer. Miner. 91, 816–825.
Zhang, S.W., Liu, R., Jiang, J.Q., Yang, C., Chen, M., Liu, X.Y., 2011. Facile synthesis of waterborne UV-curable polyurethane/silica nanocomposites and morphology, physical properties of its nanostructured films. Prog. Org. Coat. 70, 1–8.
Zhang, Z., Chen, Y., Deng, J., Jia, X., Zhou, J., Lv, H., 2014. Solid dispersion of berberine–phospholipid complex/TPGS 1000/SiO_2: preparation, characterization and *in vivo* studies. Int. J. Pharm. 465, 306–316.
Zhong, J., Li, Z., Guan, W., Lu, C., 2017. Cation-π interaction triggered-fluorescence of clay fillers in polymer composites for quantification of three-dimensional macrodispersion. Anal. Chem. 89, 12472–12479.
Zhou, Y., Rangari, V., Mahfuz, H., Jeelani, S., Mallick, P.K., 2005. Experimental study on thermal and mechanical behavior of polypropylene, talc/polypropylene and polypropylene/clay nanocomposites. Mater. Sci. Eng. A 402, 109–117.

4.3. Nanocompósitos ternários híbridos PU/talco sintético/argila: propriedades térmicas, mecânicas e morfológicas

No artigo intitulado "*Hybrid PU/Synthetic Talc/Organic Clay Ternary Nanocomposites: Thermal, Mechanical and Morphological Properties*", publicado na revista "Polymer & Polymer Composites" é apresentado a síntese de nanocompósitos ternários utilizando dois talcos sintéticos (SSMMP 7h e 24h) com processos de tratamento hidrotérmico diferentes e uma argila comercial (SPR). As cargas foram adicionadas em 3% em massa em relação ao polímero puro, variando as proporções de talco sintético/argila (75:25/25:75). Os resultados foram comparados a materiais PU/SSMMP e PU/argila (SPR). Grau de dispersão e interações carga/polímero foram acompanhadas por FTIR, DRX, MEV, TEM e AFM. As cargas apresentaram uma boa dispersão (exfoliação). Propriedades mecânicas e térmicas foram avaliadas em relação aos nanocompósitos binários (PU/SSMMPs e PU/argila(SPR)).

Hybrid Pu/Synthetic Talc/Organic Clay Ternary Nanocomposites: Thermal, Mechanical and Morphological Properties

Guilherme Dias[1], Manoela Prado[1], Rosane Ligabue[1,2], Mathilde Poirier[3], Christophe Le Roux[3], Pierre Micoud[3], François Martin[3] and Sandra Einloft[1,2]

[1]Programa de Pós-Graduação em Engenharia e Tecnologia de Materiais (PGETEMA) – Pontifícia Universidade Católica do Rio Grande do Sul (PUCRS). Porto Alegre, Brazil
[2]Faculdade de Química (FAQUI) – Pontifícia Universidade Católica do Rio Grande do Sul (PUCRS). Porto Alegre, Brazil
[3]ERT 1074 géomatériaux – GET UMR 5563 CNRS - Université de Toulouse – Toulouse, France

Received: 20 July 2017, Accepted: 13 October 2017

ABSTRACT

Polyurethane (PU) nanocomposites filled with inorganic particles, aiming at the improvement of mechanical and thermal properties, are well known. Unlike previous work we describe here the combination of two fillers, synthetic talc (silico-metallic mineral particles-SSMMP) with distinct hydrothermal processes (SSMMP 7 h and 24 h) and organically-modified commercial clay (SPR), aiming towards development of new polyurethane ternary nanocomposites by *in situ* polymerisation. Fillers were added 3 wt.% of the mass of pristine polymer, with a ranging of weight proportions (75:25/25:75) of SSMMP and SPR. Results were compared to those for nanocomposites containing pure SSMMP and SPR fillers. Dispersion degrees and filler interactions with the polyurethane matrix were followed by FTIR, XRD, SEM, TEM and AFM techniques. Results showed that the fillers presented a good dispersion and were exfoliated/well dispersed in the polyurethane matrix. Thermal and mechanical properties of nanocomposites were evaluated in comparison to the binary nanocomposites (PU/SSMMP 7 h, PU/SSMMP 24 h and PU/SPR). All nanocomposites presented superior values of Young's modulus to that of pristine PU. Results evidenced that the blend of SSMMP and SPR fillers is an interesting strategy to improve thermal and mechanical properties of nanocomposites.

Keywords: polyurethane; synthetic talc; ternary nanocomposites; organic clay; mechanical properties

1. INTRODUCTION

Polyurethanes are multifunctional polymers whose properties can be easily tailored by changing their molecular structures of 'soft segment' and 'hard segment'. To improve polyurethane properties, a common method is to add inorganic particles to the polymer matrix. The high aspect ratio of reinforcing particles such as talc, mica, silica, clay and calcium carbonate is of great importance to further increase polymers thermo-mechanical properties[1]. The best performance of polymeric nanocomposites is achieved when the silicate layers are well dispersed in the polymer matrix. Depending on the polymer's degree of interaction with the layered silicate mineral particles, hybrids nanocomposites are obtained with structures ranging from intercalated to exfoliated[2–4]. Talc, a layered magnesium silicate mineral with ideal formula $Mg_3Si_4O_{10}(OH)_2$ is used as filler in composite materials to reduce their production costs, improve their physical and chemical properties, and/or to offer new functionalities[5,6]. Montmorillonite (MMT) is also a layered silicate, but its structure consists of octahedral sheet of alumina sandwiched between two external silica tetrahedrons. The specificity of MMT is due to the presence in the interlayer of hydrated cations. MMT is a swellable clay mineral[7]. Polymer/clay nanocomposites have become important due to their improvements in mechanical strength and stiffness, thermal stability and

*Correspondent author:
E-mail: einloft@pucrs.br

gas barrier properties[8–10]. Layered silicates have often been described in the literature as fillers due to the availability of clay materials[11]. Natural talc ores consist in a mixture of several minerals, exhibiting some cationic substitutions[12] and consequently are inhomogeneous in chemical structure, crystalline phase and size distribution[13]. Manufacture of synthetic talc with a well-defined chemical composition and high purity, besides the possibility of the crystallinity, particle size and layer thickness control is a viable alternative. For example, by varying by a few tens of degrees the temperature of hydrothermal reaction, the average particle size can vary by several hundreds of nanometres[14,15]. The advantage of polymer nanocomposites is that the improvement in their properties can be achieved with a low percentage of layered silicates[16]. Several matrix polymers have been used to obtain polymer-layered silicate nanocomposites including polyurethane[1–5,7,8,10,16–34], PMMA[9], blends[14,35–40], polypropylene[41–43], polyamides[44], polylactide[45,46], polystyrene[47] and EVA[48]. In previous studies, our group investigated the performance of PU/synthetic talc nanocomposites with different filler percentages. Best results were obtained when a loading of 3 wt.% was used[21–23]. To further improve the performance of nanocomposites, the use of filler mixtures has been described. Alavi et al. produced ternary nanocomposites of PP/talc/nanoclay resulting in materials showing a better filler dispersion and an increase in mechanical properties[49]. Aguilar et al. prepared PP-based nanocomposites with organically modified montmorillonite (oMMT) and different types of $CaCO_3$ via melt blending. The resulting materials presented enhanced dispersion and better mechanical and thermal properties[50]. Kodal et al. investigated the mechanical, thermal and morphological properties of PA6 hybrid composites containing talc and wollastonite[51]. Garmabi et al. produced HDPE/nanoclay/nano $CaCO_3$ nanocomposites evidencing that the co-incorporation of this fillers improved nanocomposites' mechanical properties[52].

In this work, new polyurethane based nanocomposites were obtained by *in situ* polymerisation by mixing synthetic silico-metallic mineral particles produced by different hydrothermal treatments; SSMMP 24 h/205°C (SSMMP 24 h) and SSMMP 7 h/315°C (SSMMP 7 h) and SPR clay in different weight proportions (75:25 and 25:75) of fillers (3 wt.% regarding the mass of pristine polyurethane) were obtained.

2. EXPERIMENTAL

2.1 Materials

Polycaprolactone diol (PCL) MM: 2000 g/mol by Aldrich, hexamethylene diisocyanate (HDI) by Merck; dibutyltin dilaurate (DBTDL) by Miracema-Nuodex Ind. and methyl ethyl ketone (MEK) by Merck were used as received. Magnesium acetate tetrahydrate $(CH_3COO)_2Mg.4H_2O$), sodium metasilicate pentahydrate ($Na_2SiO_3.5H_2O$), sodium acetate trihydrate ($CH_3COONa.3H_2O$) and acetic acid were used for the syntheses of SSMMP powders (24 h/205°C and 7 h/ 315°C). All reagents were purchased from Aldrich and used without any further purification[6]. Samples were prepared as described elsewhere[53]. Organically modified commercial clay Rheotix SPR was donated by Nokxeller. Fillers were added in a percentage of 3 wt% relative to the pristine polymer without any treatments. Proportions of 75:25/25:75 of synthetic talc and SPR clay respectively, were used.

2.2 Hybrid Nanocomposites Obtained by *in situ* Polymerisation

The dispersion of SSMMP and SPR clay (in the desired proportions) was carried out in ultrasound bath (40 kHz) for 60 min, utilising methyl ethyl ketone as solvent. A glass reactor of 500 mL equipped with five inputs was used to perform the reactions. Mechanical stirring, thermocouple (to maintain the temperature at 40°C), reflux system and an addition funnel were connected to the reaction system. The reaction occurred in one step. Polycaprolactone diol (PCL) MM: 2000 g/mol, hexamethylene diisocyanate (HDI) (molar ratio between PCL and HDI = 1.1:1), DBTDL as catalyst (0.1% regarding the mass of reagents) and methyl ethyl ketone (MEK) as solvent (≅100 mL) as well as the fillers were added to the reactor. First, PCL was heated to melt with MEK. After that, a mixture of SSMMP/SPR (in the desired proportions) and the catalyst (DBTDL) were placed in the reactor. HDI was placed slowly, at the end of its addition the reaction started and was kept under reflux for 2 h and 30 min in an inert atmosphere (N_2). Lastly, films with ≅ 0.1 mm of thickness were produced by casting and dried at room temperature.

2.3 Testing and Characterisation

2.3.1 X-ray Diffraction (XRD)

Fillers in a form of powder and hybrid nanocomposites in the form of films were analysed by X-ray diffraction (XRD) recorded on a Shimadzu XRD-7000 diffractometer with CuKα Bragg-Brentano geometry θ-θ radiations, between 5 and 80 degrees with a step size of 0.02 degrees, current of 40 kV and voltage of 30 mA.

2.3.2 Transmission Electron Microscopy (TEM)

Transmission electron microscopy (TEM) was used to determine the morphology and dispersion

degree of hybrid nanocomposites. Samples of the hybrid nanocomposites in the form of films were cryomicrotomed and samples of the fillers were dispersed in water to obtain TEM images, utilising the equipment Tecnai G2 T20 FEI operating at 200 kV.

2.3.3 Fourier Transfer-infrared (FTIR) Spectroscopy

Fourier transform infrared spectroscopy (FTIR-Perkin Elmer FTIR spectrometer model Spectrum 100) was used to reveal the structural properties of fillers (powders) and hybrid nanocomposites (films), scanned from 650–4000 cm^{-1} utilising a UATR accessory.

2.3.4 Thermogravimetric Analysis (TGA)

Thermogravimetric analysis were performed to ascertain the thermal decomposition of pristine PU and hybrid nanocomposites in a SDT equipment (TA Instruments Model Q600), tests were carried out in a temperature range from 25°C to 800°C with a heating rate of 20°C min^{-1} under constant N_2 flow, utilising pristine PU and hybrid nanocomposites films and performed in triplicate.

2.3.5 Differential Scanning Calorimetry (DSC)

Melting temperature (Tm) and crystallisation temperature (Tc) of pristine PU and hybrid nanocomposites films were obtained by Differential Scanning Calorimetry (DSC) (TA Instruments model Q20 equipment). The tests were carried out under N_2 in a temperature range from −90°C to 200°C with a heating/cooling rate of 10°C min^{-1}, in two heating cycles.

2.3.6 Dynamic Mechanical Analysis (DMA)

Tensile tests (stress/strain) of pristine PU and hybrid nanocomposites were performed in DMTA equipment (TA Instruments Model Q800); tests were carried out at 25°C with rectangular shape films (thickness ~0.10 mm, length 12 mm, width ~7.0 mm) at 1 N min^{-1}. ASTMD638 was used to determine the Young moduli of samples. Analyses were carried out in triplicate until the rupture of samples.

2.3.7 Field Emission Scanning Electron Microscopy (FESEM)

Field emission scanning electron microscopy (FESEM) analyses were performed in FEI Inspect F50 equipment in secondary electrons (SE) mode and used for assessment of filler distributions in the polymer matrix. The samples (films) were placed in a stub and covered with a thin gold layer.

2.3.8 Atomic Force Microscopy (AFM)

Atomic force microscopy (AFM) was used to collect roughness data of pristine PU and hybrid nanocomposites. The cryomicrotomed samples were used to obtain the data. Analyses were performed in tapping mode to construct phase/height contrast images at different locations on the top surface of the samples using a Bruker Dimension Icon PT equipped with a TAP150A probe (Bruker, resonance frequency of 150 kHz and 5 N m^{-1} spring constant). The equipment was calibrated prior sample measurements. Scanned area of the images was 5 × 5 μm^2 with a resolution of 512 frames per area.

3. RESULTS AND DISCUSSIONS

3.1 X-ray Diffraction Analysis (XRD)

Crystalline structure of fillers (SSMMP 7 h and SPR clay) and hybrid nanocomposites were evaluated by XRD (**Figure 1**). The XRD pattern for SSMMP 7 h (**Figure 1g**) presents low intensity enlarged peaks meaning synthetic talc are formed by coherent domains with a small number of layers[14,22,23]; evidencing that crystal sizes of synthetic talc are smaller than those of natural talc which present well-defined and intense peaks in the XRD spectrum[6,22,23].

The diffractograms of fillers and hybrid nanocomposites indicated that the peak associated with the fillers ($2\theta \cong 20°$) disappeared in the nanocomposites diffractograms, indicating a good dispersion of the fillers and suggesting that silicate layers are exfoliated within the polymeric chains[33]. Baniasadi et al. described the same behaviour for PP/clay nanocomposites synthesised by *in situ* polymerisation[41]. Garmabi et al. noticed that for HDPE/nanoclay/nano $CaCO_3$, the intensity of ternary nanocomposites X-ray peaks were reduced, indicating intercalated/exfoliated morphology[52]. Likewise the diffraction peak associated with the polyurethane crystalline phase decreases for the hybrid nanocomposites indicating that the filler is well dispersed into the polymer matrix due to the interaction filler–polymeric chain[24,25]. It can be highlighted that even with two fillers mixed into the polyurethane matrix, a good dispersion was obtained, presumably due to the fillers hydroxyl groups interacting with the polyurethane chains[21,24,25].

3.2 Transmission Electron Microscopy (TEM)

From TEM images (**Figure 2** and **Figure 3**), it can be seen that for all systems individual particles and some local aggregates are present. TEM images also demonstrated that the combination of fillers did not

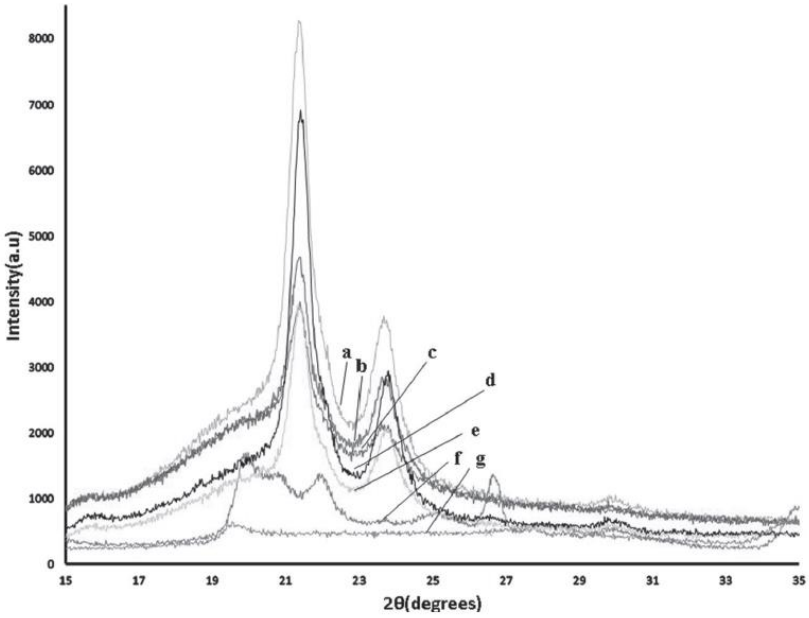

Figure 1. X-ray diffractogram patterns (a) PU, (b) PU/SSMMP 7 h+SPR 3% 25:75, (c) PU/SSMMP 7 h+SPR 3% 75:25, (d) PU/SPR 3%, (e) PU/SSMMP 7 h 3%, (f) SPR clay and (g) SSMMP 7 h

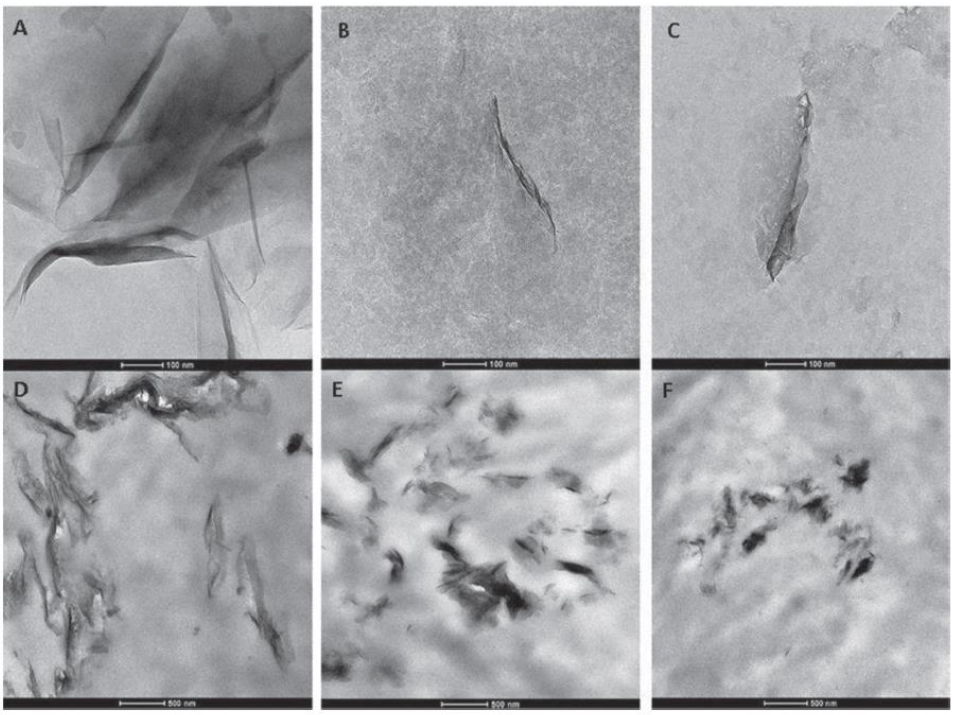

Figure 2. TEM micrographs of (a) SPR clay, (b) SSMMP 7 h, (c) SSMMP 24 h, (d) PU/SPR 3%, (e) PU/SSMMP 7 h 3% and (f) PU/SSMMP 24 h 3%

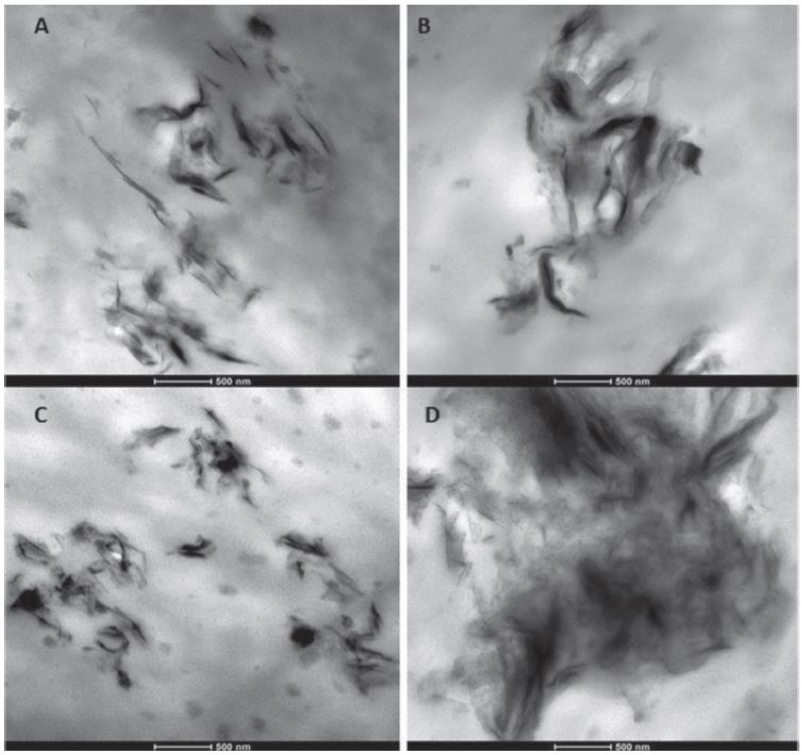

Figure 3. TEM micrographs of (a) PU/SSMMP7h+SPR 3% 75:25, (b) PU/SSMMP 7 h+SPR 3% 25:75, (c) PU/SSMMP 24 h+SPR 3% 75:25 and (d) PU/SSMMP 24 h+SPR 3% 25:75

negatively affect their good dispersion. Dark entities indicate the cross-section of intercalated or stacked clay layers; these stacked silicate layers are due to agglomeration. The bright fields in TEM micrograph represent the matrix[4,45,48].

As seen in TEM micrographs (**Figure 2** D-F and **Figure 3**), some intercalated structures can be seen along with exfoliated ones. Yet, XRD results indicated the presence of exfoliated morphology, probably related to the fact that the total number of intercalated structures, was too insignificant to provide a prominent peak in XRD diffractogram[10]. **Figure 2** and **Figure 3** prove that the layers are arranged parallel and well dispersed in the polyurethane matrix probably reflecting in the thermal and mechanical properties[7].

3.3 Fourier Transform Infrared Spectroscopy (FTIR)

FTIR was performed to evaluate the structure of hybrid nanocomposites, the fillers (SSMMPs and SPR clay) and the neat PU, as seen in **Figure 4-I**. Bands assignments of SSMMPs and SPR clay were fulfilled regarding the characteristic vibrational modes described in literature. In the spectrum of SPR clay (**Figure 4-Ig**), it can be seen that clay particles produced characteristic bands associated with stretching vibration of Si—O in Si—O—Si groups of tetrahedral sheet around 1000 cm^{-1} and small bands at 915 and 800 cm^{-1} assigned to Si—O stretching and Al—Al—OH and Al—Mg—OH (present on the edges of the clay platelets) hydroxyl bending vibrations. The absorption band at 3626 cm^{-1} is assigned to stretching vibrations of Al—OH and the hydrogen-bonded water bending band at 1633 cm^{-1}. Bands at 2930 and 2858 cm^{-1} were due to the asymmetric and symmetric –CH stretching vibrations related to the alkylammonium group, at 1460 cm^{-1} for C-H bending, and around 753 cm^{-1} the symmetric Si—O—Si stretching mode is observed[4,19,54].

In the spectrum of neat SSMMP 7 h (**Figure 4-If**), the Mg_3OH band appears at 3679 cm^{-1} and the bands around 3400 cm^{-1} and 1629 cm^{-1} are related to

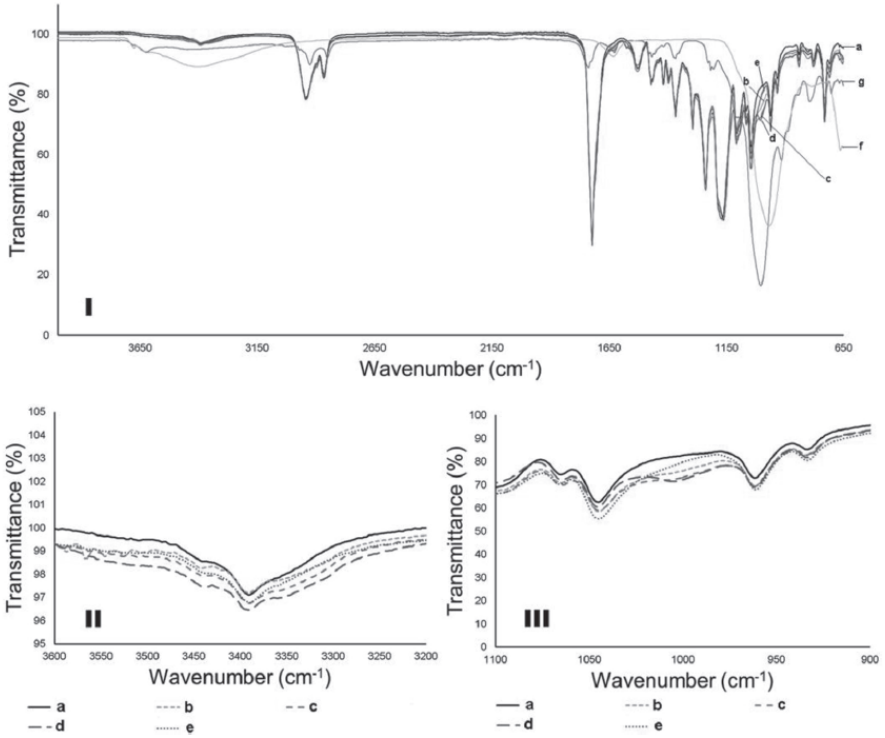

Figure 4. FTIR spectra of (a) PU pure, (b) PU/SSMMP 7 h+SPR 3% 25:75, (c) PU/SSMMP 7 h+SPR 3% 75:25, (d) PU/SSMMP 7 h 3%, (e) PU/SPR 3%, (f) SSMMP 7 h and (g) SPR clay in different wavenumber I (4000–650 cm^{-1}), II (3600–3200 cm^{-1}) and III (1100–900 cm^{-1})

the (Mg_2) O—H stretching[12]. At 1000 and 990 cm^{-1}, stretching vibrations of Si—O—Si appeared[12,22,23,55,56]. For neat PU, hybrid nanocomposites PU/SSMMP 7 h+SPR 75:25 3%, PU/SSMMP 7 h+SPR 25:75 3% and the nanocomposites PU/SSMMP 7 h 3% and PU/SPR 3% (**Figure 4-Ia-e**), the band at 3396 cm^{-1} corresponds to the urethane bonds (NH). Bands at 2946 and 2862 cm^{-1} are related to CH_2 vibrational modes. The C═O band of the urethane bonds appears at 1725 cm^{-1}. Bands around 1536 cm^{-1} represent the CN and NH bonds of the urethane groups. CO—O group bands at 1243 and 1172 cm^{-1}, and the band at 730 cm^{-1} corresponds to other vibrational modes of the CH_2 group[20–25,33]. In **Figure 4-II**, the augmentation of the band around 3400 cm^{-1} for the nanocomposites indicates that available hydroxyl groups of fillers are interacting with N-H urethane bonds of the polyurethane chains[20–25]. In **Figure 4-III**, the FTIR spectra of the nanocomposites present a new band near 1000 cm^{-1}, that can be associated with Si—O and Si—O—Si bonds stretching vibrational modes of the fillers, attesting that the fillers are incorporated into the polyurethane matrix, as noticed by our group in previous studies[22–25].

3.4 Thermogravimetric Analysis (TGA)

An increase on onset temperatures of hybrid nanocomposites with filler addition (**Figure 5**) was evidenced. Neat PU presented the lowest degradation temperature (302°C). The presence of blended fillers improved thermal stability of the hybrids (PU/SSMMP 7 h+SPR clay ≅ 336°C and PU/SSMMP 24 h+SPR clay ≅ 337°C). It can be highlight that the nanocomposites with SSMMPs presented higher values of degradation temperature[22,23] compared to the nanocomposite with SPR clay (PU/SSMMP 7 h, 340°C; PU/SSMMP 24 h, 337°C and PU/SPR, 326°C). This behaviour can be associated with filler dispersion into the polyurethane matrix. PU/SSMMP nanocomposites are better exfoliated[22,23] than PU/SPR nanocomposite, corroborating with TEM discussions. Also, SSMMPs even at lower concentrations appears to be more important when thermal properties are evidenced.

Observing DTG curves (%/°C) (**Figure 6**), an augmentation of the second peak is noticed in samples with SSMMP and SSMMP+SPR clay. In the SPR clay

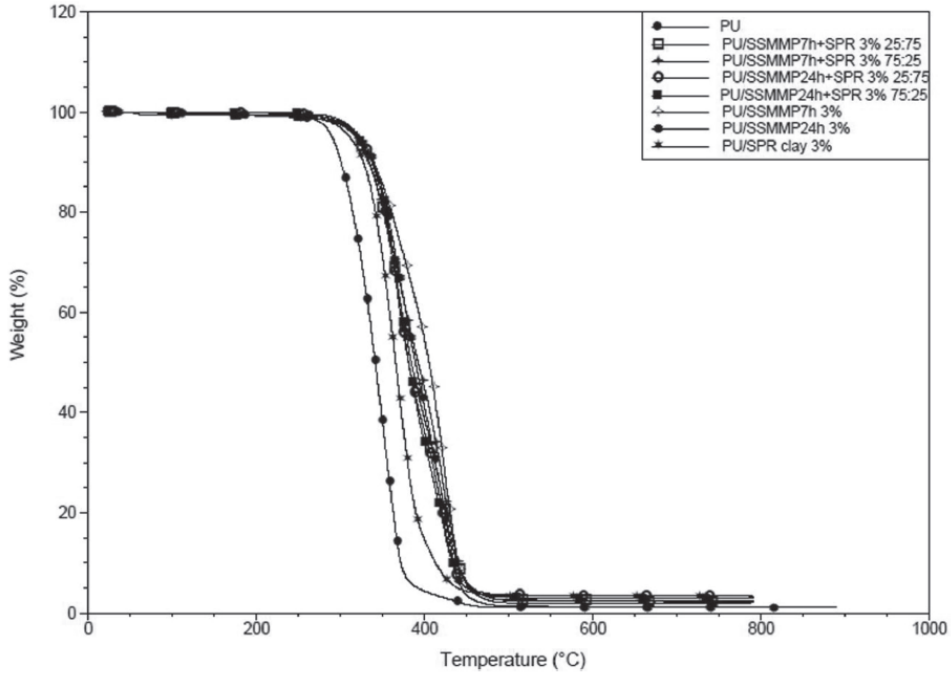

Figure 5. TGA curves for the pristine PU and the hybrid nanocomposites

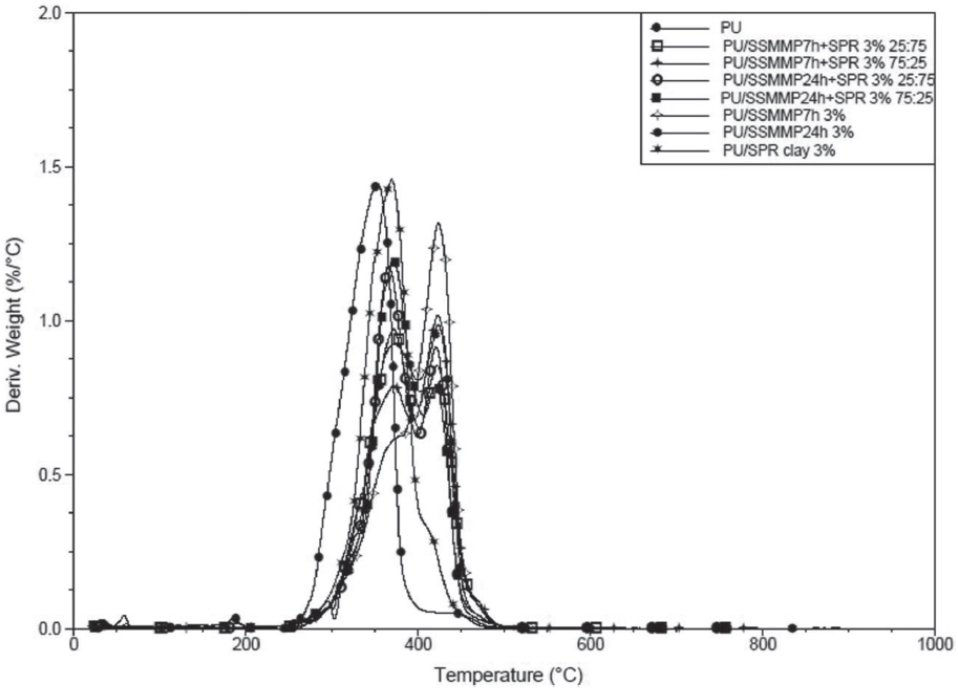

Figure 6. DTGA curves (%/°C) versus temperature of the pristine PU and the hybrid nanocomposites

Table 1. Results obtained by DSC analysis for the nanocomposites

Samples	Tc (°C)	Tm (°C)	△Hc (J/g)	ΔHm (J/g)
PU	0.26	37.61	33.40	33.49
PU/SSMMP7 h+SPR 3% 75:25	1.49	37.34	30.91	31.52
PU/SSMMP7 h+SPR 3% 25:75	−0.56	37.34	28.25	29.32
PU/SSMMP24 h+SPR 3% 75:25	0.33	37.77	33.80	35.34
PU/SSMMP24 h+SPR 3% 25:75	−1.53	37.45	28.60	32.11
PU/SSMMP7 h 3%	6.31	40.24	39.85	39.40
PU/SSMMP24 h 3%	5.95	40.10	40.75	41.92
PU/SPR 3%	8.29	44.79	41.12	42.96

sample, this behaviour was not observed. The hydroxyl groups of SSMMP can form a network structure with polyurethane chains as described in literature[22,23,44] and be responsible for the appearing of the second peak on DTG curves (**Figure 6**).

As described elsewhere thermal stability of pristine PU is improved by the presence of clay-layered crystals, which form a maze or 'tortuous path' in the PU matrix[10]. The incorporation of clay into the polymer matrix enhanced thermal stability by acting as a superior insulator and mass transport barrier to volatile products. These results can be attributed to dispersion and barrier effects of the clay layers against oxygen diffusion through the matrix[26,31,32,41,45].

3.5 Differential Scanning Calorimetry (DSC)

Table 1 presents the crystallisation temperatures (Tc) of hybrid nanocomposites. Tc temperatures of hybrid nanocomposites slightly changed once compared to neat PU, suggesting that the nucleating effect of the combined fillers is less important than when they are not blended. When fillers are combined the exfoliated structures restrict the movement of the polymeric chains retarding the crystallisation of the matrix[57]. For samples obtained with SSMMP (7 h and 24 h) and SPR clay an increase in the crystallisation temperatures values were observed. This behaviour is well known when talc and clay are added as fillers, and it is frequently reported that plate-like fillers are good nucleating agents because of their high aspect ratios[22,24,41,42,45]. For melting temperatures values the same behaviour was observed.

3.6 Dynamic Mechanical Analysis (DMA)

Stress–strain results are seen in **Figure 7**. All hybrid nanocomposites with SSMMP 7 h/24 h/SPR clay samples presented greater values of stress to small deformations when compared to PU. Fillers addition made the materials more rigid, most likely because the fillers (SSMMPs and SPR clay) and the polyurethane matrix formed crosslinks resulting from hydrogen bonding, as seen in FTIR[20–25].

Figure 8 exhibits the Young's modulus for neat polyurethane and hybrid nanocomposites. Young's modulus values presented a significant augmentation, suggesting that the materials stiffness at lower stress was affected as usual by fillers incorporation. The nanocomposite filled with SPR clay presented the higher value (366 MPa). The nanocomposite filled with SSMMP 7 h+SPR clay 25:75 presented a larger value for Young's modulus of 238 MPa, while the pristine PU presented 92 MPa (**Figure 8**). SSMMPs seem to influence directly mechanical behaviour of hybrids. But Young's Modulus augmentation is more pronounced when SPR clay is added. Young's modulus augmentation is attributed to the reinforcement provided by the dispersed fillers with a large aspect ratio, which reduces the molecular mobility of polymer chains, consequently stiffening the material[22,33]. Garmabi et al. described that for HDPE/nanoclay/nano $CaCO_3$ systems the reinforcing effect of the nanoclay was superior to $CaCO_3$, due to the nanoclay's large aspect ratio[52].

Therefore, the increase in the Young's modulus can be associated with the interfacial interaction between silicate layers and polyurethane matrix[17,29,43,45]. The surface area and shape play an important role in these properties. Yousfi et al. also related a significant increase of 39.4% on the Young's Modulus in PP/PA6 blends filled with synthetic talc (1880 MPa for the PP/PA6 blends and 2620 MPa with synthetic talc)[14] and our group noticed a maximum increment to the sample PU/synthetic Ni-talc 1 wt%, which presented an increase of 5.7% when compared to pristine PU, and an increase

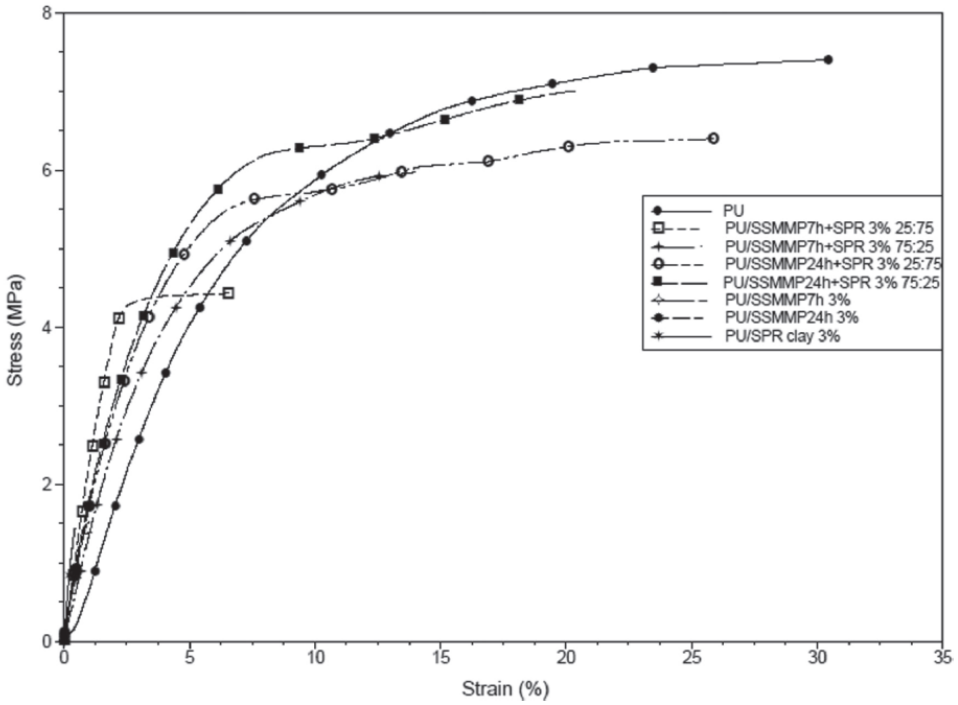

Figure 7. Stress x Strain, by DMA, for the hybrid nanocomposites and pristine PU

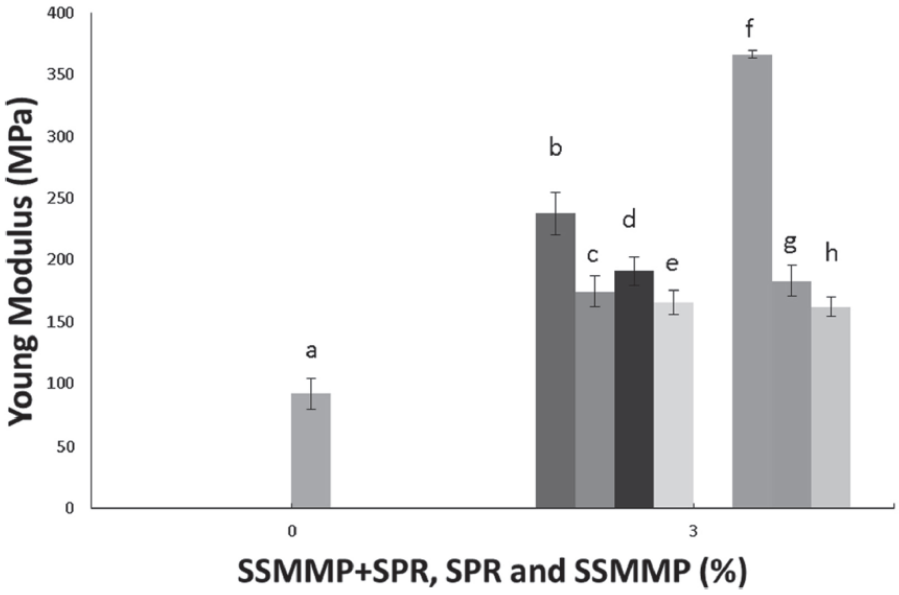

Figure 8. Young's modulus values for hybrid nanocomposites and pristine PU (a) PU Pure; (b) PU SSMMP 7 h+SPR 3% 25:75; (c) PU SSMMP 7 h+SPR 3% 75:25; (d) PU SSMMP 24 h+SPR 3% 25:75, (e) PUSSMMP 24 h+SPR 3% 75:25, (f) PU/SPR clay 3%, (g) PU/SSMMP 7 h 3% and PU/SSMMP 24 h 3%

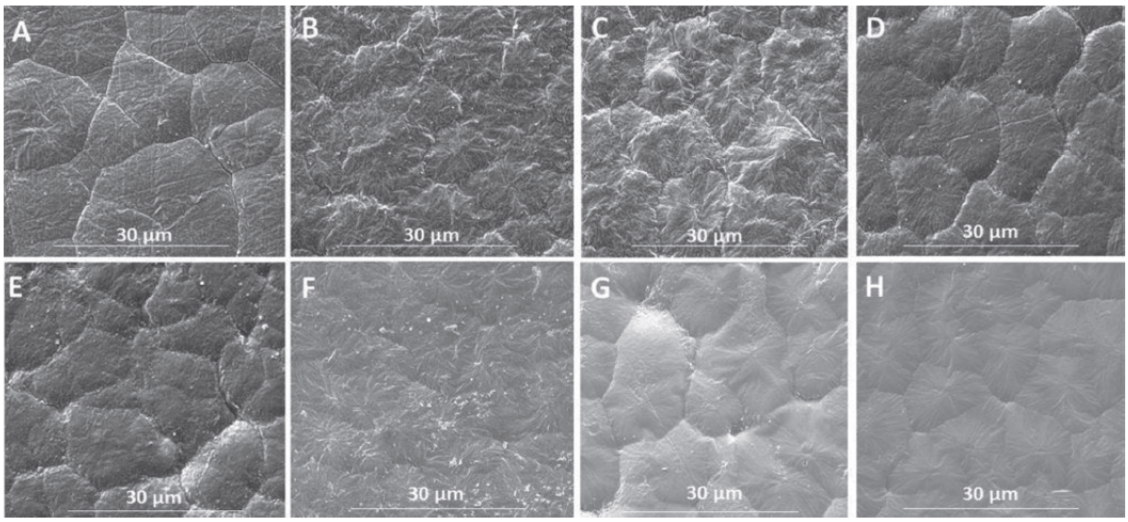

Figure 9. Micrographs, mode SE, of the materials at magnification of 5000x. (a) PU pure, (b) PU/SSMMP 7 h+SPR 3% 75:25, (c) PU/SSMMP 7 h+SPR 3% 25:75, (d) PU/SSMMP 24 h+SPR 3% 75:25, (e) PU/SSMMP 24 h+SPR 3% 25:75, (f) PU/SSMMP 7 h 3%, (g) PU/SSMMP 24 h 3% and (h) PU/SPR 3%

of 65% on the sample PU/SSMMP 7 h 3 wt%[21,22]. Therefore, when both fillers are placed together into the polyurethane matrix it is possible to obtain hybrid nanocomposites with superior mechanical properties.

3.7 Field Emission Scanning Electron Microscopy (FESEM)

On the basis of the morphological study of the prepared hybrid materials, as seen in **Figure 9**, it can be noticed that the achieved dispersion of the fillers into the polyurethane matrix was uniform and homogeneous[37]. Defects and stress concentration sites are prevented without the formation of agglomerated particles[22,35]. Good filler dispersion generated a superior contact area between matrix/filler, switching molecular mobility and consequently thermo-mechanical properties of the matrix[22,29]. **Figure 9** evidences that nucleation sites were formed in all hybrid nanocomposites; these morphological changes associated with a good dispersion of fillers and fillers-polymer interaction are probably promoting the different thermo-mechanical properties of hybrid nanocomposites[22,24].

Figure 10 shows SEM images of cryogenically fractured surface of pristine PU and hybrid nanocomposites. For pristine PU (**Figure 10A**), the appearance of grooves occurred randomly distributed on the cryo-fractured surface which looks more flat and smoother, presenting no important voids[22,23]. A different behaviour can be seen for the hybrid nanocomposites' cryo-fractured surfaces (**Figure 10B-H**). Hybrid nanocomposites presented a rough cryo-fractured surface full of voids and cracks. Similar results were found for PU/synthetic talcs, PLA/talc, PLA/clay and PLA blends composites[23,38,39,46]. An increase in the clay content modified the fracture profile, with an increase of the surface roughness, corroborating with mechanical properties results.

3.8 Atomic Force Microscopy (AFM)

A 3D height image of pristine PU and hybrid nanocomposites is shown in **Figure 11**. The hard segments appear bright due to their higher hardness, which resist penetration by the AFM probe tip. The soft segments appear with a darker contrast as they can be penetrated relatively easily by the AFM probe tip[10]. Addition of SSMMPs and SPR clay affected the morphology of this hard-soft segmental arrangement, especially when the interactions were on the nanoscale. With the addition of fillers, average roughness (Ra), root mean square roughness (Rq) and maximum height roughness (Rmax) had increased (**Table 2**). The higher values of these parameters comparing to pristine PU confirms the presence of filler particles on the surface, as reported in literature[31]. It can be seen from **Figure 11** that the layers of the fillers are well distributed both in soft and hard domain of the matrix. The presence of hydroxyl groups in both fillers seemed to significantly

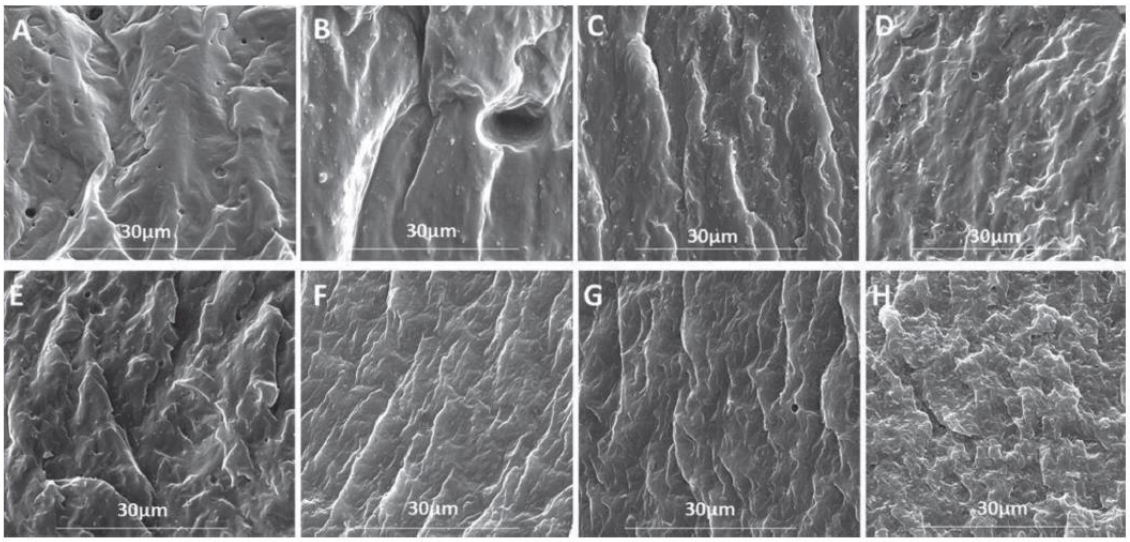

Figure 10. Micrographs from fractures, mode SE, of the materials at magnification of 5000x. (a) PU Pure, (b) PU/SSMMP 7 h+SPR 3% 75:25, (c) PU/SSMMP 7 h+SPR 3% 25:75, (d) PU/SSMMP 24 h+SPR 3% 75:25, (e) PU/SSMMP 24 h+SPR 3% 25:75, (f) PU/SSMMP 7 h 3%, (g) PU/SSMMP 24 h 3% and (h) PU/SPR 3%

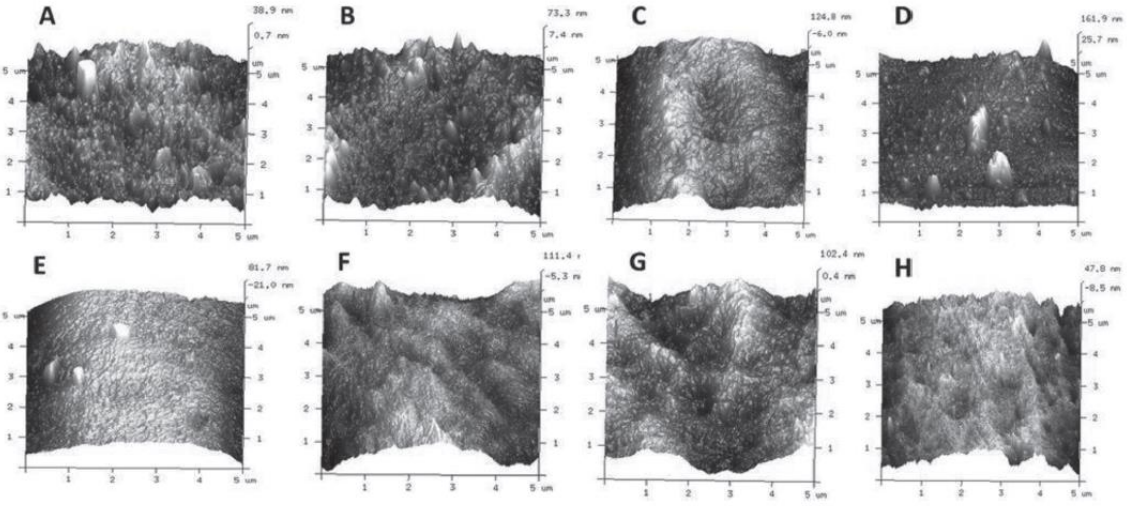

Figure 11. AFM images (height) (a) PU, (b) PU/SSMMP 7 h+SPR 3% 75:25, (c) PU/SSMMP 7 h+SPR 3% 25:75, (d) PU/SSMMP 24 h+SPR 3 % 75:25, (e) PU/SSMMP 24 h+SPR 3% 25:75, (f) PU/SSMMP 7 h 3%, (g) PU/SSMMP 24 h 3% and (h) PU/SPR 3%

influence the interactions between its layers and polyurethane chains[32].

4. CONCLUSIONS

Ternary nanocomposites were prepared by in situ polymerisation utilising SSMMPs and SPR clay as fillers, proving that it is possible to blend these fillers together. Structural analyses (XRD and FTIR) allied to morphological tests (TEM, SEM and AFM) demonstrated that the fillers are well dispersed/exfoliated into the polymeric matrix leading to nanocomposites PU/SSMMP/SPR with superior thermal and mechanical properties. Using blended fillers into a polyurethane

Table 2. Average roughness (Ra); root mean square roughness (Rq); maximum height roughness (Rmax) for the hybrid nanocomposites

Samples	Ra (nm)	Rq (nm)	Rmax (nm)
PU Pure	7.95	11	136
PU/SSMMP 7 h+SPR 3% 75:25	13.7	18	138
PU/SSMMP 7 h+SPR 3% 25:75	32.9	41.3	236
PU/SSMMP 24 h+SPR 3% 75:25	20.2	29.1	290
PU/SSMMP 24 h+SPR 3% 25:75	28.8	35	244
PU/SSMMP 7 h 3%	24.4	31.7	244
PU/SSMMP 24 h 3%	24.9	31.3	199
PU/SPR 3%	16.4	13.2	144

matrix results in materials that can perform functions that require high thermal and mechanical performance. These results corroborate previous studies showing that synthetic talcs are interesting to the development of materials with distinguished properties, and may also be combined with other fillers.

ACKNOWLEDGEMENTS

The authors would like to thank CAPES and CNPq for doctorate, post-doc and research scholarship. Also to Nokxeller – Microdispersions for providing SPR clay.

REFERENCES

1. X. Zhang, R. Xu, Z. Wu, C. Zhou, The synthesis and characterization of polyurethane/clay nanocomposites *Polymer International*, **52** (2003), 790–794.
2. B. Finnigan, D. Martin, P. Halley, R. Truss, K. Campbell, Morphology and properties of thermoplastic polyurethane nanocomposites incorporating hydrophilic layered silicates, *Polymer*, **45** (2004), 2249–2260.
3. N. Salahuddin, S.A. Abo-El-Enein, A. Selim, O.S. El-Dien, Synthesis and characterization of polyurethane/organo-montmorillonite nanocomposites, *Applied Clay Science*, **47** (2010), 242–248.
4. A.K. Barick, D.K. Tripathy, Effect of organically modified layered silicate nanoclay on the dynamic viscoelastic properties of thermoplastic polyurethane nanocomposites, *Applied Clay Science*, **52** (2011), 312–321.
5. G. Zhao, T. Wang, Q. Wang, Studies on wettability, mechanical and tribological properties of the polyurethane composites filled with talc, *Applied Surface Science*, **258** (2012), 3557–3564.
6. A. Dumas, F. Martin, C. Le Roux, P. Micoud, S. Petit, E. Ferrage, J. Brendlé, O. Grauby, M. Greenhill-Hooper, Phyllosilicates synthesis: a way of accessing edges contributions in NMR and FTIR spectroscopies. Example of synthetic talc, *Physics and Chemistry of Minerals*, **40** (2013), 361–373.
7. C. Saha, T.K. Chaki, N.K. Singha, Synthesis and characterization of elastomeric polyurethane and PU/clay nanocomposites based on an aliphatic diisocyanate, *Journal of Applied Polymer Science*, **130** (2013), 3328–3334.
8. M. Strankowski, J. Strankowska, M. Gazda, Ł. Piszczyk, G. Nowaczyk, S. Jurga, Thermoplastic polyurethane/(organically modified montmorillonite) nanocomposites produced by in situ polymerization, *Express Polymer Letters*, **6** (2012).
9. T.Y. Tsai, M.J. Lin, Y.C. Chuang, P.C. Chou, Effects of modified clay on the morphology and thermal stability of PMMA/clay nanocomposites, *Materials Chemistry And Physics*, **138** (2013), 230–237.
10. S. Anandhan, H.S. Lee, Influence of organically modified clay mineral on domain structure and properties of segmented thermoplastic polyurethane elastomer, *Journal of Elastomers & Plastics*, **46** (2014), 217–232.
11. S. Livi, J. Duchet-Rumeau, T.N. Pham, J.F. Gérard, Synthesis and physical properties of new surfactants based on ionic liquids: improvement of thermal stability and mechanical behaviour of high density polyethylene nanocomposites, *Journal of Colloid and Interface Science*, **354** (2011), 555–562.
12. F. Martin, P. Micoud, L. Delmotte, C. Marichal, R. Le Dred, P. De Parseval, A. Mari, J.P. Fortune, S. Salvi, D. Beziat, O. Grauby, J. Ferret, The structural formula of talc from the Trimouns deposit, Pyrénées, France, *The Canadian Mineralogist*, **37** (1999), 997–1006.
13. F. Martin, *International Patent*, 081046 (2009).
14. M. Yousfi, S. Livi, A. Dumas, C. Le Roux, J. Crépin-Leblond, M. Greenhill-Hooper, J. Duchet-Rumeau, Use of new synthetic talc as reinforcing nanofillers for polypropylene and polyamide 6 systems: thermal and mechanical properties, *Journal of Colloid and Interface Science*, **403** (2013), 29–42.
15. A. Dumas, F. Martin, E. Ferrage, P. Micoud, C. Le Roux, S. Petit, Synthetic talc advances: Coming closer to nature, added value, and industrial requirements, *Applied Clay Science*, **85** (2013), 8–18.
16. M. Song, D.J. Hourston, K.J. Yao, J.K. Tay, M.A. Ansarifar, High performance nanocomposites of polyurethane elastomer and organically modified layered silicate, *Journal of Applied Polymer Science*, **90** (2003), 3239–3243.
17. H. Jin, J.J. Wie, S.C. Kim, Effect of organoclays on the properties of polyurethane/clay nanocomposite

coatings, *Journal of Applied Polymer Science*, **117** (2010), 2090–2100.

18. A.F. Osman, K. Jack, G. Edwards, D. Martin, Effect of processing route on the morphology of thermoplastic polyurethane (TPU) nanocomposites incorporating organofluoromica, *In Advanced Materials Research*, **832** (2014), 27–32.
19. S. Taheri, G.M. Sadeghi, Microstructure–property relationships of organo-montmorillonite/polyurethane nanocomposites: Influence of hard segment content, *Applied Clay Science*, **114** (2015), 430–439.
20. V.D. da Silva, L.M. dos Santos, S.M. Subda, R. Ligabue, M. Seferin, C.L. Carone, S. Einloft, Synthesis and characterization of polyurethane/titanium dioxide nanocomposites obtained by in situ polymerization, *Polymer Bulletin*, **70** (2013), 1819–1833.
21. M.A. Prado, G. Dias, C. Carone, R. Ligabue, A. Dumas, C. Le Roux, P. Micoud, F. Martin, S. Einloft, Synthetic Ni-talc as filler for producing polyurethane nanocomposites, *Journal of Applied Polymer Science*, **132** (2015).
22. G. Dias, M.A. Prado, C. Carone, R. Ligabue, A. Dumas, F. Martin, C. Le Roux, P. Micoud, S. Einloft, Synthetic silico-metallic mineral particles (SSMMP) as nanofillers: comparing the effect of different hydrothermal treatments on the PU/SSMMP nanocomposites properties, Polymer *Bulletin*, **72** (2015), 2991–3006.
23. G. Dias, M. Prado, C. Carone, R. Ligabue, A. Dumas, C. Le Roux, P. Micoud, F. Martin, S. Einloft, Comparing different synthetic talc as fillers for polyurethane nanocomposites, *Macromolecular Symposia*, **367** (2016), 136–142.
24. L. M. dos Santos, R. Ligabue, A. Dumas, C. Le Roux, P. Micoud, J. F. Meunier, F. Martin, S. Einloft, New magnetic nanocomposites: Polyurethane/Fe_3O_4-synthetic talc, *European Polymer Journal*, **69** (2015), 38–49.
25. L.M. dos Santos, R. Ligabue, A. Dumas, C. Le Roux, P. Micoud, J. F. Meunier, F. Martin, M. Corvo, P. Almeioda, S. Einloft, Waterborne polyurethane/Fe_3O_4-synthetic talc composites: synthesis, characterization and magnetic properties, *Polymer Bulletin*, (2017), 1–16.
26. A. Dorigato, A. Pegoretti, A. Penati, Effect of the polymer-filler interaction on the thermo-mechanical response of polyurethane-clay nanocomposites from blocked prepolymer, *Journal of Reinforced Plastics and Composites*, **30** (2011), 325–335.
27. G. Verma, A. Kaushik, A.K. Ghosh, Preparation, characterization and properties of organoclay reinforced polyurethane nanocomposite coatings, *Journal of Plastic Film & Sheeting*, **29** (2013), 56–77.
28. M. Haghayegh, G. Mir Mohamad Sadeghi, Synthesis of shape memory polyurethane/clay nanocomposites and analysis of shape memory, thermal, and mechanical properties, *Polymer Composites*, **33** (2012), 843–849.
29. A. Kaushik, D. Ahuja, V. Salwani, Synthesis and characterization of organically modified clay/castor oil based chain extended polyurethane nanocomposites, *Composites Part A: Applied Science and Manufacturing*, **42** (2011), 1534–1541.
30. S.C. Amico, C.P. Freitag, I.C. Riegel, S.H. Pezzin, Efeito da incorporação de talco nas características térmicas, mecânicas e dinâmico-mecânicas de poliuretanos termoplásticos, *Revista Matéria*, **16** (2011), 597–605.
31. P.K. Maji, A.K. Bhowmick, Efficacy of clay content and microstructure of curing agents on the structure–property relationship of new-generation polyurethane nanocomposites, *Polymers for Advanced Technologies*, **23** (2012), 1311–1320.
32. G. Verma, A. Kaushik, A.K. Ghosh, Comparative assessment of nano-morphology and properties of spray coated clear polyurethane coatings reinforced with different organoclays, *Progress in Organic Coatings*, **76** (2013), 1046–1056.
33. S. Ramesh, K. Punithamurthy, The effect of organoclay on thermal and mechanical behaviours of thermoplastic polyurethane nanocomposites, *Digest Journal Of Nanomaterials And Biostructures*, **12** (2017), 331–338.
34. K. Malkappa, B.N. Rao, T. Jana, Functionalized polybutadiene diol based hydrophobic, water dispersible polyurethane nanocomposites: Role of organo-clay structure, *Polymer*, **99** (2016), 404–416.
35. Y. Zhou, V. Rangari, H. Mahfuz, S. Jeelani, P.K. Mallick, Experimental study on thermal and mechanical behavior of polypropylene, talc/polypropylene and polypropylene/clay nanocomposites, *Materials Science and Engineering: A*, **402** (2005), 109–117.
36. E. G Bajsić, V. Rek, B. O. Pavić, The influence of talc content on the thermal and mechanical properties of thermoplastic polyurethane/polypropylene blends, *Journal of Elastomers & Plastics*, **45** (2013), 501–522.
37. J. Pavlićević, M. Špírková, O. Bera, M. Jovičić, K.M. Szécsényi, J. Budinski-Simendić, The influence of bentonite and montmorillonite addition on thermal decomposition of novel polyurethane/organoclay nanocomposites, *Macedonian Journal of Chemistry and Chemical Engineering*, **32** (2013), 319–330.
38. Z.W. Liu, H.C. Chou, S.H. Chen, C.T. Tsao, C.N. Chuang, L.C. Cheng, C.H. Yang, C.K. Wang, K.H. Hsieh, Mechanical and thermal properties of thermoplastic polyurethane-toughened polylactide-based nanocomposites, *Polymer Composites*, **35** (2014), 1744–1757.

39. Y. Qin, J. Yang, M. Yuan, J. Xue, J. Chao, Y. Wu, M. Yuan, Mechanical, barrier, and thermal properties of poly(lactic acid)/poly (trimethylene carbonate)/talc composite films, *Journal of Applied Polymer Science*, **131** (2014).

40. M. Yousfi, S. Livi, A. Dumas, J. Crépin-Leblond, M. Greenhill-Hooper, J. Duchet-Rumeau, Compatibilization of polypropylene/polyamide 6 blends using new synthetic nanosized talc fillers: Morphology, thermal, and mechanical properties, *Journal of Applied Polymer Science*, **131** (2014).

41. H. Baniasadi, S. J S. A.A.R. Nikkhah, Investigation of in situ prepared polypropylene/clay nanocomposites properties and comparing to melt blending method, *Materials & Design*, **31** (2010), 76–84.

42. K. Wang, N. Bahlouli, F. Addiego, S. Ahzi, Y. Rémond, D. Ruch, R. Muller, Effect of talc content on the degradation of re-extruded polypropylene/talc composites, *Polymer Degradation and Stability*, **98** (2013), 1275–1286.

43. L.A. Castillo, S.E. Barbosa, N.J. Capiati, Influence of talc morphology on the mechanical properties of talc filled polypropylene, *Journal of Polymer Research*, **20** (2013), 152.

44. G.P. Balamurugan, S.N. Maiti, Effects of nanotalc inclusion on mechanical, microstructural, melt shear rheological, and crystallization behavior of polyamide 6-based binary and ternary nanocomposites, *Polymer Engineering & Science*, **50** (2010), 1978–1993.

45. A.K. Mohapatra, S. Mohanty, S.K. Nayak, Dynamic mechanical and thermal properties of polylactide-layered silicate nanocomposites, *Journal of Thermoplastic Composite Materials*, **27** (2014), 669–716.

46. T.F. Cipriano, A.L. Silva, A.H. Silva, A.M. Sousa, G.M. Silva, M.G. Rocha, Thermal, rheological and morphological properties of poly (lactic acid) (PLA) and talc composites, *Polímeros*, **24** (2014), 276–282.

47. A. Arora, V. Choudhary, D.K. Sharma, Effect of clay content and clay/surfactant on the mechanical, thermal and barrier properties of polystyrene/organoclay nanocomposites, *Journal of Polymer Research*, **18** (2011), 843–857.

48. H.M. Hassanabadi, D. Rodriguez, Effect of particle size and shape on the reinforcing efficiency of nanoparticles in polymer nanocomposites, *Macromolecular Materials and Engineering*, **299** (2014), 1220–1231.

49. S.M. Alavi, M. Esfandeh, J. Morshedian, Y. Jahani, Study of the Mechanical and Dynamic Mechanical Properties of Polypropylene/Talc/Nanoclay Ternary Nanocomposites, *Polymers & Polymer Composites*, **20** (2012), 299.

50. H. Aguilar, M. Yazdani-Pedram, P. Toro, R. Quijada, M. López-Manchado, Synergic effect of two inorganic fillers on the mechanical and thermal properties of hybrid polypropylene composites, *Journal of the Chilean Chemical Society*, **59** (2014), 2468–2473.

51. M. Kodal, S. Erturk, S. Sanli, G. Ozkoc, Properties of talc/wollastonite/polyamide 6 hybrid composites, *Polymer Composites*, **36** (2015), 739–746.

52. H. Garmabi, S.E.A. Tabari, A. Javadi, H. Behrouzi, G. Hosseini, An investigation on morphology and mechanical properties of HDPE/nanoclay/nano $CaCO_3$ ternary nanocomposites, *AIP Conference Proceedings*, **1713** (2016), 090005.

53. A. Dumas, C. Le Roux, F. Martin, P. Micoud, Process for preparing a composition comprising synthetic mineral particles and composition, WO2013004979 A1 (2013).

54. A.K. Mishra, S. Allauddin, R. Narayan, T.M. Aminabhavi, K.V. Raju, Characterization of surface-modified montmorillonite nanocomposites, *Ceramics International*, **38** (2012), 929–934.

55. J.D. Russell, V.C. Farmer, B. Velde, Replacement of OH by OD in layer silicates, and identification of the vibrations of these groups in infra-red spectra, *Mineralogical Magazine*, **37** (1970), 869–879.

56. M. Zhang, Q. Hui, X.J. Lou, S.A. Redfern, E.K. Salje, S.C. Tarantino, Dehydroxylation, proton migration, and structural changes in heated talc: An infrared spectroscopic study, *American Mineralogist*, **91** (2006), 816–825.

57. H. Chen, M. Wang, Y. Lin, C.M. Chan, J. Wu, Morphology and mechanical property of binary and ternary polypropylene nanocomposites with nanoclay and $CaCO_3$ particles, *Journal of Applied Polymer Science*, **106** (2007), 3409–3416.

4.4. Talco sintético como catalisador e carga na síntese de nanocompósitos de poliuretano base aquosa

No artigo intitulado “Synthetic talc as catalyst and filler for waterborne polyurethane based nanocomposites synthesis”, submetido na revista “Polymer Bulletin” talco sintético foi utilizado como catalisador e carga para a produção de nanocompósitos de poliuretano base aquosa por meio da polimerização *in situ*. Foi utilizado talco sintético na forma de gel e pó a fim de comparar o efeito da morfologia do talco na obtenção dos nanocompósitos. Para comparação foi sintetizado uma dispersão aquosa de poliuretano utilizando um catalisador comercial DBTDL. Os materiais foram caracterizados por FTIR, DRX, TEM, MEV-FEG, AFM, DMA, TGA e DSC. Os nancompósitos foram produzidos utilizando 0,5%, 1% e 3% de talco sintético em gel e em pó. A análise de FTIR mostrou que é possível obter dispersões aquosas de poliuretano utilizando talco sintético como catalisador e que foram formadas ligações de hidrogênio entre carga/matriz. Uma boa dispersão das cargas foram evidenciadas por DRX, TEM, MEV-FEG e AFM. Propriedades mecânicas e térmicas foram aumentadas com a adição das cargas. A T_g dos nanocompósitos foi afetada pela presença das cargas, provavelmente devido a boa dispersão das mesmas dentro da matriz polimérica.

Synthetic talc as catalyst and filler for waterborne polyurethane based nanocomposites synthesis

Guilherme Dias[1], Manoela Prado[1], Christophe Le Roux[4], Mathilde Poirier[4], Pierre Micoud[4], Rosane Ligabue[1,2], François Martin[4], Sandra Einloft[1,3].

1 - Post-Graduation Program in Materials Engineering and Technology, Pontifical Catholic University of Rio Grande do Sul – PUCRS, Brazil;

2 - School of Science, Pontifical Catholic University of Rio Grande do Sul – PUCRS, Brazil;

3 - School of Technology, Pontifical Catholic University of Rio Grande do Sul – PUCRS, Brazil;

4 - ERT Géomatériaux, GET, Université de Toulouse, CNRS, IRD, UPS, France.

ABSTRACT

In this work synthetic talc was used as catalyst and filler aiming to obtain waterborne polyurethane (WPU) nanocomposites by *in situ* polymerization. Filler were used both in gel and powder form in order to compare its effects into the WPU matrix. The use of synthetic talc as filler is interesting due to the possibility of hydrogen bonds formation between WPU chains/ Si-O-Si and OH groups in synthetic talc edges promoting changes in physical, mechanical and thermal properties. Moreover, WPUs are environmental friendly polymers replacing organic solvents by water as dispersion medium reducing pollutants emission in the atmosphere. Materials structure analyzed by FTIR evidenced that it is possible to synthesize WPU using synthetic talc as catalyst and proved hydrogen bonding formation between synthetic talcs and WPU matrix. Synthetic talcs were well dispersed even with higher filler content, as supported by XRD, TEM, FESEM and AFM analyses. Thermal and mechanical performance were improved with synthetic talc fillers addition in order to obtain WPU nanocomposites. Also, T_g of WPU nanocomposites was affected by fillers addition as presented by DSC corroborating synthetic talcs good dispersion as evidenced by XRD and TEM analyses. Synthetic talcs used as catalyst/filler resulted in nanocomposites with superior thermal and mechanical properties being a new path to utilize synthetic talcs to obtain multifunctional materials.

Keywords: waterborne polyurethane; synthetic talc; *in situ* polymerization; hydrogen bond.

INTRODUCTION

Waterborne polyurethane (WPU) is a polyurethane system in which water is used as dispersion medium replacing conventional organic solvents (toluene and acetone).The use of water as solvent reduce volatile organic compounds (VOCs) release to the atmosphere contributing to environment protection [1]. WPU has interesting applications such as adhesives, coatings and membranes owing to its good processing properties, abrasion resistance, non-toxicity, low cost and great adhesion [2,3].

However, thermal stability, insolubility and mechanical properties of WPU are lower when compared to the organic solvent-born PU needing to be improved. Using nanoparticle fillers is an effective way to alter and enhance WPU properties [4]. In this context, various inorganic particles are used to obtain new nanocomposites, like Fe_3O_4 [1,2,5], silica [6-9], attapulgite [4], clay [10-13], metallic oxides [14-17], etc. Among all potential nanocomposite precursors, those based on clay and layered silicates have been most widely investigated, probably due to the easy availability of starting clay materials. Moreover, talc particles are widely used as plate-like mineral filler because it is a low cost material [18]. Despite their good performance as filler and low price, natural talc presents some drawbacks. Natural talc cannot be ground homogeneously below 5 µm without leading to structure amorphization. To solve this issue and also to control particle size, we turned to talc obtained from hydrothermal synthesis [19]. Synthetic talcs used as fillers were reported by many researches to produce new materials such as solvent-born polyurethanes [20-24], polypropylene and polyamide 6 (PA6) nanocomposites [18], PP/PA6 blends [25], PP/PA6 blends using ionic liquids/nanotalc as fillers [26], PA6 and PA12 nanocomposites [27],

ternary nanotalc reinforced PA6/SEBS-g-MA composites [28] and also WPUs [29,30]. Moreover, tin catalysts as dibutyl tin dilaurate (DBTDL), widely used as catalyst in PU synthesis, are known as toxic compounds [31], for this reason it is interesting to use environmental friendly catalysts, like synthetic talc. As far as we know in this work we describe for the first time the use of synthetic talc as catalyst. Filler effect in polymerization reaction as catalyst and as reinforcement in waterborne polyurethane nanocomposites properties was evaluated as well.

EXPERIMENTAL

Materials

Synthetic talcs were manufactured using the following materials: magnesium acetate tetrahydrate ($Mg(CH_3COO)_2 \cdot 4H_2O$), sodium metasilicate pentahydrate ($Na_2SiO_3 \cdot 5H_2O$), sodium acetate trihydrate ($NaCH_3COO \cdot 3H_2O$), and acetic acid. All reagents were purchased from Aldrich and used without further purification.

Isophorone diisocyanate (IPDI, for synthesis, Bayer, Germany), polyester diol (Mn=1000 g/mol) and 2,2- bis(hydromethyl) propionic acid (DMPA, 99%, Perstorp, Sweden) were used to obtain waterborne polyurethanes. NCO/OH molar ratio of 1.7 was utilized. Dibutyl tin dilaurate [DBTDL Miracema-Nuodex Ind., Brazil (0.1% w/w)] was used as catalyst for pristine WPU. DMPA carboxylic acid was neutralized with trimethylamine (J.T Baker, Center Valley, Pennsylvania, USA). Free NCO content was measured by titration with n-dibutylamine (Bayer, Leverkusen, Germany) and hydrazine (Merck, Kenilworth, New Jersey, USA) was used as chain extender.

Synthetic talc preparation

Synthetic talc was obtained by hydrothermal synthesis as described in literature [31]. First, talc precursor was obtained by reacting sodium metasilicate pentahydrate with magnesium acetate tetrahydrate in a proportion of Si/Mg=4/3, in the presence of sodium acetate. In a second step, talc precursor was hydrothermally treated under high temperature (300°C) and pressure (85 bar) during a period of time of 6h in order to obtain well-crystallized nano-sized talc gel it. Synthetic talc (ST) was obtained in gel form (ST-g) or in powder form (ST-p) after dried in an oven at 120°C and ground. Specific surface area of synthetic talc manufactured in this conditions is 130 m^2g^{-1}, as reported previously by our group [29].

Waterborne polyurethanes nanocomposites preparation method

Waterborne polyurethanes nanocomposites and pristine waterborne polyurethane were prepared by *in situ* polymerization. In a glass reactor the following reagents were placed: IPDI, a polyester diol and DMPA (NCO/OH molar ratio of 1.7 and 5% w/w of DMPA in relation to prepolymer solids content). The NCO terminated prepolymer reaction was carried out under constant mechanical stirring and inert atmosphere (N_2) at 80°C for 1 h. To quantify the residual free isocyanate content, titrations were performed with n-dibutylamine based on the ASTM 2572 standard technique. Then, to neutralize the acid groups from DMPA, molar equivalent of trimethylamine was added to the reactor and stirred for 30 min at 50 °C. Lastly, a mixture of the previously neutralized prepolymer and hydrazine (chain extender in amount equivalent to the residual free NCO content) was poured in water and kept under mild agitation (200 rpm) at room temperature for 30 min. To prepare pristine WPU, DBTDL was used as catalyst. To produce WPU nanocomposites synthetic talc

in gel and powder form were used aiming to substitute DBTDL as catalyst and perform as reinforcement. Fillers content were 0.5wt%, 1wt% and 3wt%. The average solids content were 37% w/w.

Characterization Methods

WPU nanocomposites and neat WPU characterizations were performed using dried films of 70 µm of thickness produced by casting, samples of these films were analyzed by: Fourier transform infrared spectroscopy (FTIR, PerkinElmer Spectrum100 spectrometer) in transmission mode in the range 4000–650 cm^{-1}, was used to ascertain fillers and nanocomposites structural properties; X-ray diffraction (Shimadzu XRD-7000) patterns were recorded with $CuK\alpha_{1,2}$ Bragg–Brentano geometry θ–θ radiations, between 5 and 80 º with a step size of 0.028, current of 40 kV and voltage of 30 mA; Differential scanning calorimetry (DSC, TA Instruments Q20 calorimeter,) was used to determine glass transition temperature (Tg) from -90 to 200 °C, with a heating rate of 10°C/min under an inert atmosphere of nitrogen, from the heat second cycle; Thermogravimetric analysis (TA Instruments Q600 simultaneous thermal analyzer,) was carried out with a heating rate of 20°C/min, from room temperature to 800°C under nitrogen atmosphere; Mechanical tests were performed in triplicate according to ASTM D822 standard technique (TA Instruments Q800 dynamic mechanical analyzer,) for determination of Young's modulus and stress X strain tests; Field emission scanning electron microscopy (FESEM, FEI Inspect F50) analyses were performed in secondary electrons (SE) mode and used for assessment of fillers distribution in the polymer matrix; Atomic force microscopy (AFM) was used to collect roughness data of the WPU and its nanocomposites. The AFM analyses were performed in tapping mode to construct phase/height contrast

images at different locations on the top surface of the samples using a Bruker Dimension Icon PT equipped with a TAP150A probe (resonance frequency of 150 kHz and 5 $N.m^{-1}$ spring constant)and calibrated prior to samples measurements. The scanned area of images was 5 X 5 μm^2 with a resolution of 512 frames per area.

RESULTS AND DISCUSSION

FTIR Analysis

WPU nanocomposites, neat WPU, synthetic talc in gel and in powder form were characterized by FTIR spectroscopy (Figure 1). In synthetic talc spectra (ST-p and ST-g), it was observed characteristic bands assigned to talc around 1650 cm^{-1} related to Si-O vibrations [33] and the band between 1200–800 cm^{-1} characteristic of Si-O and Si-O-Si bonds [20,23,24,33,34]. For neat WPU and its nanocomposites the bands in regions of 3500–3400 cm^{-1} are attributed to urethane linkage N-H. The bands in 2950 and 2870 cm^{-1} are associated to different vibrational modes of polymeric chain CH_2 group. The band in 1731 cm^{-1} is characteristic of C=O of urethane bond. Region around 1520 cm^{-1} is related to CN and NH of urethane bonds. CO-O bond appears in 1243 cm^{-1} region. In 1185 and 1135 cm^{-1} appears the bands associated to N-CO-O and C-O-C groups [13,15,20-24,29,30]. WPU nanocomposites formation is proved by FTIR (Fig.1), confirming synthetic talc as a substitute for commercial catalyst in polymerization reaction. It also can be observed that the band related with C=O decreases as fillers content increased and a shoulder appeared around 1650 cm^{-1} in the nanocomposites, probably due to hydrogen bond formation between C=O of polymeric chain and hydroxyl groups available on synthetic talc layers edges [16].

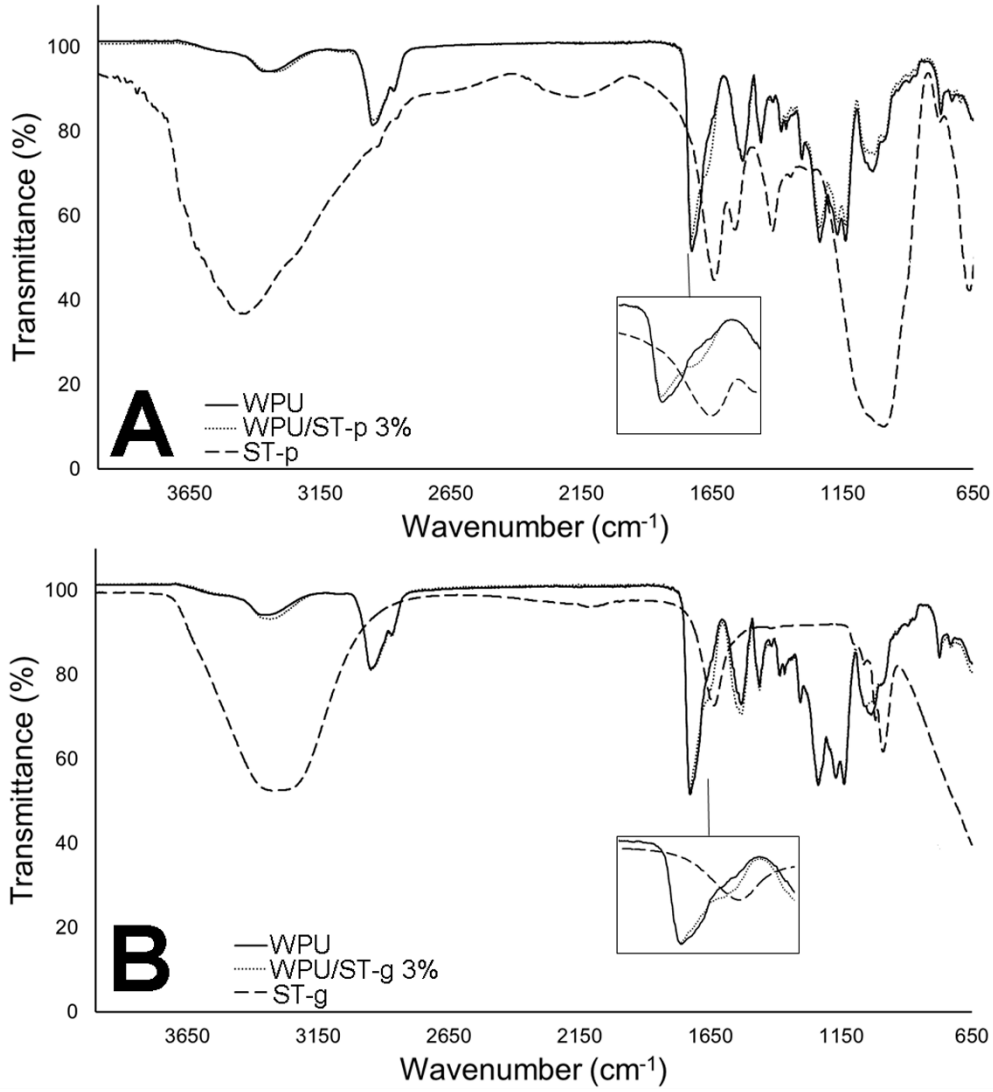

Fig. 1 FTIR spectra of (A) neat WPU, WPU/ST-p 3% and ST-p and (B) neat WPU, WPU/ST-g 3% and ST-g.

XRD-TEM analysis

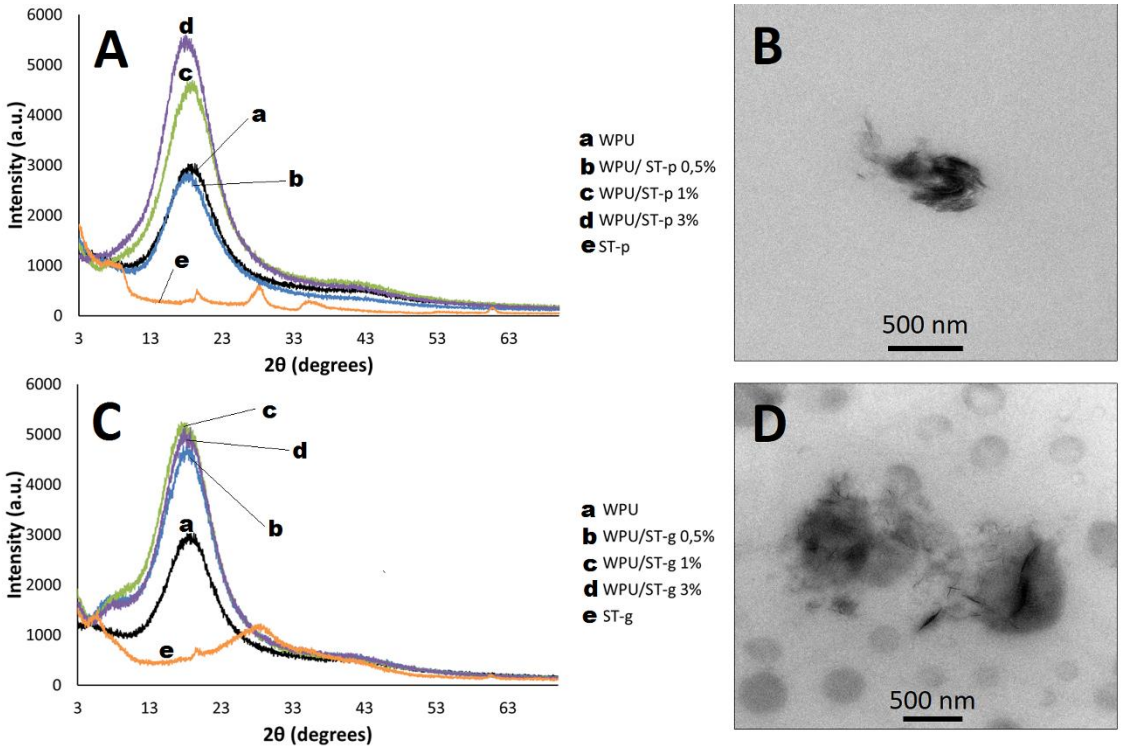

Fig. 2 XRD patterns of (A) WPU/ST-p and (C) WPU/ST-g nanocomposites, compared to neat WPU and synthetic talc. TEM images of (B) WPU/ST-p 3% and (D) WPU/ST-g 3%.

Figure 2 (A, C) shows diffraction patterns of pristine WPU, synthetic talcs and their nanocomposites. Characteristic XRD diffraction peaks associated to natural talc are observed, but for synthetic talcs these diffraction peaks are broader and less intense. This behavior indicates that synthetic talc layers are smaller compared to natural talc [18,19,22,29]. For pure WPU films, a broad diffraction peak is located around 2θ= 20°; this diffraction is associated to PU amorphous phase and appeared in all nanocomposite samples [2]. The diffraction peak around 2θ≅ 9° for synthetic talc in powder form disappeared in WPU/ST-p nanocomposites XRD pattern. This disappearance suggests that polymer chains are intercalated between fillers layers

inducing its delamination or intercalated between two individual nanoparticles, resulting in good filler dispersion throughout WPU films [3]. Characteristic diffraction peaks of synthetic talc in gel form appeared in WPU/ST-g nanocomposites diffraction patterns. Moreover, this peak located at 2θ≅ 9° raised in XRD patterns of WPU nanocomposites with ST-g content, indicating that synthetic talc in gel form layers are intercalated or intercalated between two individual nanoparticles [35,36]. Fig. 2 (B, D) shows TEM images of WPU/ST nanocomposites samples which contained 3 wt% synthetic talc. As illustrated in TEM images, the dark areas are attributed to ST fillers and lighter colored region attributed to WPU matrix [2]. Even with 3 wt% of fillers content into the WPU matrix a good filler dispersion was achieved; other studies performed with synthetic talc fillers presented the same results for TEM analysis [20,22,23,25,28,30]

Mechanical properties

Table 1. Mechanical properties of the nancomposites and neat WPU.

Samples	Young Modulus (MPa)	Strain (%)	Stress (MPa)
WPU	31 ± 3	136 ± 9	6 ± 0.6
WPU/St-p 0.5%	80 ± 9	97 ± 13	11 ± 1
WPU/ST-p 1%	38 ± 4	137 ± 12	7 ± 2
WPU/ST-p 3%	64 ± 12	115 ± 21	10 ± 2
WPU/St-g 0.5%	35 ± 10	93 ± 30	6.5 ± 0.6
WPU/ST-g 1%	108 ± 1	4 ± 1	4 ± 0.8

WPU/ST-g 3%	49 ± 4	77 ± 39	8 ± 1

Table 1 presents stress/strain properties of neat WPU and WPU nanocomposites. Synthetic talc addition affected nanocomposites mechanical properties. The nanocomposites do not break at tests conditions. Interactions between filler/polymer alternatively to filler/filler interactions are probably associated with mechanical properties enhancement [21-23,29]. Well-dispersed fillers in polymer matrix as well as strong interfacial interaction between polymer/filler improved the stress transfer between polyurethane matrix and fillers increasing polymer resistance to deformation. This augmentation in mechanical properties can be related to hydrogen bonding between synthetic talcs and WPU in nanocomposites [37]. Young Modulus tended to increase with increasing of fillers content into the WPU nanocomposites; sample with 1 wt% of synthetic talc in gel form presented a different behavior, probably because some agglomeration occurred and affected WPU film formation and its mechanical performance. Moreover, talcs with high aspect ratio tend to stiffen materials [38]. Yet, this stiffening may be related to hydrogen bonding interactions, corroborating FTIR results [29,39]. Our group showed in previous works that synthetic talc filler improved Young Modulus of WPU nanocomposites, like for WPU/synthetic talc nanocomposites formed by blending method [29] and WPU/Fe_3O_4-synthetic talc nanocomposites also by blending method [30]. These results corroborate with TEM results and reinforce the fact that dispersion affects nanocomposites mechanical properties.

Thermal Properties

Table 2. Thermal properties of the nanocomposites and neat WPU.

Samples	T_{onset} (°C)	$T_{peakmax1}$ (°C)	$T_{peakmax2}$ (°C)	$T_{g\text{-}DSC}$ (°C)
WPU	330.2	373.2	430.6	-33.3
WPU/St-p 0.5%	341.7	367.1	435.2	-34.9
WPU/ST-p 1%	348.3	376.9	439.7	-33.5
WPU/ST-p 3%	336.9	358.8	431.4	-37.1
WPU/St-g 0.5%	344.8	372.4	440.6	-37.2
WPU/ST-g 1%	338.4	369.4	431.9	-40.1
WPU/ST-g 3%	338.2	364.1	435.9	-40.6

In order to investigate thermal stability of neat WPU, WPU nanocomposites and the effect of the synthetic talcs on their thermal behavior, TGA was carried out. Results are listed in Table 2. It was observed from TGA data that WPU films thermal stability was enhanced by fillers addition, which can be attributed to the action of nanoparticles as thermal insulator. Also the good fillers dispersion into the WPU matrix resulted in an improvement of thermal stability of nanocomposites films [2]. The first stage is related to hard segment degradation and the second stage to soft segment degradation. Layered silicates can make the path longer for thermally decomposed volatiles to escape. It is clearly observed that the initial stage thermal decomposition temperature is the major and sharp which involve the thermal decomposition of the intercalated polymers [13]. The increase of the decomposition

temperature is likely due to the interaction between WPU and fillers. Synthetic talc structure into the WPU matrix could limit the segmental movement of polymer chains or act as thermal insulator and mass transport barrier to the volatile products generated during decomposition, as a consequence retarding material degradation [8,14]. In previous works, was reported that the thermal stability of nanocomposites is improved by the use of synthetic talc, because the large amount of hydroxyl groups present at the filler layer edges favors interactions between filler and polymer [21-23,40]. But when nanocomposites with synthetic talc in gel form were prepared by physical mixture thermal stability did not increase as when nanocomposites prepared by in situ polymerization, as reported in a previous work [29].

Thermal property of neat WPU and WPU nanocomposites films was studied by DSC. No melting peak was found in the DSC analysis for the pristine WPU and WPU/ synthetic talc samples, indicating that no crystallization domain was formed in their hard or soft phases. This corroborated with XRD results, that shows these polymers are amorphous [12]. Higher concentration of synthetic talc slightly decreased T_g this effect could be associated to filler dispersion, as shown by XRD, TEM and FESEM results [41]. Also, this reduction in T_g values for the nanocomposites could be related to the breaking of the hydrogen bonds between soft and hard segments by nanoparticles which disrupts the phase separation of polyurethanes and increases the mobility of the polymer chains [2,17].

Morphological study

FESEM was employed to inspect nanocomposites microstructure. FESEM images of samples fractured section were illustrated in Fig 3. Figure 3 shows FESEM micrographs of neat WPU and WPU nanocomposites. All samples showed deeper

and longer cracks when fractured with liquid nitrogen comparing with neat WPU. However, with fillers content increasing fracture surfaces became rough. This is related to the alteration of WPU matrix after adding higher fillers content. This trend could be explained by supposing a homogenous nanoparticles distribution and an improvement of polymer/filler interaction in the nanocomposites, and therefore a crack propagation path occurring inside the polyurethane matrix [8]. The rough fracture surface indicates that there was a strong resistance to further cracks propagation. Meanwhile, the rough fracture surface means that a large crack would encounter difficulties in propagating. This effect can be responsible for nanocomposites mechanical properties improvement [42].

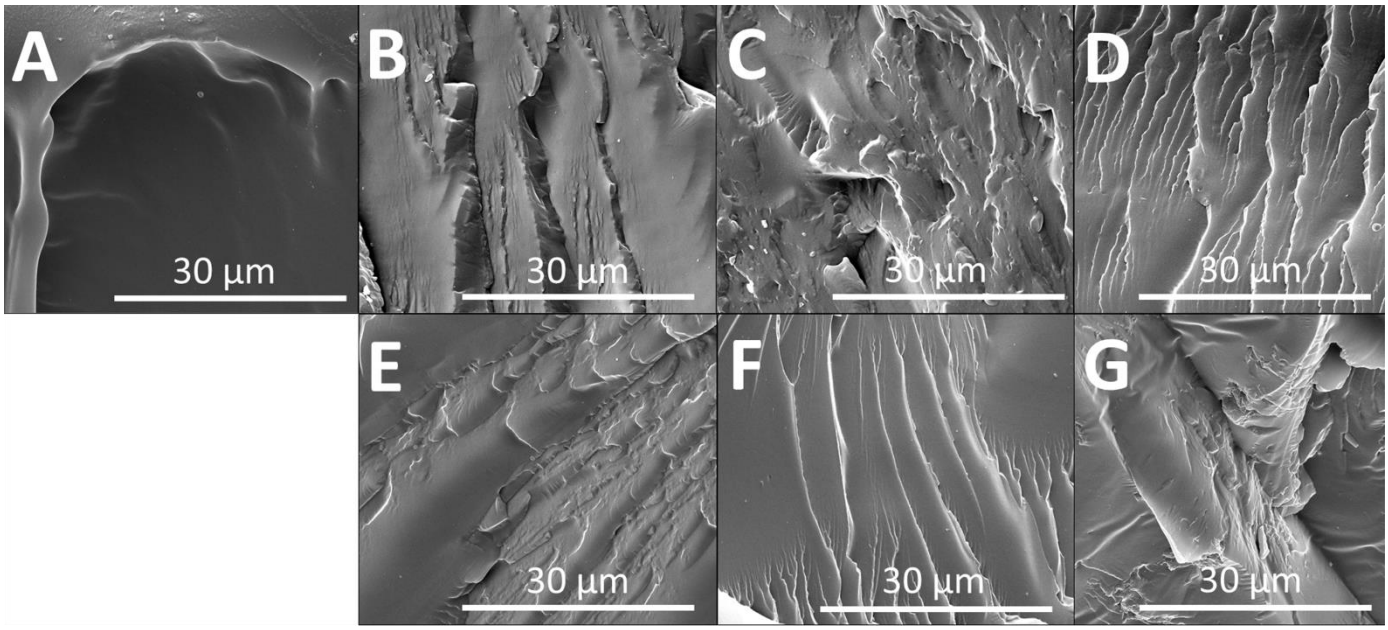

Fig. 3 Micrographs from cryogenically fractures of the materials at magnification of 5000X, mode SE, (A) WPU, (B) WPU/St-p 0,5%, (C) WPU/ST-p 1%, (D) WPU/ST-p 3%, (E) WPU/St-g 0,5%, (F) WPU/ST-g 1% and (G) WPU/ST-g 3%.

AFM results

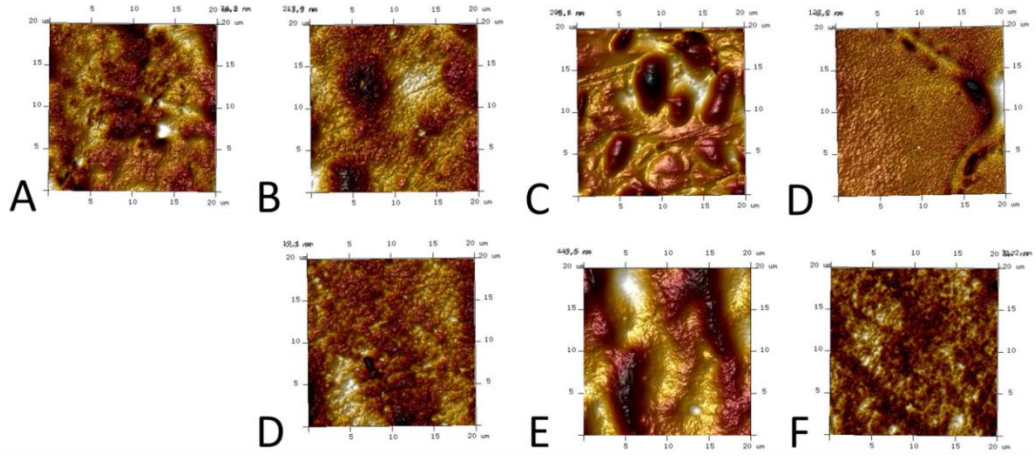

Fig. 4 AFM images (height). (A) WPU, (B) WPU/St-p 0.5%, (C) WPU/ST-p 1%, (D) WPU/ST-p 3%, (E) WPU/St-g 0.5%, (F) WPU/ST-g 1% and (G) WPU/ST-g 3%.

Figure 4 shows the height AFM topographic images and Table 3 shows the average roughness (Ra), root mean square roughness (Rq), and maximum height roughness (Rmax) for neat WPU and its nanocomposites measured by AFM in tapping mode. In WPU matrix (Fig 4-A), dark regions are associated with amorphous domains (soft segments) and bright regions are associated with crystalline domains (hard segments). The results of Ra, Rq, and Rmax demonstrates that with fillers addition surface roughness of nanocomposites increased, indicating fillers influence on the surface morphology of systems [29,43]. As seen in Figure 4, with fillers addition on nanocomposites the rugged domains come more prominent evidencing the interactions between filler/polymer probably by hydrogen bonding among fillers and hard segments of the WPU [9,29]. It can be seen that when 3wt% of fillers were added to the WPU matrix, roughness decreased. Introducing higher fillers content into WPU matrix restricted the shrinkage of the polymer surface, reducing nanocomposites roughness [10]. The higher values of these parameters comparing

to pristine WPU confirms the presence of filler particles on the surface, as reported in literature [11]. This interaction corroborates the mechanical properties improvements in nanocomposites once compared to pristine WPU.

Table 3. AFM Results: Average Roughness (Ra), Root Mean Square Roughness (Rq), and Maximum Height Roughness (Rmax) of neat WPU and its nanocomposites.

Samples	Rq (nm)	Ra (nm)	Rmax (nm)
WPU	9	7	116
WPU/St-p 0,5%	59	46	431
WPU/ST-p 1%	78	58	585
WPU/ST-p 3%	24	13	330
WPU/St-g 0,5%	55	49	362
WPU/ST-g 1%	142	115	805
WPU/ST-g 3%	20	16	148

CONCLUSIONS

New waterborne polyurethane nanocomposites were synthesized using synthetic talcs as catalyst and as filler by in situ polymerization. FTIR confirmed that is possible to produce WPU/synthetic talc nanocomposites without adding the commercial catalyst. Also, FTIR indicated hydrogen bonds between filler and polymer chains. Synthetic talcs were well dispersed into the WPU matrix as supported by XRD, TEM, FESEM and AFM analyses. Thermal stability of WPU nanocomposites increased when compared to pristine WPU. DSC indicated that the

glass transition temperature of nanocomposites was affected by the addition of synthetic talcs, probably due to good filler dispersion. Mechanical properties improvement can be associated to hydrogen bonding between filler/polymer and good filler dispersion. It has been proved that synthetic talc can be used as catalyst and filler to produce WPU nanocomposites with desired properties. This new waterborne polyurethane synthetic talc nanocomposites can be used for flexible films and/or coating industries.

ACKNOWLEDGEMENTS

GD and MP thanks CAPES for their PhD scholarship. SE acknowledges CNPq for DT grant (number 303467/2015-0). This study was financed in part by the Coordenação de Aperfeiçoamento de Pessoal de Nível Superior – Brasil (CAPES) – Finance Code 001. Thanks to Nokxeller – Microdispersions by the supply of part of the reagents used in this work.

REFERENCES

1 - Chen S, Zhang S, Jin T, Zhao G (2016) Synthesis and characterization of novel covalently linked waterborne polyurethane/Fe_3O_4 nanocomposite films with superior magnetic, conductive properties and high latex storage stability. Chem Eng J 286: 249-258.

2 - Hoseini Z, Nikje, M.M.A (2018) Synthesis and characterization of a novel thermally stable water dispersible polyurethane and its magnetic nanocomposites. Iran Polym J 27:733. https://doi.org/10.1007/s13726-018-0650-5.

3 – Gurunathan T, Mohanty S, Nayak S K (2015) Effect of reactive organoclay on physicochemical properties of vegetable oil-based waterborne polyurethane nanocomposites. RSC Adv 5: 11524.

4 - Peng L, Zhou L, Li Y, Pan F, Zhang S (2011) Synthesis and properties of waterborne polyurethane/attapulgite nanocomposites. Compos Sci Tech 71: 1280-1285.

5 – Zhang S, Li Y, Peng L, Li Q, Chen S, Hou K (2013) Synthesis and characterization of novel waterborne polyurethane nanocomposites with magnetic and electrical properties. Compos Part A: Appl Sci Manufact 55: 94-101. https://doi.org/10.1016/j.compositesa.2013.05.018.

6 - Chen J J, Zhu C F, Deng H T et al. (2009) Preparation and characterization of the waterborne polyurethane modified with nanosilica. J Polym Res 16: 375. https://doi.org/10.1007/s10965-008-9238-7.

7 – Zhang SW, Liu R, Jiang J Q, Yang C, Chen M, Liu X Y (2011) Facile synthesis of waterborne UV-curable polyurethane/silica nanocomposites and morphology, physical properties of its nanostructured films. Prog Org Coat 70: 1-8.

8 – Peruzzo P J, Anbinder P S, Pardini F M, Pardini O R, Plivelic T S, Amalvy J I (2016) On the strategies for incorporating nanosilica aqueous dispersion in the synthesis of waterborne polyurethane/silica nanocomposites: Effects on morphology and properties. Mat Today Commun 6: 81-91.

9 – Han Y, Chen Z, Dong W, Xin (2015) Improved water resistance, thermal stability, and mechanical properties of waterborne polyurethane nanohybrids reinforced by fumed silica via in situ polymerization. High Perfor Polym 27: 824–832.

10 - Kuan H, Ma C M, Chuang W, Su H (2005) Hydrogen bonding, mechanical properties, and surface morphology of clay/waterborne polyurethane nanocomposites. J Polym Sci B Polym Phys 43: 1-12. doi:10.1002/polb.20256.

11 - Maji P K, Bhowmick A K (2012) Efficacy of clay content and microstructure of curing agents on the structure–property relationship of new-generation polyurethane nanocomposites. Polym. Adv. Technol. 23:1311–1320.

12 – Rafiemanzelat F, Adli V, Mallakpour S (2015) Effective preparation of clay/waterborne Azo-containing polyurethane nanocomposite dispersions incorporated anionic groups in the chain termini, Design Mono Polym 18: 303-314. doi: 10.1080/15685551.2014.999459.

13 – Ramesh S, Punithamurthy K (2017) The effect of organoclay on thermal and mechanical behaviors of thermoplastic polyurethane nanocomposites. Digest J Nanomater Biostruct 12:331 – 338.

14 – Gao X, Zhu Y, Zhou S, Gao W, Wang Z, Zhou B (2011) Preparation and characterization of well-dispersed waterborne polyurethane/$CaCO_3$ nanocomposites. Coll Surf A: Physicochem Eng Aspects 377:312-317, https://doi.org/10.1016/j.colsurfa.2011.01.025.

15 - Demétrio da Silva V, dos Santos L M, Subda S M et al. (2013) Synthesis and characterization of polyurethane/titanium dioxide nanocomposites obtained by in situ polymerization. Polym Bull 70: 1819. https://doi.org/10.1007/s00289-013-0927-y.

16 - Soares R R, Carone C, Einloft S et al. (2014) Synthesis and characterization of waterborne polyurethane/ZnO composites. Polym Bull 71: 829. https://doi.org/10.1007/s00289-014-1095-4.

17 - Malik M, Kaur R (2018) Mechanical and Thermal Properties of Castor Oil–Based Polyurethane Adhesive: Effect of TiO_2 Filler. Adv Polym Technol 37: 24-30. doi:10.1002/adv.21637.

18 – Yousfi M, Livi S, Dumas A, Le Roux C, Crépin-Leblond J, Greenhill-Hooper M, Duchet-Rumeau J (2013) Use of new synthetic talc as reinforcing nanofillers for polypropylene and polyamide 6 systems: Thermal and mechanical properties. J Coll Interf Sci 403: 29-42.

19 – Dumas A, Martin F, Ferrage E, Micoud P, Le Roux C, Petit S (2013) Synthetic talc advances: Coming closer to nature, added value, and industrial requirements. Appl Clay Sci 85:8-18.

20 - Dias G, Prado M A, Carone C et al. (2015) Synthetic silico-metallic mineral particles (SSMMP) as nanofillers: comparing the effect of different hydrothermal treatments on the PU/SSMMP nanocomposites properties. Polym Bull 72: 2991. https://doi.org/10.1007/s00289-015-1449-6.

21 - Prado M A, Dias G, Carone C, Ligabue R, Dumas A, Roux C, Micoud P, Martin F, Einloft S. (2015), Synthetic Ni-talc as filler for producing polyurethane nanocomposites. J Appl Polym Sci 132: 41854, doi: 10.1002/app.41854.

22 - dos Santos L M, Ligabue R, Dumas A, Le Roux C, Micoud P, Meunier J F, Martin F, Einloft S (2015) New magnetic nanocomposites: Polyurethane/ Fe_3O_4-synthetic talc. Euro Polym J 69: 38-49.

23 – Dias G, Prado M, Ligabue R, Poirier M, Le Roux C, Martin F, Fery-Forgues S, Einloft S (2018) Synthetic talc as a new platform for producing fluorescent clay polyurethane nanocomposites. Appl Clay Sci 158: 37-45.

24 – Dias G, Prado M, Ligabue R, Poirier M, Le Roux C, Micoud P, Martin F, Einloft S (2018) Hybrid Pu/Synthetic Talc/Organic Clay Ternary Nanocomposites: Thermal, Mechanical and Morphological Properties. Polym Polym Comp 26:127-140.

25 - Yousfi M, Livi S, Dumas A, Crépin-Leblond J, Greenhill-Hooper M, Duchet-Rumeau J (2014) Compatibilization of polypropylene/polyamide 6 blends using new synthetic nanosized talc fillers: Morphology, thermal, and mechanical properties. J Appl Polym Sci 131:40453, doi: 10.1002/app.40453.

26 – Yousfi M, Livi S, Dumas A, Crépin-Leblond J, Greenhill-Hooper M, Duchet-Rumeau J (2015) Ionic compatibilization of polypropylene/ polyamide 6 blends using an ionic liquids/nanotalc filler combination: morphology, thermal and mechanical properties. RSC Adv 5: 46197, doi: 10.1039/c5ra00816f.

27 – Beuguel Q, Ville J, Crepin-Leblond J, Mederic P, Aubry T (2015) Comparative study of the structural and rheological properties of PA6 and PA12 based synthetic talc nanocomposites. Polym 62:109-117. https://doi.org/10.1016/j.polymer.2015.02.031.

28 - Hemlata, Maiti S N (2014) Mechanical, morphological, and thermal properties of nanotalc reinforced PA6/SEBS-g-MA composites. J Appl Polym Sci 132: 41381. doi: 10.1002/app.41381.

29 - Dias G, Prado M, Le Roux C, Poirier M, Micoud P, Ligabue R, Martin F, Einloft S (2017) Analyzing the influence of different synthetic talcs in waterborne polyurethane nanocomposites obtainment. J Appl Polym Sci 135:46107. doi: 10.1002/app.46107.

30 - dos Santos L M, Ligabue R, Dumas A et al. (2018) Waterborne polyurethane/Fe_3O_4-synthetic talc composites: synthesis, characterization, and magnetic properties. Polym Bull 75:1915. https://doi.org/10.1007/s00289-017-2133-9.

31 – Fernandes I P, Costa M R P F N, Ferreira M J, Barreiro M F (2015) Water-based poly(urethane-urea) dispersions — meeting the European Union legislation. Polymery 60: 536-540. doi: dx.doi.org/10.14314/polimery.2015.536.

32 - Le Roux C, Martin F, Micoud P, Dumas A (2013) Process for Preparing a Composition Comprising Synthetic Mineral Particles and Composition. (Int. Pat. WO 2013/ 004979 A1).

33 – Zhang M, Hui Q, Lou X J, Redfern S A T, Salje E K H, Tarantino S C (2006) Dehydroxylation, proton migration, and structural changes in heated talc: An infrared spectroscopic study. Amer Miner 91:816–825. doi: https://doi.org/10.2138/am.2006.1945.

34 - Martin F, Micoud P, Delmotte L, Marichal C L, Dred R D, Parseval P, Mari A, Fortune J P, Salvi S, Beziat D, Ferret O G (1999) The Structural Formula of Talc from the Trimouns Deposit, Pyrenees, France. J Can Miner 37: 997.

35 – Ray S S, Okamoto M (2003) Polymer/layered silicate nanocomposites: a review from preparation to processing. Prog Polym Sci 28:1539-1641.

36 – Paul D R, Robeson L M (2008) Polymer nanotechnology: Nanocomposites. Polym 49:3187-3204.

37 - Hajializadeh S, Barikani M, Bellah S M (2017) Synthesis and characterization of multiwall carbon nanotube/waterborne polyurethane nanocomposites. Polym Int 66:1074-1083. doi:10.1002/pi.5362.

38 – Castillo L A, Barbosa S E, Capiati N J (2013) Influence of talc morphology on the mechanical properties of talc filled polypropylene. J Polym Res 20:152. https://doi.org/10.1007/s10965-013-0152-2.

39 - Han W (2013) Synthesis and Properties of Networking Waterborne Polyurethane/Silica Nanocomposites by Addition of Poly(ester amine) Dendrimer. Polym Compos 34, 156. doi 10.1002/pc.22388.

40 - Dumas A, Martin F, Le Roux C et al (2013) Phyllosilicates synthesis: a way of accessing edges contributions in NMR and FTIR spectroscopies. Example of synthetic talc. Phys Chem Minerals 40:361. https://doi.org/10.1007/s00269-013-0577-5

41 - Romo-Uribe A, Santiago-Santiago K, Zavala-Padilla G, Reyes-Mayer A, Calixto-Rodriguez M, Arcos-Casarrubias J A, Baghdachi J (2016) Waterborne layered

silicate/acrylate nanocomposites by in-situ emulsion polymerization: Thermal and mechanical reinforcement, Prog Org Coat 101:59-70.

42 - Wu Y, Du Z, Wang H, Cheng X (2016) Preparation of waterborne polyurethane nanocomposite reinforced with halloysite nanotubes for coating applications. J Appl Polym Sci 43949. doi: 10.1002/app.43949.

43 - Santamaria-Echart A, Ugarte L, García-Astrain C, Arbelaiz A, Corcuera M A, Eceiza A (2016) Cellulose nanocrystals reinforced environmentally-friendly waterborne polyurethane nanocomposites. Carbo Polym 151:1203-1209.

5. CONCLUSÕES

As conclusões serão divididas em quatro partes: nanocompósitos de DPUs com três diferentes talcos sintéticos por mistura física, nanocompósitos fluorescentes de poliuretano obtidos por mistura física, nanocompósitos ternários de talcos sintéticos misturados com argila comercial por polimerização *in situ* e nanocompósitos de DPUs utilizando talco sintético como carga e catalisador obtidos por polimerização *in situ*.

Os resultados mostraram que é possível obter nanocompósitos de DPUs foram por mistura física utilizando os talco sintéticos como carga, produzindo materiais com um baixo impacto ambiental. A área superficial específica dos talcos sintéticos influenciou nas propriedades finais dos nanocompósitos de DPU. As análises de DRX, TEM MEV-FEG, e AFM indicaram que os talcos sintéticos apresentaram uma boa dispersão dentro da matriz polimérica. Os resultados de módulos de armazenamento e perda evidenciaram uma boa incorporação dos talcos sintéticos na matriz de DPU. A compatibilidade dos talcos sintéticos em forma de nano-gel com os DPUs está relacionada com a interação que ocorre entre carga-polímero através do meio aquoso, por meio da ligação de hidrogênio. O aumento das propriedades mecânicas dos nanocompósitos está relacionada com a boa dispersão dos talcos sintéticos e interação entre carga/polímero. Além disso, as condições de síntese distintas dos talcos sintéticos resultando em diferentes áreas superficiais específicas é uma plataforma interessante para se obter nanocompósitos de DPU com uma vasta gama de possíveis propriedades mecânicas e térmicas.

Novos nanocompósitos fluorescentes de poliuretano foram obtidos pela incorporação de talcos natural e sintético através da mistura física. Os resultados demonstraram que as partículas de talco foram bem dispersas na matriz de PU mesmo quando em maiores quantidades, isto pode estar relacionado a interação entre os grupos OH disponíveis dos talcos sintéticos com as cadeias de PU. As propriedades térmicas e mecânicas dos nanocompósitos aumentaram quando adicionados os talcos sintéticos e natural fluorescentes em relação ao PU puro. Porém, as características dos talcos natural e sintético influenciaram nas propriedades de fluorescência dos nanocompósitos. O talco sintético fluorescente com as partículas menores apresentou uma maior fluorescência. A presença do agente fluorescente disperso na superfície da carga de talco evitando a aglomeração das moléculas fluorescentes é o grande diferencial destes novos nanocompósitos fluorescentes de poliuretano, pois a aglomeração ocorre naturalmente quando se obtêm o polímero misturado com a berberina pura. Berberina não é o melhor agente fluorescente, mas os resultados obtidos sugerem que o conceito pode ser facilmente aplicado a outros corantes fluorescentes ou eletroluminescentes, abrindo novas rotas para materiais altamente emissivos também dotados de boas propriedades térmicas e mecânicas. Finalmente, a forte adsorção da berberina no talco sugere que muitas moléculas biologicamente ativas que são insolúveis em água devem comportar-se de forma semelhante.

Nanocompósitos ternários foram preparados por meio da polimerização *in situ* utilizando talcos sintéticos (SSMMP 7h e 24h) distintos e uma argila comercial (SPR) como carga, provando que é possível obter materiais utilizando esta mistura de cargas. Os resultados das análises estruturais (DRX e FTIR) aliados aos testes morfológicos (TEM, SEM e AFM) demonstraram que as cargas foram bem dispersas/esfoliadas na matriz polimérica levando a obtenção de nanocompósitos PU/SSMMP/SPR com propriedades térmicas e mecânicas superiores. Essa mistura de cargas em uma matriz de poliuretano resulta em materiais que podem executar funções que exigem alto desempenho térmico e mecânico. Esses resultados corroboram com estudos prévios, demonstrando que os talcos sintéticos são interessantes para o desenvolvimento de materiais com propriedades distintas, e que também podem ser combinados com outras cargas.

Novos nanocompósitos de poliuretano à base de água foram sintetizados utilizando-se talco sintético em gel e em pó como catalisador e como carga por meio da polimerização *in situ*. Os resultados de FTIR provou que é possível produzir nanocompósitos de DPU/talco sintético sem adicionar o catalisador comercial. Além disso, o FTIR indicou ligações de hidrogênio entre carga/polímero. Os resultados das análises de DRX, TEM, MEV-FEG e AFM mostraram que os talcos sintéticos foram bem dispersos nas dispersões aquosas de poliuretanos. Os nanocompósitos apresentaram um aumento na estabilidade térmica quando comparados ao DPU puro. A boa dispersão das cargas afetou a temperatura de transição vítrea dos nanocompósitos, como reportado pela análise de DSC. O aumento das propriedades mecânicas pode ser relacionado as ligações de hidrogênio entre carga/polímero e boa dispersão do talco sintético. Este trabalho comprovou que é possível utilizar o talco sintético como catalisador e carga para produzir nanocompósitos de DPU com as propriedades desejadas.

Este trabalho demonstrou que os talcos sintéticos são uma nova plataforma para obtenção de materiais com diferentes funcionalidades e aplicações, onde é possível moldar as metodologias e processos para se obter propriedades diferenciadas que possam atender a diferentes demandas da indústria.

CONCLUSIONS

Les objectifs de la thèse étaient multiples mais surtout de montrer l'intérêt de développer des charges nanométriques qui quand la dispersion dans la matrice est maitrisée, permettent d'obtenir des matériaux composites avec des propriétés renforcées, de créer de nouveaux métariaux multicomposites non présents sur les marchés en utilisant par exemple des propriétés des nanocharges comme la fluorescence, mais aussi de comprendre les effets des charges nanométriques sur les propriétés physiques et chimiques des polymères créés en les comparant avec les effetds d'autres charges utilisées comme les argiles naturelles commerciales, qui sont elle pour la plus part de tailles microniques. Les objectifs sont atteints et comme le travail de cette thèse est basée sur 4 études menées en parallèle, les conclusions seront divisées en quatre parties pour faciliter la lecture à savoir 1) les

nanocomposites de DPU obtenus avec trois talcs synthétiques différents par mélange physique, 2) les nanocomposites fluorescents à base de polyuréthane obtenus par mélange physique, 3) les nanocomposites ternaires de talcs synthétiques mélangés à une argile commerciale par polymérisation in situ, et 4) les nanocomposites de DPU utilisant des talc synthétiques comme charge et catalyseur obtenus par polymérisation in situ.

1) Les résultats ont montré qu'il est possible d'obtenir des nanocomposites de DPU par mélange physique en utilisant du talc synthétique comme charge, produisant des matériaux ayant un faible impact sur l'environnement. La surface spécifique des talcs synthétiques a influencé les propriétés finales des nanocomposites de DPU. Les analyses par XRD, TEM MEB-FEG et AFM ont montré que les talcs synthétiques présentaient une bonne dispersion dans la matrice polymère. Les résultats des modules de stockage et de perte ont montré une bonne incorporation des talcs synthétiques dans la matrice de DPU. La compatibilité des talcs synthétiques sous forme nano-gel avec les DPU est liée à l'interaction entre le polymère de charge à travers le milieu aqueux, via la liaison hydrogène. L'augmentation des propriétés mécaniques des nanocomposites est liée à la bonne dispersion des talcs synthétiques et à l'interaction charge / polymère. De plus, les conditions de synthèse distinctes du talc synthétique donnant lieu à différentes surfaces spécifiques constituent une plate-forme intéressante pour obtenir des nanocomposites de DPU avec une large gamme de propriétés mécaniques et thermiques possibles.

2) De nouveaux nanocomposites de polyuréthane fluorescents ont été obtenus par incorporation de talcs naturels et synthétiques par mélange physique. Les résultats ont démontré que les particules de talc étaient bien dispersées dans la matrice de polyuréthane, même en quantités plus importantes, ce qui peut être lié à l'interaction entre les groupes OH disponibles des talcs synthétiques avec les chaînes du polyuréthane. Les propriétés thermiques et mécaniques des nanocomposites ont augmenté lorsque des fluorescents synthétiques et naturels ont été ajoutés à du PU pur. Cependant, c’est avec les talcs synthétiques que les meilleures propriétés de fluorescence des nanocomposites ont été obtenues. La présence de l'agent fluorescent dispersé à la surface de la charge de talc évitant l'agglomération des molécules fluorescentes est le principal différentiel de ces nouveaux

nanocomposites fluorescents à base de polyuréthane, car l'agglomération se produit naturellement lorsque le polymère mélangé à la berbiérine pure est obtenu. La berbérine n'est pas le meilleur agent fluorescent, mais les résultats suggèrent que le concept peut être facilement appliqué à d'autres colorants fluorescents ou électroluminescents, ouvrant de nouvelles voies pour les matériaux thermiques et mécaniques. Enfin, la forte adsorption de la berbiérine sur le talc suggère que de nombreuses molécules biologiquement actives insolubles dans l'eau devraient se comporter de la même manière.

3) Des nanocomposites ternaires ont été préparés par polymérisation in situ en utilisant des talcs synthétiques distincts (SSMMP 7h et 24h) et une argile commerciale (SPR), prouvant qu'il est possible d'obtenir des matériaux avec ce mélange de charges. Les résultats des analyses (DRX et FTIR), ainsi que des tests morphologiques (TEM, SEM et AFM), ont montré que les charges étaient bien dispersées /exfoliées dans la matrice polymère, en obtenant des nanocomposites PU/SSMMP/SPR avec des propriétés thermiques et mécaniques supérieures. Ce mélange de charges dans une matrice de polyuréthane permet d'obtenir des matériaux capables de remplir des fonctions nécessitant des performances thermiques et mécaniques élevées. Ces résultats corroborent des études antérieures démontrant que les talcs synthétiques sont intéressants pour le développement de matériaux ayant des propriétés différentes, et peuvent également être combinés avec d'autres charges.

4) De nouveaux nanocomposites de polyuréthane à base d'eau ont été synthétisés à l'aide de talc synthétique sous forme de gel et de poudre en tant que catalyseur et en tant que charge par polymérisation in situ. Les résultats FTIR ont prouvé qu'il était possible de produire des nanocomposites DPU / talc synthétique sans ajouter le catalyseur commercial. De plus, en FTIR des liaisons hydrogène entre charge / polymère ont été mis en évidence. Les résultats des analyses DRX, TEM, MEB-FEG et AFM ont montré que les talcs synthétiques étaient bien dispersés dans les dispersions aqueuses de polyuréthanes. Les nanocomposites ont montré une augmentation de la stabilité thermique par rapport à la DPU pure. La bonne dispersion des charges a affecté la température de transition vitreuse des nanocomposites, comme l'a montré l'analyse DSC. L'augmentation des propriétés mécaniques

peut être liée aux liaisons hydrogène entre charge / polymère et à une bonne dispersion du talc synthétique. Ces travaux ont montré qu'il était possible d'utiliser du talc synthétique comme catalyseur et charge pour produire des nanocomposites de DPU présentant les propriétés voulues.

Ainsi, il a été possible de répondre à la quasi-totalité des questions induites par l'insertion de charges nanométriques dans des matrices PU. De nouvelles fonctionnalités sont apparues (fluorescence, catalysuer), de nouveaux champs d'investigation ont été ouverts en mélangeant des argiles naturelles (peu chères 10 euros la tonne) avec des charges synthétiques chères (10 euros le kilogramme), …Les talcs synthétiques constituent une nouvelle plate-forme permettant d'obtenir des matériaux dotés de fonctionnalités et d'applications différentes, dans lesquels il était possible de façonner les méthodologies et les processus afin d'obtenir des propriétés différenciées pouvant répondre aux différentes demandes du secteur.

Les prospectives de travail sont nombreuses et sans dévoiler les travaux en cours qui sont sous le sceau de de la confidentialité, il est évident pour l'homme de l'art, que les grandes surfaces spécifiques de ces nanocharges sont un régal pour les phénomènes de sorption, d'absorption, d'absorption, de greffage, … de molécules variées comme par exemple CO_2, molécules photoluminescentes, nanominéraux magnétiques, …. pouvant s'insérer dans des polymères, polymères fabriqués en respectant les normes environnementales, ce qui est une très grande avancée réalisée dans cette thèse.

6. REFERÊNCIAS BIBLIOGRÁFICAS

AKYNDOYO, J. O; et al. Polyurethane types, synthesis and applications – a review. **RSC Advances**, v. 6, p. 114453–114482, 2016.

ALEXANDRE, M; Dubois, P. Polymer-layered silicate nanocomposites: preparation, properties and uses of a new class of materials. **Materials Science and Engineering**, v. 28, 1-63, 2000.

BAJSIC, E. G; Rek, V; Pavic, O. B. The influence of talc content on the thermal and mechanical properties of thermoplastic polyurethane/ polypropylene blends. **Journal of Elastomers & Plastics**, v. 45, p. 501–522, 2012.

BARNI, A; Levi, M. Aqueous polyurethane dispersions: a comparative study of polymerization processes. **Journal of Applied Polymer Science**, v. 88, p. 716–723, 2003.

BEUGUEL, Q.; et al. Comparative study of the structural and rheological properties of PA6 and PA12 based synthetic talc nanocomposites. **Polymer**, v. 62, p. 109-117, 2015.

BEUGUEL, Q.; et al. Influence of clay mineral structure and polyamide polarity on the structural and morphological properties of clay polypropylene/ polyamide nanocomposites. **Applied Clay Science**, v. 135, p. 253-259, 2017.

CAO, X; Habibi Y.; Lucia L. A. One-pot polymerization, surface grafting, and processing of waterborne polyurethane-cellulose nanocrystal nanocomposites. **Journal of Materials Chemistry**, v. 19, p. 7137-7145, 2009.

CASTILLO L. A; Barbosa S. E; Capiati N. J. Influence of talc morphology on the mechanical properties of talc filled polypropylene. **Journal of Polymer Research**, v. 20, 2013.

CASTILLO, L; et al. Thermoplastic starch films reinforced with talc nanoparticles. **Carbohydrate Polymers**, v. 95, p. 664-674, 2013.

CHABROL, K.; et al. Functionalization of synthetic talc-like phyllosilicates by alkoxyorganosilane grafting. **Journal of Materials Chemistry**, v. 20, 9695-9706, 2010.

CHATTOPADHYAY D. K; Raju, K. V. S. N. Structural engineering of polyurethane coatings for high performance applications. **Progress in Polymer Science**, v. 32, p. 352-418, 2007.

CLAVERIE, M; et al. Synthetic talc and talc-like structures: preparation, features and applications. **Chemistry A European Journal**, v. 24, p. 519-542, 2018.

CORNILLE, A; et al. A perspective approach to sustainable routes for non-isocyanate polyurethanes. **European Polymer Journal**, v. 87, p. 353-552, 2017.

CZLONKA, S; et al. Linseed oil as a natural modifier of rigid polyurethane foams. **Industrial Crops & Products**, v. 115, p. 40-51, 2018.

DIAS, G; et al. Comparing different synthetic talc as fillers for polyurethane nanocomposites. **Macromolecular Symposia**, v. 367, p. 136-142, 2016.

DIAS, G; et al. Synthetic silico-metallic mineral particles (SSMMP) as nanofillers: comparing the effect of different hydrothermal treatments on the PU/SSMMP nanocomposites properties. **Polymer Bulletin**, v. 72, p. 2991-3006, 2015.

DOS SANTOS, L. M; et al. New magnetic nanocomposites: Polyurethane/ Fe_3O_4-synthetic talc. **European Polymer Journal**, v. 69, p. 38-49, 2015.

DOS SANTOS, L. M; et al. Waterborne polyurethane/Fe_3O_4-synthetic talc composites: synthesis, characterization, and magnetic properties. **Polymer Bulletin**, v. 75, p. 1915-1930, 2018.

DUMAS, A; et al. Synthetic talc advances: Coming closer to nature, added value, and industrial requirements. **Applied Clay Science**, v. 85, p. 8-18, 2013.

FIORENTINO, B; et al. Chemical modification routes of synthetic talc: Influence on its nucleating power and on its dispersion state. **Applied Clay Science**, v. 109-110, p. 107-118, 2015.

GAO, X; et al. Preparation and characterization of well-dispersed waterborne polyurethane/CaCO3 nanocomposites. **Colloids and Surfaces A: Physicochemical and Engineering Aspects**, v. 377, p. 312-317, 2011.

GURUNATHAN, T; Mohantya, S.; Nayakab, S. K. Effect of reactive organoclay on physicochemical properties of vegetable oil-based waterborne polyurethane nanocomposites, **RSC Advances**, v. 5, p. 11524–11533, 2015.

HECK, C. A; dos Santos, J. H. Z; Wolf, C. R. Waterborne polyurethane: the effect of the addition or in situ formation of silica on mechanical properties and adhesion. **International Journal of Adhesion & Adhesives**, v. 58, p. 13-20, 2015.

JIN, H; Wie, J; Kim, S. C. Effect of organoclays on the properties of polyurethane/ clay nanocomposite coatings. **Journal of Applied Polymer Science**, v. 117, p. 2090–2100, 2010.

KAUSHIK, A; Ahuja, D; Salwani, V. Synthesis and characterization of organically modified clay/castor oil based chain extended polyurethane nanocomposites. **Composites Part A: Applied Science and Manufacturing**, v. 42, p. 1534-1541, 2011.

KHUDYAKOV, I. V; Zopf, D. R; Turro, N. J. Polyurethane Nanocomposites. **Designed Monomers and Polymers**, v. 12, p. 279-290, 2009.

KIM, B. K; Aqueous polyurethane dispersions. **Colloid & Polymer Science**, v. 274, p. 599-611, 1996.

LAFLAMME, P; Beaudoin, A; Chapaton, T; Spino, C; Soldera, A. Simulated infrared spectra of triflic acid during proton dissociation. **Journal of Computational Chemistry**, v. 33, p. 1190–1196, 2012.

LEE, H-T; Hwang, J-J; Liu, H-J. Effects of ionic interactions between clay and waterborne polyurethanes on the structure and physical properties of their nanocomposite dispersions. **Journal of Polymer Science: Part A: Polymer Chemistry**, v. 44, p. 5801–5807, 2006.

LEI, S. G; S.V. Hoa, S. V; Ton-That M. T. Effect of clay types on the processing and properties of polypropylene nanocomposites. **Composites Science and Technology**, v. 66, p. 1274-1279, 2006.

MAJI, P. K.; Bhowmick, A. K. Efficacy of clay content and microstructure of curing agents on the structure–property relationship of new-generation polyurethane nanocomposites. **Polymer Advanced Technology**, v. 23, p. 1311-1320, 2012.

MOREIRA DOS SANTOS, L **Preparação de Nanocompósitos de Poliéster Aromáticos/TiO_2 por polimerização in situ.** Porto Alegre. 2013. Dissertação. Programa de Pós-Graduação em Engenharia e Tecnologia de Materiais, Pontifícia Universidade Católica Do Rio Grande Do Sul, Brasil.

NGUYEN, Q. T; Baird, D G. Preparation of polymer–clay nanocomposites and their properties. **Advances in Polymer Technology**, v. 25, p. 270–285, 2006.

NOREEN, A; et al. Recent trends in environmentally friendly water-borne polyurethane coatings: A review. **Korean Journal of Chemical Engineering**, v. 33, p. 388-400, 2016.

PAVLIDOU, S; C.D. Papaspyrides, C. D. A review on polymer–layered silicate nanocomposites. **Progress in Polymer Science**, v. 33, p. 1119-1198, 2008.

POKHAREL, P; Sunwoong Choi, S; Lee D. S. The effect of hard segment length on the thermal and mechanical properties of polyurethane/graphene oxide nanocomposites. **Composites: Part A**, v. 69, p. 168-177, 2015.

PRADO, M; et al. Synthetic Ni-talc as filler for producing polyurethane nanocomposites. **Journal of Applied Polymer Science**, v. 132, 2015.

RAY, S. S; Okamoto, M. Polymer/layered silicate nanocomposites: a review from preparation to processing. **Progress in Polymer Science**, v. 28, p. 1539-1641, 2003.

SAHA, C; Chaki, T. K; Singha N. K. Synthesis and characterization of elastomeric polyurethane and PU/clay Nanocomposites based on an aliphatic diisocyanate. **Journal of Applied Polymer Science**, v. 130, p. 3328-3334, 2013.

SALAHUDDIN, N; et al. Synthesis and characterization of polyurethane/organo-montmorillonite nanocomposites. **Applied Clay Science**, v. 47, p. 242-248, 2010.

SATTAR, R; Ayesha Kausar, A; Siddiq, M. Advances in thermoplastic polyurethane composites reinforced with carbon nanotubes and carbon nanofibers: A review. **Journal of Plastic Film & Sheeting**, v. 31, p. 186-224, 2015.

SONG, M; High performance nanocomposites of polyurethane elastomer and organically modified layered silicate. **Journal of Applied Polymer Science**, v. 90, p. 3239–3243, 2003.

TAN, B; Thomas N. L. A review of the water barrier properties of polymer/clay and polymer/graphene nanocomposites. **Journal of Membrane Science**, v. 514, p. 595-612, 2016.

WANG, J; Somasundaran, P. Study of galactomannose interaction with solids using AFM, IR and allied techniques. **Journal of Colloid and Interface Science**, v. 309, p. 373-383, 2007.

WANG, K; et al. Effect of talc content on the degradation of re-extruded polypropylene/talc composites. **Polymer Degradation and Stability**, v. 98, p. 1275-1286, 2013.

WANG, W; Guo, Y; Otaigbe, J. U. Synthesis and characterization of novel biodegradable and biocompatible poly(ester-urethane) thin films prepared by homogeneous solution polymerization. **Polymer**, v. 49, p. 4393-4398, 2008.

YAMASAKI, S; Industrial synthetic methods for rubbers. 8. Polyurethane elastomers. **International Polymer Science and Technology**, v. 1, p. 29-35, 2016.

YANG, H; et al. Preparation of porous material from talc by mechanochemical treatment and subsequent leaching. **Applied Clay Science**, v. 31, 290-297, 2006.

YOUSFI, M; et al. Compatibilization of polypropylene/polyamide 6 blends using new synthetic nanosized talc fillers: morphology, thermal, and mechanical properties. **Journal of Applied Polymer Science**, v.131, 2014.

YOUSFI, M; et al. Use of new synthetic talc as reinforcing nanofillers for polypropylene and polyamide 6 systems: thermal and mechanical properties. **Journal of Colloid and Interface Science**, v. 403, p. 29-42, 2013.

YOUSFI, M; Ionic compatibilization of polypropylene/ polyamide 6 blends using an ionic liquids/nanotalc filler combination: morphology, thermal and mechanical properties. **RSC Advances**, v. 5, p. 46197-46205, 2015.
YU, F; et al. Effects of talc on the mechanical and thermal properties of polylactide. **Journal of Applied Polymer Science**, v. 125, p.99–109, 2012.

ZHANG, Q; et al. In situ miniemulsion polymerization for waterborne polyurethanes: Kinetics and modeling of interfacial hydrolysis of isocyanate. **Colloids and Surfaces A: Physicochemical Engineering Aspects**, v. 393, p. 17– 26, 2012.

ZHANG, S; et al. Synthesis and characterization of novel waterborne polyurethane nanocomposites with magnetic and electrical properties. **Composites: Part A**, v. 55, p. 94-101, 2013.

ZHANG, X; et al. The synthesis and characterization of polyurethane/clay nanocomposites. **Polymer International**, v. 52, p. 790–794, 2003.

ZHAO, G; Wanga, T.; Wanga, Q. Studies on wettability, mechanical and tribological properties of the polyurethane composites filled with talc. **Applied Surface Science**, v. 258, p. 3557-3564, 2012.

ZHOU, X; et al. Recent advances in synthesis of waterborne polyurethane and their application in water-based ink: a review. **Journal of Materials Science & Technology**, v. 31, p. 708-722, 2015.

ZIA, K. M; Bhatti, H. N; Bhatti, I. A. Methods for polyurethane and polyurethane composites, recycling and recovery: A review. **Reactive & Functional Polymers**, v. 67, p. 675-692, 2007.

ZOU, H; Wu, S; Shen, J. Polymer/silica nanocomposites: preparation, characterization, properties, and applications. **Chemical Reviews**, v. 108, p. 3893-3957, 2008.